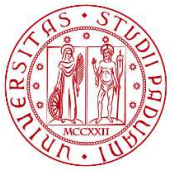

UNIVERSITÀ
DEGLI STUDI
DI PADOVA

Sede Amministrativa: Università degli Studi di Padova

Dipartimento di Scienze Cardiologiche, Toraciche e Vascolari

DOTTORATO DI RICERCA IN SCIENZE MEDICHE, CLINICHE E SPERIMENTALI

INDIRIZZO "SCIENZE CARDIOVASCOLARI"

CICLO XXIX

Development and characterisation of Bioengineered percutaneous heart valves using Xenogeneic decellularised pericardia

This research project was funded by the People Programme (Marie Curie Actions) of the European Union's Seventh Framework Programme FP7/2007-2013/ under REA grant agreement n° 317512.

Coordinatore: Ch.mo Prof. Annalisa Angelini

Supervisore: Ch.mo Prof. Gino Gerosa

Co-Supervisore: Prof. Laura Iop

Dottorando: Sugat Ratna Tuladhar

ABSTRACT

Heart valve disease (HVD) represents a major health problem, causing significant morbidity and mortality worldwide. The gold standard for treating HVD is surgical replacement of the diseased valve with a prosthetic one. However, many patients affected by HVD cannot receive surgical treatment due to their old age or multiple comorbidities, such as poor left ventricular function, coronary artery disease, kidney failure or chronic lung diseases. The alternative solution for these patients is transcatheter implantation of a valve prosthesis, i.e. a percutaneous heart valve (PHV), by minimally invasive techniques. Current heart valve prostheses for this approach are composed of chemically treated xenogeneic tissue. As such, a limitation common to all of them is the inability of remodelling, repair, and regeneration, which are particularly problematic in case of paediatric patients.

Decellularised scaffolds presenting a natural histoarchitecture have been shown to be a good alternative to chemically processed xenograft. Decellularisation is a process, which removes cells and other xenogeneic components from the treated tissue while retaining the integrity of its extracellular matrix components, which are essential for supporting cell engraftment and function. Importantly, decellularisation has the potential to remove immunogenic factors rendering decellularised xenografts potentially biocompatible in an in-human implantation.

In this project, decellularised pericardium has been applied with the aim to develop bioengineered percutaneous heart valves (bioPHVs) with possibly superior potential of long-term performance in comparison to conventional cardiac valve prostheses.

Porcine and bovine pericardia were decellularised using an established protocol combining Triton X-100, sodium cholate and endonucleases. Decellularisation was verified through histology, immunofluorescence, and biochemistry. BioPHVs were fabricated by sewing the decellularised pericardia onto commercially available stents. The bioPHVs were as first evaluated by hydrodynamic performance according to ISO 5840-3 standard requirements. Second, the possible effects of valve crimping on bioPHV decellularised pericardial tissues were assessed through histological and morphometrical analysis.

Histology, immunofluorescence, and biochemical analyses revealed TRICOL to be equally successful for the decellularisation of both porcine and bovine pericardia. Hydrodynamic tests showed that bioPHVs satisfied the minimum performance requirements indicated by ISO 5840-3. The hydrodynamic behaviour of the bioPHVs was comparable, or even superior, to the one exhibited by the control valves. BioPHVs were also able to withstand extreme back pressure conditions without any severe regurgitations. Examination, both macroscopic and microscopic, of the valve samples after crimping showed no major trauma or injury on the pericardial cusps.

This study demonstrated the suitability of the decellularised pericardium, either bovine or porcine, as an alternative to the glutaraldehyde-treated equivalent. Among the two types of pericardial species tested, preliminary results indicated that the porcine tissue would be preferable to fabricate advanced PHV replacements.

TABLE OF CONTENTS

1. INTRODUCTION

Among the diseases affecting the heart, one of the most prevalent is heart valve disease (HVD) (1), which can be classified as either stenosis or regurgitation. Treatment of HVD is performed through surgical valve replacement or repair, i.e. the second major heart intervention in the Western world (2). However, many patients diagnosed with HVD cannot receive surgical treatment due to their old age or multiple comorbidities, such as poor left ventricular function, coronary artery disease, kidney failure or chronic lung diseases. In the case of aortic stenosis, about one-third of patients cannot undergo surgical treatment (3).

For these 'high risk' patients, the alternative solution is transcatheter valve implantation by minimally invasive techniques. This approach utilises a catheter, which is inserted into the patient's artery or vein to deliver the heart valve into the desired location. Such an interventional technique has been successfully applied for the replacement of the aortic valve by a procedure called transcatheter aortic valve implantation (TAVI) (4-6). TAVI does not require open heart surgery, can be performed on a beating heart and, thus, has significantly reduced surgical risks (7).

Several heart valve replacements, i.e. percutaneous heart valves (PHVs) (or transcatheter heart valves (THVs)), are currently available for TAVI procedure and they are manufactured with a stent and sutured cusp material. The stent is the structural support of the PHV and depending on the chosen metal alloy frame, it can possess self-expanding or balloon-expandable properties (8). Self-expanding PHVs are characterised by a structure composed of shape memory materials, usually nitinol, which acquire their final shape once released. On the other hand, the balloon-expandable devices, constructed from stainless steel or cobalt-chromium alloy, require balloon dilatation to reach their final shape.

The cusps are formed of xenogeneic materials, mainly porcine or bovine pericardium or porcine aortic cusps, that have been submitted to glutaraldehyde treatment. Processing these tissues with glutaraldehyde stabilises their extracellular matrix (ECM) components and prevents graft rejection by significantly reducing their immunogenicity. However, the chemical fixation of these materials is associated to several potential limitations (9). Following glutaraldehyde treatment, these tissues are

no more viable, thus lacking the ability to grow and/or repair. Cell remnants, such as free phosphate groups (i.e. phospholipids and degraded nucleic acids), act as sites of calcific nucleation (10), which in due course of time results in the mineralisation of the cusps. Another hypothesis for the degeneration onset relates to the recipient's immune response to specific antigens expressed on xenogeneic cells and ECM. Although glutaraldehyde treatment shields such epitopes, *in vivo* tissue fatigue could cause their exposure, rendering the graft material vulnerable to immunologic reactions and hence triggering the failure of the implant (11). As a result of all these factors, progressive degeneration leads to failure of the implanted bioprostheses employed for classic surgical implantation in 10 to 15 years post-implantation.

Since both bioprosthetic heart valves and PHVs are fabricated from glutaraldehyde-treated tissues, a similar degeneration path can be hypothesised also for the latter replacement alternatives.

In order to overcome these drawbacks, the development of a glutaraldehyde-free and non-immunogenic PHV is mandatory to improve TAVI clinical performance. Ideally, this PHV replacement should also be viable with the incorporation of cells either through *in vitro* seeding or by recipient's endogenous cell repopulation. In this respect, decellularised xenograft material could have the potential to offer a suitable alternative to glutaraldehyde-treated tissue for the manufacturing of PHV cusps.

The decellularisation process removes cells and their components, whilst grossly preserving the ECM proteins (12). As a result, the decellularised ECM scaffold maintains intact the natural fibre architecture comprised of collagen, elastin, glycosaminoglycans (GAGs), and growth factors (12). These preserved components hold specific informative clues for guiding cell adhesion, engraftment, differentiation and/or maintenance of differentiated phenotypes (13). This is a unique benefit offered by the decellularised tissue in comparison to synthetic biomaterials.

In this regard, two general strategies might be pursued for developing a PHV using decellularised tissue. One option is to fabricate the PHV using a decellularised tissue scaffold and implant the valve unseeded, with a view to attracting endogenous cells once *in vivo,* following the principle of *in vivo* tissue guided regeneration. Another option is to seed the decellularised tissue-based PHV *in vitro* with the patient's own cells to generate a living, functional and autologous PHV prior to implantation.

Potential sources of cells for this last approach are differentiated tissue-specific cells (endothelial and/or smooth muscle cells) and stem cells (14). Following seeding, the cell-scaffold construct needs to be placed in a functional simulation system (bioreactor), to promote appropriate cell differentiation and subsequent appropriate tissue development (15).

This thesis is structured into five main sections. The first section gives an introduction about the project. The second section states the aims and objectives of the research. The third section describes the experimental methodology followed during tissue decellularisation, assessment of decellularised tissues, bioPHVs fabrication and characterisation. The fourth section presents all the results related to the characterisation of decellularised tissues and bioPHVs. The thesis concludes with a discussion on the work performed till date and an outlook for the future.

1.1 Heart and heart valves

The heart is one of the vital organs of the body. The ceaselessly beating activity of heart has fascinated people for centuries. It is part of the cardiovascular system (CVS), which transports nutrients to and removes waste products from the cells through a vast network of blood vessels.

The heart is a muscular organ enclosed within the mediastinum, the medial cavity of the thorax (Figure 1-1). The size of a human heart is about the size of the person's fist and is cone shaped. It has a mass between 250 and 350 grams and beats approximately 100,000 times a day pumping roughly 8000 liters of blood (16). The heart is enclosed in a double walled sac, called the pericardium. The heart wall, richly supplied with blood vessels, is composed of three layers: the epicardium, the myocardium, and the endocardium.

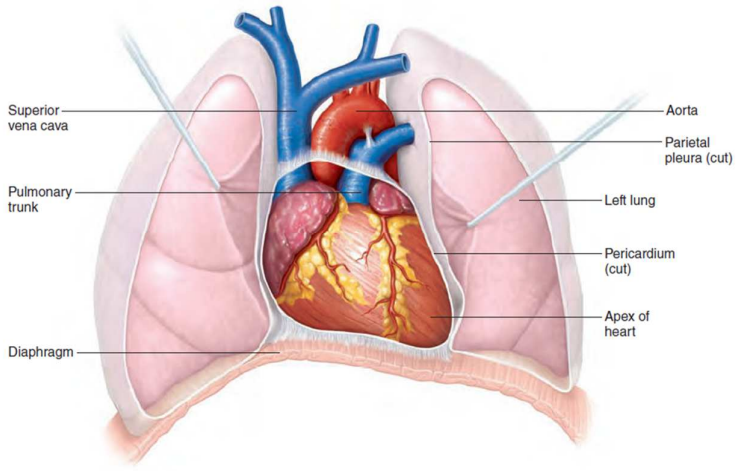

Figure 1-1 Location of heart in mediastinum. From (16)

The human heart consists of four chambers: the right atrium and ventricle, and the left atrium and ventricle (17). Blood flows through the heart in one direction: from atria to ventricles and out to the great arteries leaving the superior aspect of the heart (Figure 1-2). Four valves enforce this unidirectional flow. In response to the difference in blood pressure on their two sides, the valves open and close about 40 million times a year and 3 billion times over the average human lifetime (18)(19).

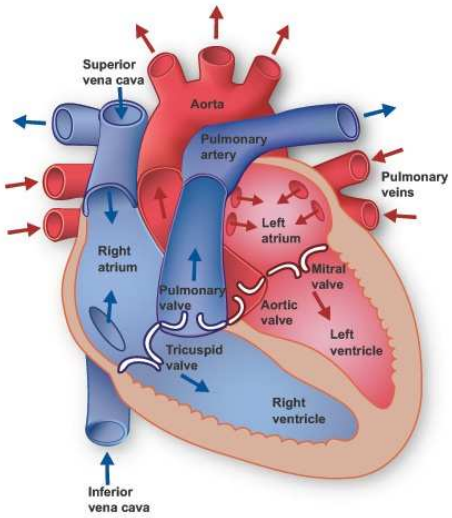

Figure 1-2 The heart valves and the blood vessels connecting to the heart. From (16)

The two atrioventricular (AV) valves, located at each atrioventricular junction, prevent backflow into the atria when the ventricles are contracting. The aortic and pulmonary valves guard the bases of the large arteries arising from the ventricles (aorta and pulmonary truck, respectively) and prevent backflow of blood into the heart.

1.1.1 Anatomical features of the heart valves

The four heart valves: aortic, pulmonary, mitral, and tricuspid valves are all situated in a plane, which forms the 'base' of the heart (Figure 1-3). This area, known as the 'fibrous skeleton' of the heart, is composed of densely collagenous fibers and remains almost stationary during the cardiac cycle, in contrast to the dynamic movements of the myocardium, leaflets/cusps and arteries (20).

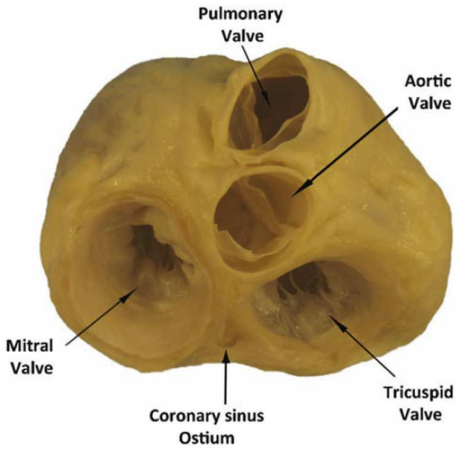

Figure 1-3 Anatomical plate of a human heart with the atria and great arteries removed showing the relationship between the four valves at the base of the heart. From (21)

Semilunar valves

The two semilunar valves, aortic and pulmonary, are composed of three cusps each attached to its respective sinus. When closed, the three cusps co-apt along zones of apposition. The cusp margins are attached to the arterial wall in the shape of half-moon (Figure 1-4) (21). The aortic valve is positioned between the left ventricle and the aorta, while the pulmonary valve between the right ventricle and the pulmonary artery.

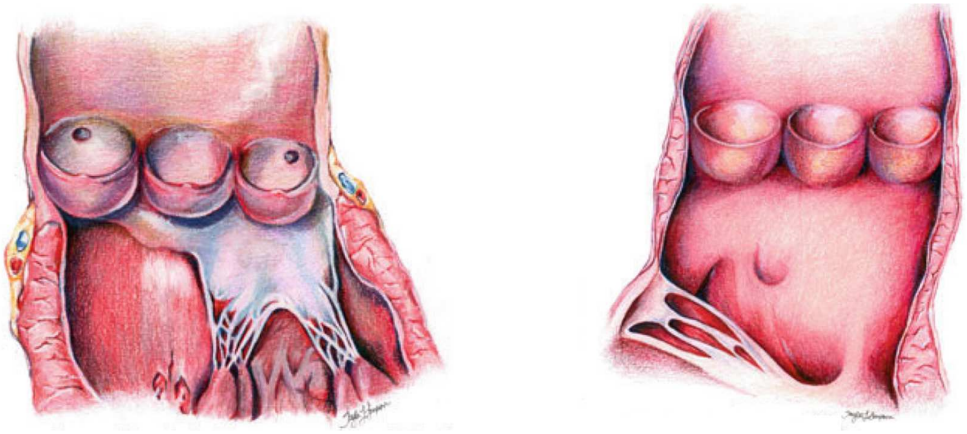

(a) Aortic Valve (b) Pulmonary Valve

Figure 1-4 An artistic depiction of the healthy (a) aortic and (b) pulmonary valves. From (21)

The cusps of the aortic valve are named after the coronary arteries that branch from its sinuses and supply blood to the left and the right sides of the heart (Figure 1-5). The cusp, whose sinus contains the ostium of the left coronary artery, is called left coronary cusp, while the one, whose sinus contains the ostium of the right coronary artery, is named right coronary cusp. The third aortic sinus is not associated with any coronary artery and the cusp is referred to as non-coronary one.

The cusps of the pulmonary valves are named according to their relationship with the aortic valve (Figure 1-5). Two cusps of the pulmonary valve lie opposite the left and right coronary ones of the aortic valve and thus are called left and right facing cusps, respectively. The third cusp is consequently termed non-facing one (21).

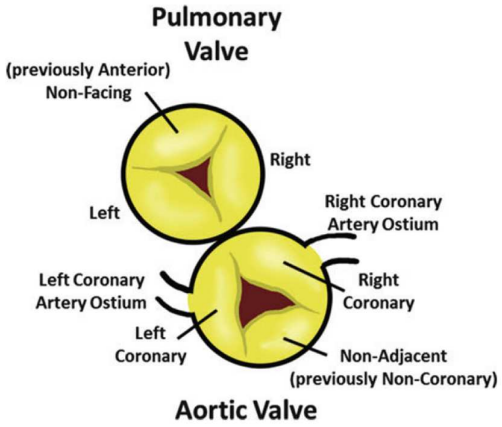

Figure 1-5 Nomenclature of individual cusps for aortic and pulmonary valves. From (21).

Atrioventricular valves

The two AV valves are the tricuspid and the mitral valves (Figure 1-6). The tricuspid valve is the right AV valve has three flexible cusps. The left AV valve with two flaps is called bicuspid valve or alternatively the mitral valve because of its resemblance to the two-sided bishop's mitre or hat (22). The tricuspid valve is located between the right atrium and the right ventricle, while the mitral valve between the left atrium and the left ventricle. Attached to each AV valve flap are tiny white collagen cords, called *chordae tendineae*, which anchor the cusps to the papillary muscles protruding from the ventricular walls (23).The leaflets of the tricuspid valve are referred to as the anterior, posterior, and septal. The mitral valve normally presents two leaflets commonly referred to as the anterior and posterior.

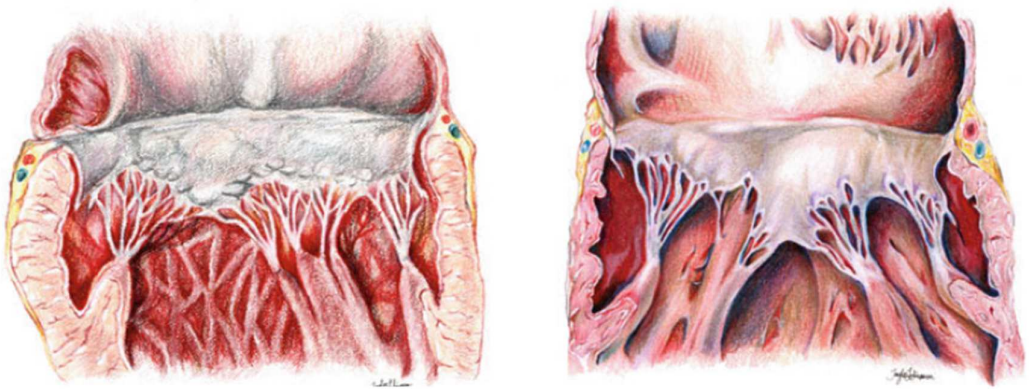

(a) Mitral Valve (b) Tricuspid Valve

Figure 1-6 Schematic representation of (a) Mitral and (b) Tricuspid valve. From (21)

1.1.2 Aortic heart valve structure

The ability of the valves to permit unobstructed forward flow depends on their mobility, pliability, and structural integrity, meaning that the valves need to have enough strength and durability to cope with the repetitive movements and the consequent mechanical stress and strain imposed on them. The functional requirements of the heart valves are accomplished by a specialised set of cells and a heterogeneous ECM, arranged in a spatially specific and differentiated tissue structure. The cellular component of the valve cusps includes the valvular endothelial cells (VECs) at the blood-contacting surfaces, and the valvular interstitial cells (VICs) at the main inner bulk of the valve. The ECM mainly includes collagen, elastin, and amorphous extracellular matrix (predominantly GAGs) (24). The valve ECM undergoes continuous damage due to the repetitive loading cycles during normal function and is subsequently remodelled and repaired by the residing cells (25).

The aortic cusps can be divided into three distinct layers: *fibrosa*, *ventricularis*, and *spongiosa* (Figure 1-7) (26). The *fibrosa* is located on the aortic side of the cusp, and is composed of collagen bundles arranged circumferentially with very little elastin (27). The *ventricularis* is a thinner layer that constitutes the ventricular layer of the cusp and has considerably more elastin. Between the *fibrosa* and the *ventricularis* is the *spongiosa*, which makes up a central core of loose connective tissue. The *spongiosa* is comprised of a large amount of GAGs and few loosely connected fibrous proteins. Healthy human valve cusps are avascular, being thin enough (<1 mm) to receive nourishment through convection and diffusion (28).

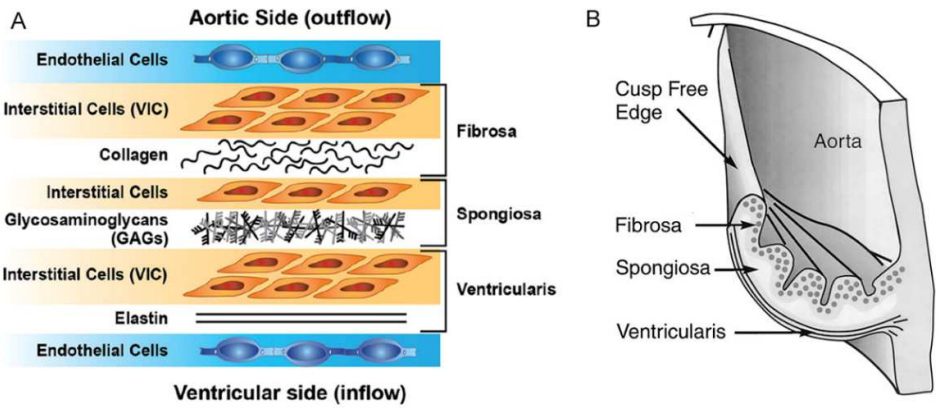

Figure 1-7 Different layers of aortic valve cusp. A) Demonstration of the histoarchitecture of a normal aortic valve. Adapted from (24); B) A section through the cusp and aortic wall showing the internal configuration of the *fibrosa, spongiosa and ventricularis*. From (27)

From the biomechanical point of view, the majority of the stresses and strains experienced by the cusps occur during diastole and early valve opening. Although an exact *in vivo* measurement is very difficult to perform, a reasonable approximation based on elementary beam mechanics can be performed. Assuming that valves deform under blood pressure by a combination of axial stretch and bending, the total stresses in the cusp in systole have been calculated to be in the order of 50 kPa and 500 kPa in diastole (29). The *fibrosa* layer of the cusp bears the higher diastolic load, while the *ventricularis* supports the systolic one. Considerations on the geometry of the load bearing surfaces during systole and diastole have generated estimates of maximum physiological cusp stress between 200–400 kPa (30). *In vivo* cusp strains have been calculated to be 0.1 in the circumferential direction and 0.4 in the radial one (30). The aortic root also experiences significant mechanical loads *in vivo* that arises from pressure and its connection to the contracting ventricle (30).

Aortic VECs maintain a non-thrombogenic blood contact surface, and are responsible for transmitting nutrient and biochemical signals to the interstitial cells (31). Aortic VECs form single cell monolayers on the cusp surfaces, express von Willebrand factor, produce nitric oxide and possess cell junctions similar to arterial endothelial cells. VECs are oriented circumferentially across the cusps, perpendicular to the direction of blood flow (32). However, the cells on the aortic and ventricular sides behave differently and express different markers (33).

Aortic VICs can be defined as the mesenchymal cell within the aortic valve cusp (34). VICs are a heterogeneous cell population that comprises at least five different cell phenotypes, including embryonic progenitor endothelial/mesenchymal cells (eVICs), quiescent VICs (qVICs), activated VICs (aVICs), post developmental/adult progenitor VICs (pVICs), and osteoblastic VICs (obVICs) (34). Most VICs in the normal valve are quiescent and fibroblast-like. VICs are responsible for organizing and remodelling the ECM proteins to withstand the dynamic cusp strains during the cardiac cycle. VICs are strongly attached to the ECM and they express ECM-degrading enzymes (including matrix metalloproteinases) and their inhibitors that remodel collagen and other ECM components (35). It has been observed that normal aortic VICs secrete and turnover proteins and GAGs at a dramatically increased rate in comparison to other cell types *in vivo*, with a significantly higher index of proliferation (36). This suggests that VICs continually repair the mechanically-induced tissue microdamage to enable long-term durability. Besides, the endothelial and interstitial cells, smaller populations of smooth muscle cells (37) and nerve cells have also been reported (38).

1.1.3 Heart valve disease

Heart valves are affected by mainly two types of diseases: stenosis and regurgitation. Stenosis refers to narrowing of valve orifice that results in obstruction of the blood flow while regurgitation is the condition, where the valve becomes incompetent causing back flow of blood. Among the four heart valves, the one most prone to disease and requiring substitution is the aortic valve, followed by the mitral valve.

Valve stenosis

The aortic valve has the highest occurrence of stenosis (Figure 1-8), being the most common valvular heart disease in developed countries (39). There are several ways, by which a normal aortic valve can become stenotic. Calcification and congenital bicuspid defect account for most of aortic stenosis cases, followed by rheumatic fever (40).

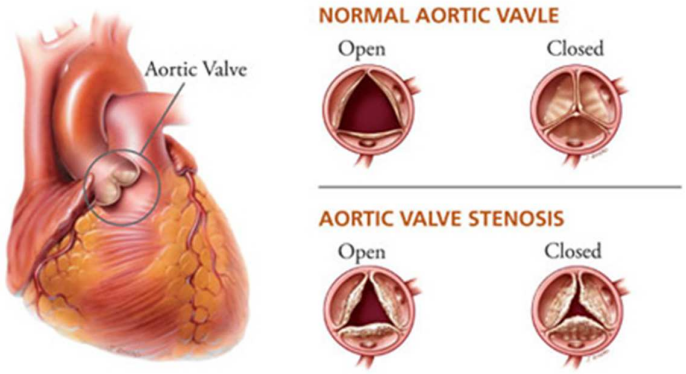

Figure 1-8 Aortic stenosis in comparison to normal aortic valve. From (41)

Calcific aortic valve disease occurs because of calcification of the cuspal tissue of either previously anatomically normal or congenital bicuspid aortic valves (Figure 1-9). Calcific aortic stenosis affects approximately 2% to 3% of those older than 75 years and the main cause of the disease on most of them is congenital bicuspid aortic stenosis (40). Aortic valve calcification occurs approximately a decade earlier in patients with a bicuspid aortic valve than in those who have an anatomically normal valve. The calcific deposits typically occur in the attachments of the cusps in the regions of highest functional valve stresses (25), which suggests that mechanical factors potentiate valve calcification. Mineralisation is initiated predominantly in VICs, and it is a degenerative process with passive accumulation of hydroxyapatite mineral in dead or damaged cells (42). Observations from animal models of aortic valve disease and *in vitro* calcification models have even led to hypothesis that osteoblastic differentiation of VICs contributes to calcific aortic valve disease, since heart valves and bone share common regulatory mechanisms for connective tissue formation and remodelling (43).

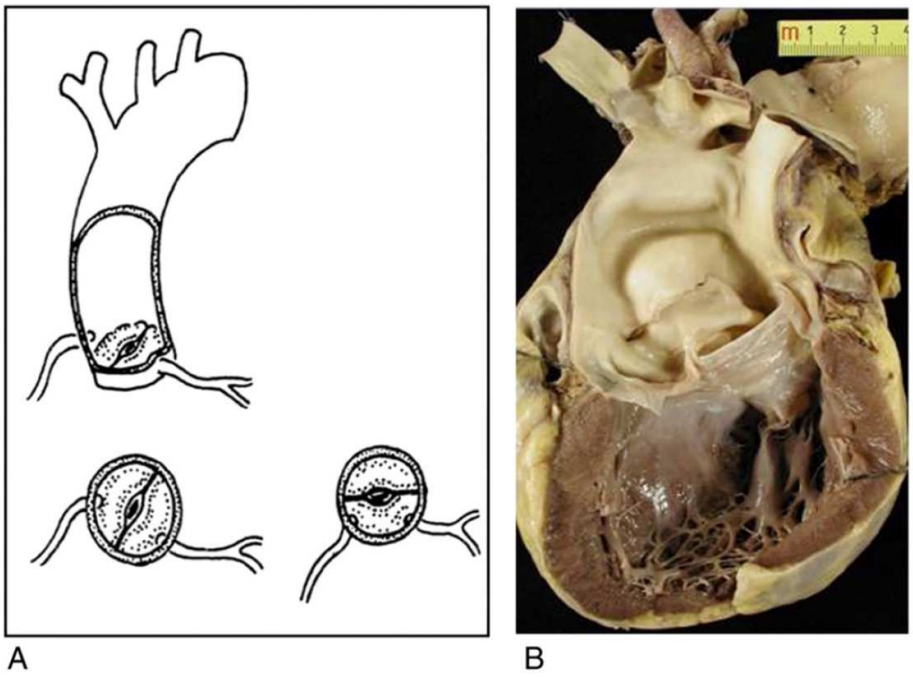

Figure 1-9 Bicuspid aortic valve (BAV), one of the main causes leading to aortic valve stenosis. (A) Schematic representation of BAV. (B) View from the left ventricle and the ascending aorta. From (44)

In developing countries, the most common cause of aortic stenosis is rheumatic heart disease (RHD) (40). This disease is linked to acute rheumatic fever (ARF), which is an immunologically mediated, multisystem inflammatory disease. Cardiac involvement during the active phase of rheumatic fever could progress to chronic rheumatic heart disease. This is characterised by microscopic organisation of acute inflammation and subsequent post-inflammatory scarring leading to chronic fibrotic valvular deformities. This is still an important socio-economical problem in developing countries as RHD accounts for a major proportion of all cardiovascular disease in children and adults (40).

Stenosis can also occur in the mitral valve, narrowing the valve orifice and resulting in reduced flow of blood into the left ventricle. The most common cause of mitral stenosis is rheumatic fever. Other less common causes of mitral stenosis are calcification of the mitral valve leaflets and congenital heart disease (45).

There is no current treatment proven to prevent or delay the development of valve stenosis. Due to the similarity of risk factors between aortic stenosis and coronary artery disease, statins are proposed as a possible therapeutic treatment; however, to

date, no randomised clinical trials have supported this hypothesis (40). Aortic valve replacement is indicated once symptoms develop.

Valve Regurgitation

Valve regurgitation is most prevalent in the case of the mitral valve. Mitral regurgitation is a condition where the mitral valve does not close properly, leading to leakage of blood back into the left atrium during systole. Mitral regurgitation can occur if the valve is weakened or damaged. Causes of mitral regurgitation include degenerative changes, rheumatic heart disease, mitral valve prolapse, myocardial infarction or congenital heart problems (21).

In the case of degenerative changes, the tissues, which connect the mitral valve leaflets to the heart wall, become weak and stretched over time such that the valves do not close together properly. In RHD, inflammation of the valve causes permanent damage and leads to thickening and scarring. Another reason of mitral regurgitation is heart attack, which can sometimes damage the ventricle, where the chordae are attached and thus distorting the mitral valve apparatus (21).

In mitral regurgitation, since the valve does not close properly, during every beat some blood is pumped back into the left atrium when the left ventricle contracts. As the volume of blood leakage increases, it causes a rise in the pressure in the atrium. As a result, the wall of the atrium becomes thicker and enlarged. In addition, due to the leakage, there is a drop in forward stoke volume and cardiac output, causing the ventricle to work harder to compensate and leading to its enlargement (21).

1.2 Pericardium

The pericardium is a double-walled fibroserous sac enclosing the heart and the roots of great vessels. It is composed of two parts: fibrous and serous.

The fibrous pericardium is the external layer made of dense connective tissue and forms a flask-like sac, the neck of which is closed by its attachment to the great vessels. It is attached ventrally to the manubrium of the sternum and the xiphoid process, dorsally to the vertebral column, and caudally to the central tendon of the diaphragm (46).

The serous pericardium is the thin internal layer, comprising again two layers, i.e. parietal and visceral. The outer parietal layer lines the internal surface of the fibrous pericardium and is difficult to separate from it. The internal visceral layer, also known as epicardium, forms the outer layer of the heart (Figure 1-10). Each of the serous layer is made up of a sheet of simple squamous epithelial cells, known as mesothelium. The parietal layer reflects at the roots of the great vessels and runs directly over the external surface of the heart as the visceral layer. Hence, in between the parietal and visceral pericardial layer, a space is located, called pericardial cavity, which is filled with lubricating serous fluid, called pericardial fluid.

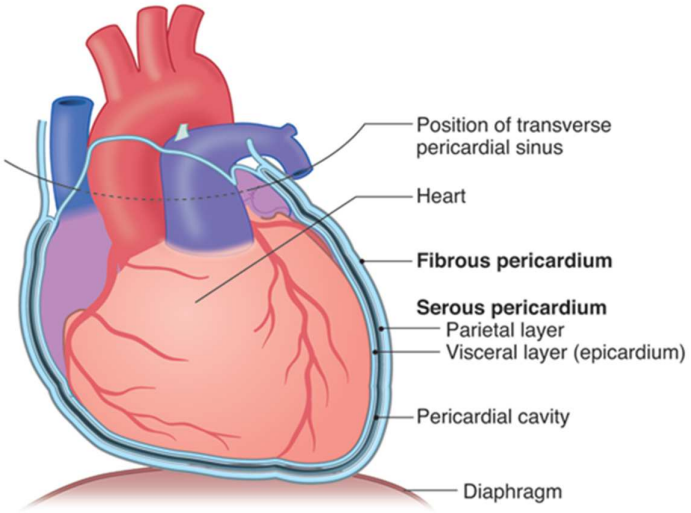

Figure 1-10 Different components of the pericardium. From (17)

Blood is supplied to the pericardium from the pericardiacophrenic arteries and the internal thoracic arteries while the internal thoracic veins are responsible for the venous drainage. The innervation of the pericardium is governed by several different branches including the phrenic nerves, which give sensory fibers that control pain sensation, and the sympathetic trunks, which carry vasomotor fibers (47).

The main functions of the pericardium are:

- Fix the heart in the mediastinum: the pericardium through its attachment to the diaphragm, the sternum and the *tunica adventitia* of the great vessels limits the motion of the heart and holds it in the mediastinum.
- Prevent overfilling and excessive dilation of the heart: the relatively inextensible fibrous layer of the pericardium prevents the heart from rapidly increasing in size.

- Lubrication: the pericardial fluid between the two layers of the serous pericardium reduces the friction generated by the cardiac organ, as it moves within the thoracic cavity.
- Protection from infection: the fibrous pericardium serves as a physical barrier between the muscular body of the heart and adjacent organs prone to infection, such as the lungs. Pericarditis is the most common disorder affecting the pericardium. In this pathological condition, it becomes swollen or inflamed, affecting also the normal heart function. Pericarditis can manifest in acute or chronic settings sue to several causes, including bacterial or viral infections, cancer, kidney failure, certain medicines, and heart (48).

1.2.1 Histological and Ultrastructural features of Pericardium

The human parietal pericardium has been reported to be composed of three layers: the *serosa*, the *fibrosa* and an outer layer of epipericardial connective tissue (49). The *serosa* consists of a surface layer of flattened irregular polygonal mesothelial cells, giving it a smooth and glistening appearance. A narrow submesothelial space (about 2 μm in width) separates the mesothelial cells from the *fibrosa*. The submesothelial layer is thin and contains few fibrocyte-like cells, elastic fibers, and abundant wavy collagen fibers. The submesothelial layer merges with an underlying *fibrosa*, which is composed of connective tissue cells (mainly fibroblast-like cells), small vessels, variously oriented layers of collagen fibrils (a) and small inconspicuous elastic fibers (Figure 1-11b). Several distinct layers of collagen exist in the *fibrosa*. Immediately subjacent to the mesothelial cells, the bundles are oriented along the cephalo-caudal axis. In deeper layers, the collagen bundles run in various directions and showing more weaving pattern. Elastic fibers are usually oriented perpendicular to the collagen bundles. The elastic fibers close to the mesothelium are smaller than those in deeper areas. In the *fibrosa* are embedded slender, greatly elongated connective tissue cells with long, thin nuclei and very little cytoplasm. The *fibrosa* transforms gradually into the dense epipericardial connective tissue layer containing mainly large coarse bundles of collagen, elastic fibers, adipose tissue cells, neural elements and blood vessels (49) .

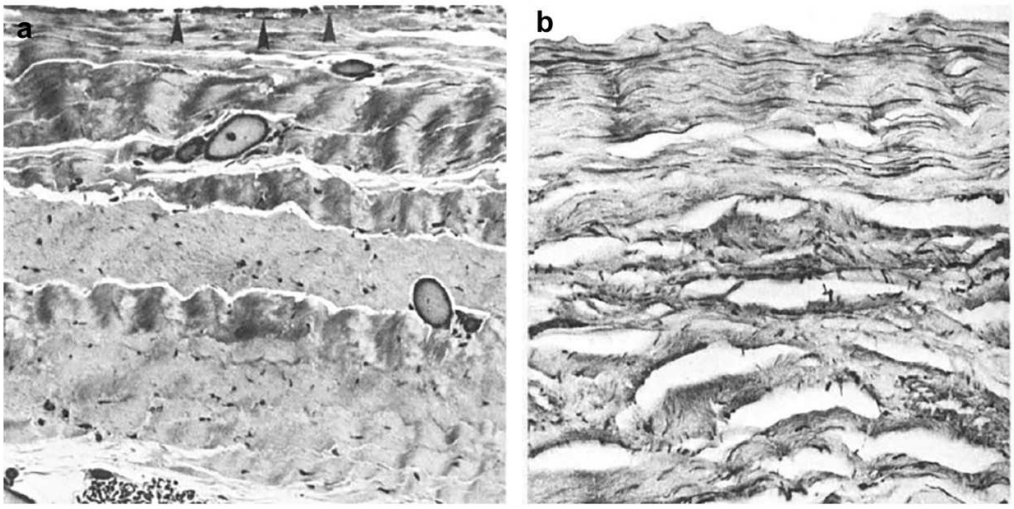

Figure 1-11 Histology of human parietal pericardium (a) Alkaline toluidine blue staining of a section through entire thickness of the pericardium showing the mesothelial cell layer (arrowheads), collagen fibers, vessels and connective tissue cells (b) Elastic-van Gieson staining demonstrating presence of small elastic fibers (shown in black). From (49)

When observed under scanning electron microscopy, at low magnification, the serosal surface of the pericardium appears completely covered by mesothelial cells with polygonal outline. The surface of the mesothelial cells contains numerous microvilli measuring up to 3 µm in length and 0.1 µm in width. Areas of intercellular junctions can be observed as discrete narrow ridges with no intercellular spaces present between adjacent mesothelial cells (Figure 1-12a). Immediately below the mesothelial cells, the serosal surface is composed of bundles of collagen fibrils that have wavy appearance. This layer corresponds to the basal lamina of the mesothelial cells (Figure 1-12b, c). The mediastinal surface of parietal pericardium contains large collagen bundles that run in various directions. These bundles are much larger than those subjacent to the serosal surface.

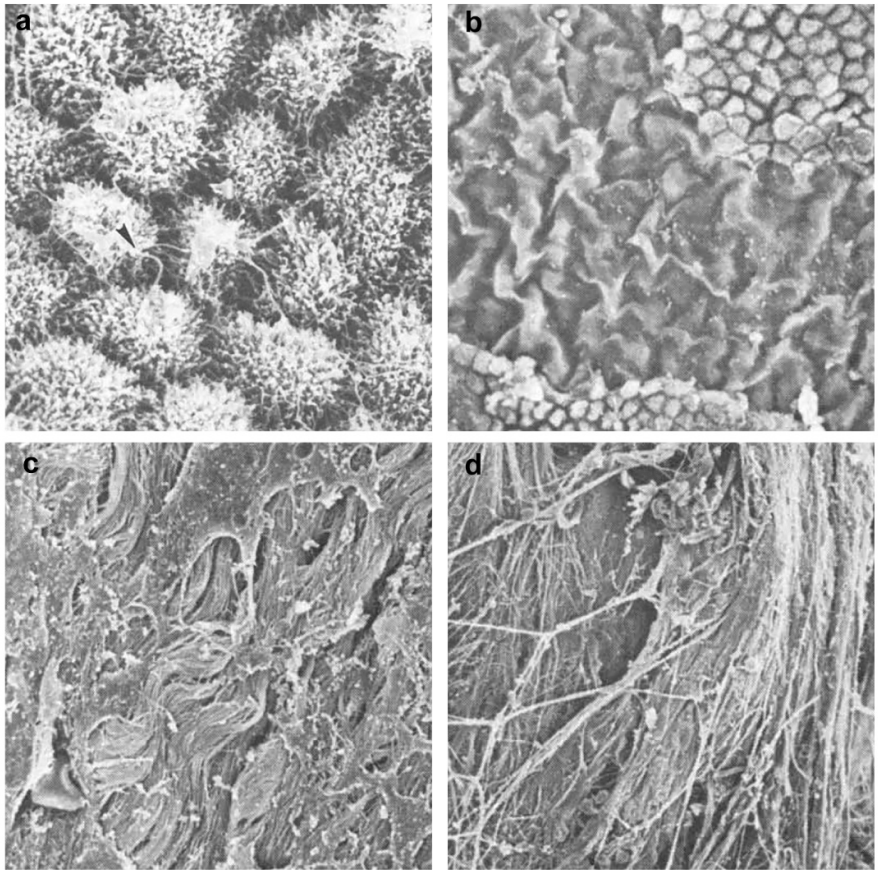

Figure 1-12 Scanning Electron Microscope image of human parietal pericardium: (a) View of mesothelial cells with microvilli; (b) Bundles of collagen fibrils immediately below the mesothelium; (c) Basal lamina of the mesothelium cells showing individual collagen fibrils; (d) Mediastinal surface of parietal pericardium. From (49)

In humans, the geometric configuration of the collagenous fibers in the parietal pericardium varies with age. In the fetus, the fibers are practically straight. After birth they become wavy, reaching the largest wave amplitude in young adults, and becoming nearly straight again in old age. The waves in the collagenous fibers are closely related to the development of the elastic fibers. These latter in the fetus are few, but they increase in number and thickness from birth to adult life. The total quantity of elastic fibers in older persons is approximately the same or somewhat greater than that in younger adults. These findings suggest that the pericardium of young adults is more elastic than that of the elderly (46).

1.3 Surgical heart valve replacement

There is currently no pharmacological treatment for a diseased heart valve. Most of the mechanisms involved in the pathophysiology and progression of HVD are not completely understood. As a consequence, the development of effective medical therapies is challenging.

Repair or replacement of the dysfunctional heart valve remains the only option that can significantly reduce the associated morbidity and mortality (50). The annual number of patients requiring valve replacement worldwide is projected to triple from approximately 290,000 in 2003, to over 850,000 by 2050 (51).

The gold standard procedure for heart valve replacement is surgical implantation of a prosthetic substitute, which involves open heart surgery and placing the patient on heart-lung machine support during intervention. Two categories of prostheses are available for surgical valve replacement: non-biological and biological (50). Non-biological prostheses are fabricated from artificial materials and include mechanical and polymeric heart valves. Biological valves include bioprosthetic valves, fabricated from chemically-treated valvular or pericardial xenografts, as well as cryopreserved homograft valves, obtained from human donors, and autografts valves (pulmonary valve of a patient implanted into aortic position during the Ross intervention).

Since the development of the first heart valve replacement in 1960, prosthetic valve technology has progressed rapidly (52). Similarly, to any other field in medicine, the treatment of HVD has experienced a total revolution in the last 30 years. The following paragraphs will discuss the brief history and the current state-of-the-art of surgical heart valve replacements.

1.3.1 Mechanical heart valves

Mechanical heart valves (MHVs) are fabricated using hemocompatible, non-biological materials, such as metals, ceramics, or polymers. The first MHVs were characterised by central occluders in the form of a ball (53), moving passively in response to the pressure differences (Figure 1-13).

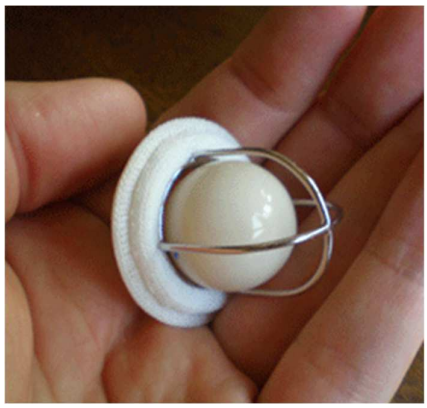

Figure 1-13 Starr-Edwards caged ball valve. From (54)

In 1970s, MHVs with a tilting disc design were introduced. The most clinically employed tilting disc valve was the Björk–Shiley device (Figure 1-14a). Other tilting disc valves included the Medtronic Hall and Sorin valves (Monocast, Carbocast and Allcarbon) (Figure 1-14 b-c). The various tilting disc valves could achieve opening angles varying from 60° to 85° and in the fully open position, the flow passed through both the major and minor orifices.

a. b. c.

Figure 1-14 Tilting disc MHVs: (a) Björk-Shiley valve (b) Medtronic Hall valve (c) Sorin valve. From (55)

In the late 1970s, another major change was introduced to the MHV design in the form of bileaflet valves. These devices were assembled with two semilunar discs (acting as leaflets), attached to a rigid valve ring either by hinge mechanism or open pivots. The bileaflet valve technology proved to be superior to the tilting disc counterpart, being the only mechanical prosthesis currently in clinical use. Among the popular bileaflet valves are the Master HP Series from St. Jude Medical, Medtronic Open Pivot

standard and Open Pivot AP and Sorin Group's Carbomedics and Bicarbon (Figure 1-15)

(a) (b) (c)

Figure 1-15 Bileaflet MHVs: (a) St. Jude valve; (b) Medtronic Open Pivot; (c) Sorin Bicarbon. From (56, 57)

1.3.2 Bioprosthetic heart valves

Bioprosthetic heart valves (BHVs) are made of chemically-treated animal tissue. These xenogeneic valves are fabricated using valvular or pericardial tissues of porcine or bovine origin (58). These tissues undergo special chemical treatment in order to render them suitable for implantation into humans. Early clinical use of xenografts employed treatment of the tissues with organic mercurial salts (59) or formaldehyde (60) to overcome the problems of rejection of the implanted foreign biomaterials by human recipients. Formaldehyde-treated valves suffered from durability issues with a failure rate of up to 60% at 2 years after implantation (53). This led to the conclusion that tissue crosslinks are fundamental in maintaining the structural integrity of the BHVs. Novel crosslinking agents were tested and glutaraldehyde revealed not only to be valid as preservation fluid, but also to effectively reduce the antigenicity of the foreign tissues (58).

BHVs are available in two forms: stented and stentless. In the stented version, the porcine heart valve is mounted on a flexible stent, which acts as its frame. The supporting stent is generally composed of three upright wide posts with a circular base in metal or plastic covered with fabric (Figure 1-16). A sewing flange or ring is attached to the base of the covered stent and used to suture the prosthesis in place during implantation. The stented valve is fixed with glutaraldehyde with the valve in the closed position. Glutaraldehyde solution with concentrations ranging from 0.2 to 0.625% have been used for heart valve fixation, also applying different transvalvular pressures.

Studies have shown that the low pressure fixation maintains the microstructure of collagen (53).

Figure 1-16 Stents for stented porcine BHVs. From (61)

The first glutaraldehyde-treated porcine aortic valve prosthesis mounted on a metallic stent was implanted in 1969. Just a year later, the Hancock Porcine Xenograft based on this same technology was introduced in the market. The stent in this valve was made of polypropylene with stainless steel radiopaque marker, a sewing ring made of silicone rubber foam fibres and a cloth covering of polyester.

An improved version of this valve, i.e. the Hancock II (Figure 1-17a), was introduced by Medtronic. The Hancock II demonstrated very low rates of structural deterioration and overall low amount of valve-related complications (53).

Other stented BHVs include the Carpentier-Edwards Aortic Porcine and S.A.V. Aortic Porcine, introduced by Edwards Lifesciences. Both the Carpentier-Edwards and the Hancock-II were of supra-annular type, designed to be implanted on top of the aortic annulus, while aligning the internal diameter of the valve to the patient's annulus (53).

a. b. c.

Figure 1-17 Stented porcine BHVs: (a) Medtronic Hancock II; (b) Carpentier-Edwards Aortic Porcine; (c) Carpentier-Edwards S.A.V. Aortic Porcine. From (52)

BHVs using porcine valvular tissue were also developed following a stentless design due to some drawbacks observed in the stented formulation. In the stented bioprostheses, elevated stress concentration was observed at the cusp stent junction. In addition, the stented designs provided little or no dilation during the cardiac cycle, further elevating the stress concentration in the tissue. This had more implications in the cusps as in native condition their opening and closing assisted by the dilation of the valve annulus. To avoid such regions prone to increased stress concentration, BHV stentless versions were designed. The absence of the supporting stents implies less obstruction to flow, increased annular dilation and improved hemodynamics allowing larger size valve to be implanted for a given orifice (53). Examples of stentless bioprostheses currently available are the Edwards Prima™ Plus, Medtronic Freestyle and St. Jude Medical Toronto SPV valves (Figure 1-18). These prostheses are comprised of the pig's aortic valve with its preserved aortic root and a polymer cloth sewn around the inflow opening.

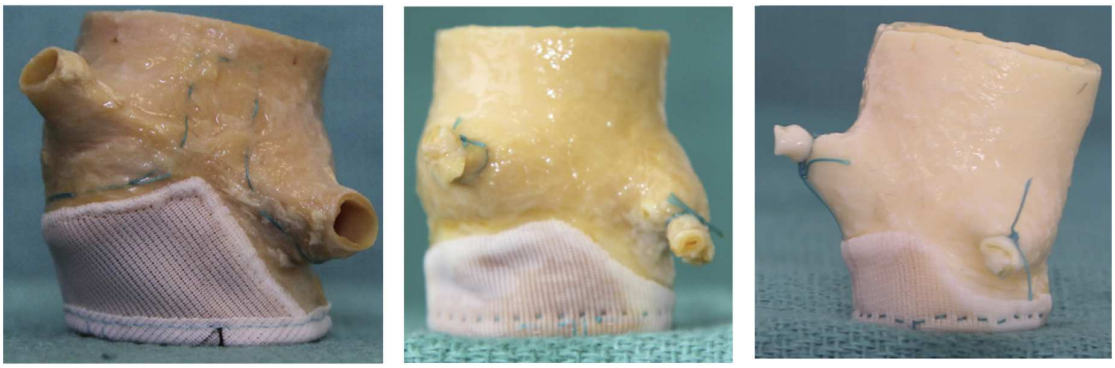

a. b. c.

Figure 1-18 Stentless porcine BHVs: (a) Edwards Prima™ Plus; (b) Medtronic Freestyle; (c) St. Jude Medical Toronto SPV. From (62)

Pericardial BHVs are available only in stented version and are made using bovine pericardium to form the cusps. The pericardium is harvested and processed to remove fatty deposits. An appropriate region of the pericardium is selected and fixed in glutaraldehyde. Following fixation, cusps are cut out from the selected areas of the pericardial tissue and sewn to the cloth-covered stent, in such a fashion to obtain coapting and fully sealing cusps (53).

The Ionescu-Shiley valve was one of the first pericardial valves introduced into the market in the 1970s but had to be discontinued within a decade due to problems associated with calcification and decreased durability. With advances in tissue processing and valve manufacturing technology, pericardial valves were reintroduced into commercial market in the 1990s.

The Edwards Lifesciences marketed the Carpentier-Edwards PERIMOUNT Bioprostheses. Other examples of pericardial BHVs are the Trifecta (St. Jude Medical) and Mitroflow Aortic Pericardial Valve (Sorin Group) (Figure 1-19).

a. b. c.

Figure 1-19 Pericardial BHVs: (a) Carpentier-Edwards PERIMOUNT; (b) St. Jude Medical Trifecta; (c) Sorin Mitroflow. From (53)

1.3.3 Homografts

Homografts valves are allogeneic prostheses harvested from humans. These valves are isolated either from recipients of heart transplantation, organ donors, whose hearts are not accepted for transplantation for reasons other than valve problems, or from cadavers, i.e. from patients who had died due to noncardiac reasons. The tissues are usually taken from donors under the age of 60. Unlike the xenogeneic BHVs, after harvesting, homografts are not fixed with glutaraldehyde (63). After the retrieval, proper disinfection/sterilisation and preservation treatment are applied on the homografts. Heimbecker and colleagues performed the first aortic homograft valve implantation, although they did not disclose good results (64).

The first successful aortic homograft valve implantation was reported by Ross (65). The sterilisation of cadaveric homografts was initially performed with γ-radiation or ethylene-oxide. Later, antibiotics-disinfected, and wet-stored allografts were used, but they showed poor durability.

For preservation, the grafts are commonly frozen at -150°C in liquid nitrogen (cryopreservation) facilitating their preservation for up to 5 years (63). Another preservation method was developed by Yacoub *et al*. In their study, fresh homograft valves stored at 4 °C ("homovital") showed good long-term results with 97% of patients (30 years of age or older), remaining free from valve degeneration after 10 years (66).

The most important advantage of the homografts with respect to the other biological or mechanical prostheses is the superior physiological flow pattern or hemodynamics and their resistance to infection. Moreover, homografts are not fixed with

glutaraldehyde and therefore their proteins are not crosslinked. Also, in comparison to mechanical and xenogeneic bioprostheses, homografts undergo lower rate of thromboembolic events after implantation, thus avoiding the need for life-time anti-coagulation treatment. This might in part be a result of the younger age of most patients at the time of valve replacement, as the incidence of thromboembolism increases with age.

However, since homografts are allogenic, they induce an immunologic response comprised mainly of activated T-cells. This chronic rejection and inflammation results in the degeneration of graft (67). This immunologic process is more evident in infants since the immune system of children is more active and aggressive. Though the durability of homografts is higher compared with most xenogeneic valves, it is still inferior to that of mechanical prostheses. Also, the availability of homografts is limited because of the need for human organ donors. The allograft valve substitutes are also unable to grow with the patient body, thus necessitating reoperations in paediatric patients.

Overall, homograft durability after implantation depends on factors such as method of harvesting, preservation protocol, technique of implantation and selection of patient. Today, “Homograft Banks”, i.e. specialized Tissue Banks, play a vital role in the supply and distribution of homografts.

1.3.4 Autografts

Autograft valves represent a special category of surgical valve prostheses, for which the patient’s own pulmonary valve is used to reconstruct the diseased aortic. This famous technique was developed by Ross in 1967 (68). During the procedure, the healthy pulmonary valve is removed and sewn into the position of the damaged aortic valve (Figure 1-20). A homograft or a xenograft valve is then placed in the pulmonary position.

The advantages of the use of an autograft is given by several factors, i.e. excellent hemodynamic properties, resistance to infection, no anti-coagulation therapy and importantly, the possibility of pulmonary valve adaptation with the growth of the patient. This is particularly advantageous for paediatric patients. However, the main disadvantage is represented by the surgical need to perform two valve operations to treat a single diseased valve (69).

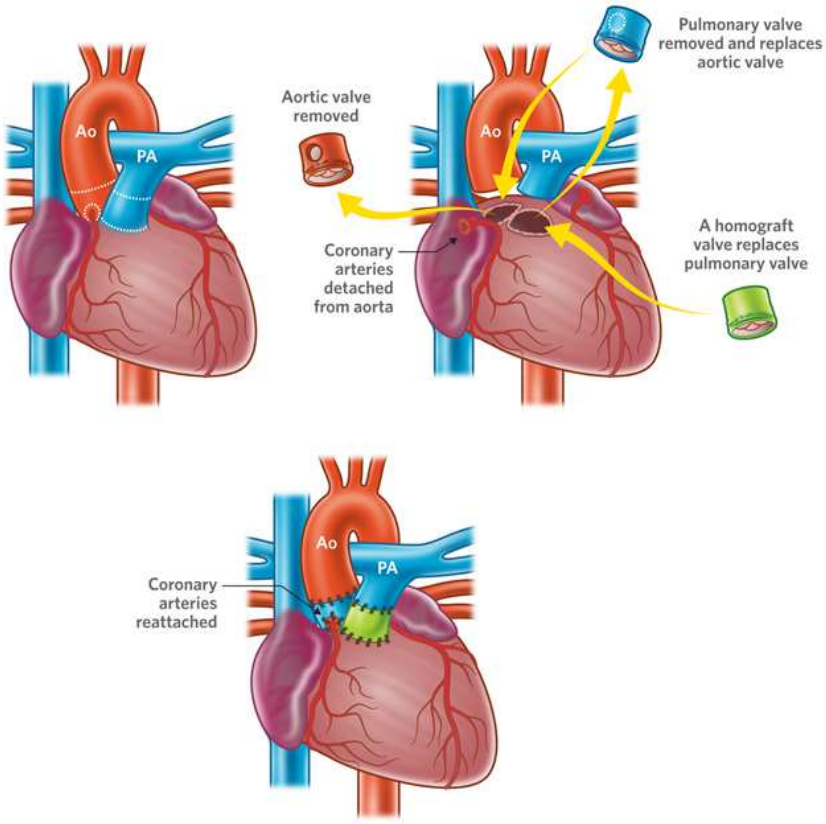

Figure 1-20 Ross procedure for autograft valves. From (69)

1.4 Percutaneous heart valves / Transcatheter heart valves

Transcatheter aortic valve implantation (TAVI) is a technology, in which valve mounted on a stent frame is implanted using minimally invasive technique through a catheter-based delivery system. The remarkable feature of TAVI is that it avoids the need to perform open-heart surgery for HVR. The valve prostheses used during TAVI procedure are called percutaneous heart valves (PHVs) or transcatheter heart valves (THVs). The first study of PHVs on animals was carried out by Anderson *et al* (1992), using a porcine aortic valve (70). The stent consisted of two wires folded about 15 times, with three of the folds higher than the rest to accommodate the commissures of the valve (Figure 1-21). Anderson used a retrograde transaortic approach to implant this hand-made device in nine pigs. Hemodynamic assessment showed low pressure gradients and trivial paravalvular regurgitation. However, coronary flow reduction was observed in one-third of cases.

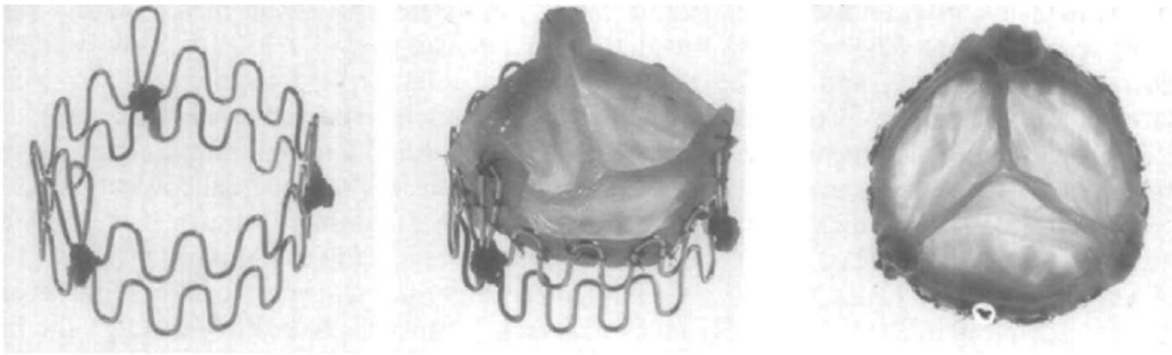

Figure 1-21 One of the first PHV showing the stent and the valve fabricated with porcine aortic valve. From (70)

In 2000, Bonhoeffer *et al* reported the feasibility of delivering a valve, fabricated by mounting bovine jugular vein within an expandable stent, inside the native pulmonary valve of lambs (71). Later, this group performed the first successful in human percutaneous replacement of a pulmonary valve onto a right ventricle to pulmonary artery prosthetic conduit (72). Although today the TAVI procedure follows the concept first pioneered by Anderson, a further decade was necessary to improve and ultimately translate the technique into clinical practice. In 2002, Cribier *et al.* performed the pioneering TAVI procedure using an antegrade trans-venous approach (73). The valve consisted of equine pericardium sewn inside a balloon-expandable metal stent. Unfortunately, the technical complexity and the risks associated with the trans-venous approach limited its widespread application and was rapidly abandoned in favour of the retrograde trans-femoral procedure, which is technically a more feasible and reliable approach.

Nowadays, a number of valves and delivery systems have been developed by several companies for TAVI. Some have been more widely used while others are investigational. These PHVs can be classified as first and second generation. The first generation PHVs could not be retrieved or repositioned once deployed. As such with the first generation PHVs, there were high chances that correct valvular alignment and positioning might not be attained, leading to incidence of paravalvular leakage and obstruction of the coronary ostia. Furthermore, it could result in other complications such as stent migration, fracture and mitral regurgitation (74). In order to address these issues, the second generation of PHVs has been developed by various companies. These improved PHVs can be fully retrieved and repositioned in cases where the valve

has been deployed in a suboptimal position. The following paragraphs describe some of the notable PHV devices.

Edwards Lifesciences Sapien valves

The PHVs used in the studies by Cribier *et al.* (2002) were acquired by Edwards Lifesciences and became known as the Cribier-Edwards valve. Since then, this PHV underwent several design changes. First, the equine pericardium was replaced with the more durable bovine pericardium to develop the Edwards SAPIEN valve. In November 2011, the Edwards SAPIEN valve became the first transcatheter aortic valve approved by the FDA for implantation in the United States. In addition to this initial design, Edwards Lifesciences developed other Sapien Valve versions, which include the SAPIEN XT and SAPIEN 3 (75). All of these bioprostheses were manufactured from bovine pericardium sutured onto a balloon-expandable stent frame. They possessed no capability to be repositioned and retrieved. Several differences exist between the SAPIEN iterations including the use of different stent materials. The SAPIEN valve was based on a stainless steel stent, which was replaced with a cobalt chromium alloy stent in the SAPIEN XT and SAPIEN 3 (76). Additionally, in SAPIEN XT and SAPIEN 3, the cusps adapted a scalloped shape, reducing the delivery profile of the valve (Figure 1-22).

a. b. c.

Figure 1-22 Edwards Lifesciences PHVs: (a) SAPIEN Valve (b) SAPIEN XT (c) SAPIEN3. From (75)

The SAPIEN 3, the most recent in the SAPIEN series, has several features to improve its functionality. The stent geometry has four rows and columns between each

commissure for high radial strength, wide strut angles for reduced crimp profile, small cells on inflow side to adjust outer skirt and large cells on outflow side for coronary access (Figure 1-23). The SAPIEN 3 design includes commissure windows: it is different than the commissural post from previous SAPIEN valves and helps to reduce frame material. The valves also incorporates an external polymer skirt for reducing paravalvular leak. Each valve comes in multiple sizes, with the SAPIEN being available in 23 and 26 mm sizes, while the SAPIEN XT and SAPIEN 3, also in 29 mm sizes.

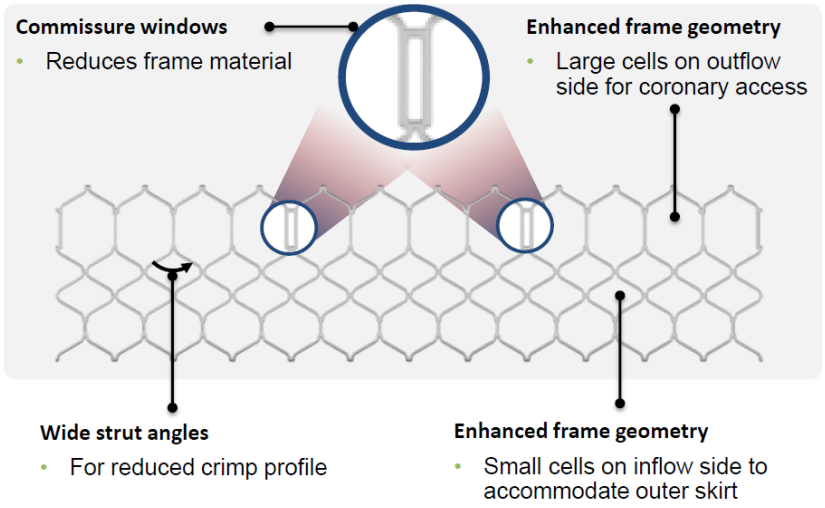

Figure 1-23 Architecture of SAPIEN 3 stent. From (77)

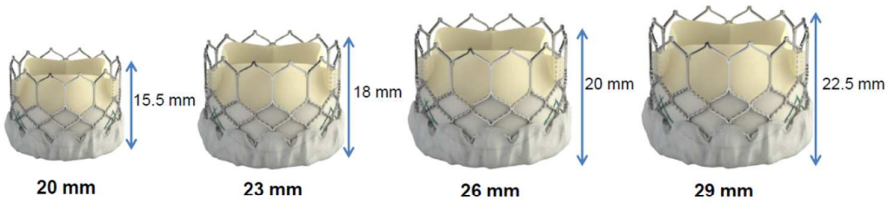

SAPIEN 3 Valve size	20 mm	23 mm	26 mm	29 mm
Crimped Height	21 mm	24.5 mm	27 mm	31 mm
Expanded Height	15.5 mm	18 mm	20 mm	22.5 mm
Foreshortening	5.5 mm	6.5 mm	7 mm	8.5 mm

Figure 1-24 The SAPIEN 3 valve is available in four sizes: 20, 23, 26 and 29 mm. This figure shows the specific dimensions related to SAPIEN 3, demonstrating that this PHV undergoes foreshortening when expanded. From (77)

Medtronic CoreValve series

The CoreValve was developed by Medtronic Inc. It was the second PHV approved for use in the United States by the FDA. The CoreValve is composed of self-expanding Nitinol frame while the cusps are constructed of glutaraldehyde-treated porcine pericardium. This PHV has a conforming frame and a sealing skirt with the aim to minimise paravalvular leak (78).

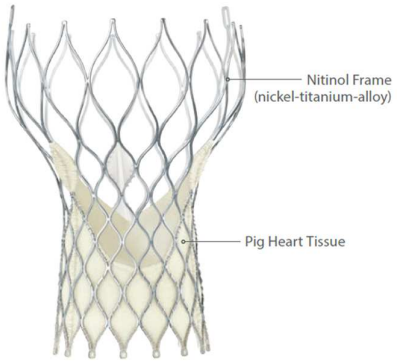

Figure 1-25 The Medtronic CoreValve. From (78)

The latest generation of PHVs from Medtronic is the Evolut R, which follows on the foundation of the CoreValve.

The main design focus of this PHV was to improve annular sealing and reduce paravalvular leakage. The outflow has been shortened and redesigned to provide improved alignment with the native sinus and less stress on the LVOT. The Evolut R (26 and 29 mm) has extended skirt at inflow and scalloped design for enhanced sealing (Figure 1-26). It also has consistent radial force (inflow) across the operating range.

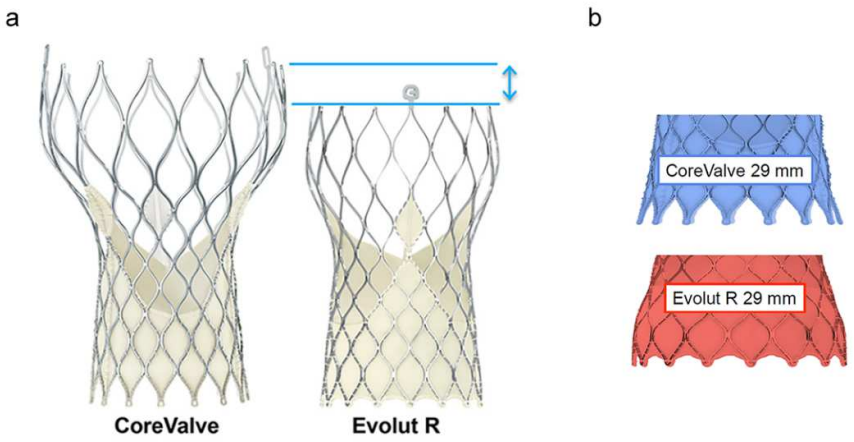

Figure 1-26 Design improvements in Evolut R with respect to CoreValve. From (79)

The Evolut R is currently available in three sizes: 23, 26, and 29 mm. The Evolut R 34 mm is still under clinical trial.

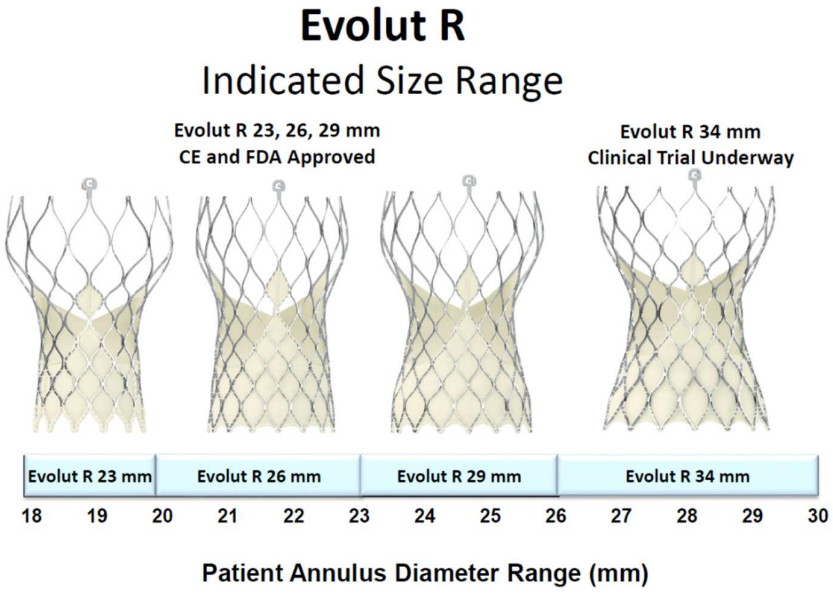

Figure 1-27 Size ranges of Evolut R. From (79)

Symetis ACURATE

Symetis has two versions of PHVs: ACURATE TA and ACURATE neo TF. The ACURATE TA is a transapical prosthesis (Figure 1-28). It is composed of three elements: a self-expanding nitinol stent, a valve made of three non-coronary native porcine cusps and a polyethylene terephthalate (PET) skirt, sutured onto the inner and the outer surfaces of the nitinol stent (80). The ACURATE TA is optimised for an antegrade transapical implantation. The stent frame architecture features three

segments with different functions. Stabilisation arches at the distal segment support coaxial alignment and prevent tilting of the device. The middle segment is composed of an upper crown creating the distal portion of an hourglass-shaped stent waist. The upper crown provides hooks into the native aortic valve and generates a tactile feedback sensation. The upper crown also stabilises the stent during delivery in the supra-annular position. The proximal segment with its lower crown completes the lower part of the stent waist and together with the upper crown wedges the native aortic annulus. During the deployment, the lower crown – when fully released – defines the final position and axial alignment of the stent. The prosthesis, when implanted, compresses native calcified cusps tissue in between the “upper crown” and the annular level. The balanced stent geometry limits protrusion into the LV outflow tract in order to reduce the risk of conduction disturbance. Three different sizes are commercially offered allowing for the treatment of patients presenting an annulus diameter (AD) ranging from 20 mm up to 27 mm. The valves are accordingly labelled as small (S: AD 20-23 mm), medium (M: AD 23-25mm) and large (L: AD 25-27 mm).

Figure 1-28 Symetis ACURATE TA valve. From (81)

The ACURATE *neo* TF is the transfermoral TAVI system of Symetis. It is based on the same self-seating, self-sealing design and stepped deployment concept as the ACURATE TA system. ACURATE *neo* TF is also composed of a self-expanding nitinol stent with an architecture similar to that of ACURATE TA. However, differently from ACURATE TA, the cusps of *neo* TF are composed of a porcine pericardial tissue. Also, the skirt on the outer and inner surfaces of the stent body is constructed with pericardial tissue (Figure 1-29). The ACURATE *neo* is available in three sizes (S, M, L) and its delivery system has an outer diameter of 18F.

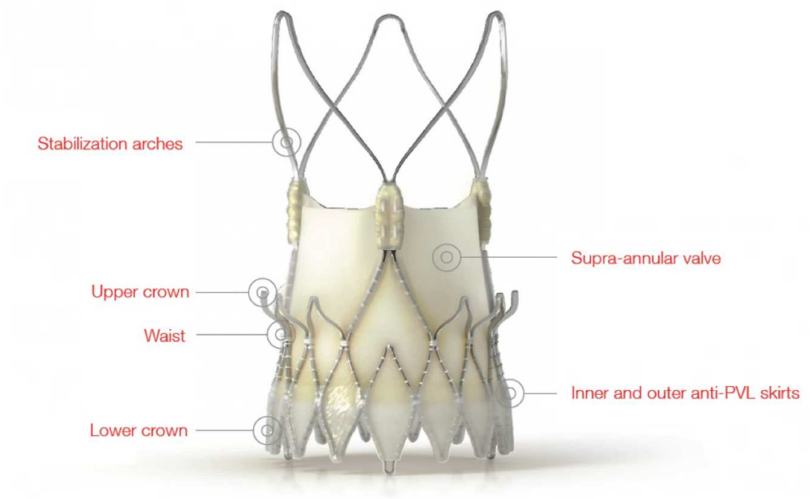

Figure 1-29 Symetis ACURATE *neo* TF. From (82)

Boston scientific Lotus valve

The Lotus Valve System from Boston Scientific is a transcatheter valve model that was designed to be fully repositionable and retrievable (Figure 1-30). This PHV is comprised of a unique braided Nitinol frame along with a central radiopaque position marker, while the cusps are realised in bovine pericardium. The Lotus Valve System includes a controlled mechanical expansion, which allows for precise placement. If necessary, it can be repositioned even at 100% deployment (83).

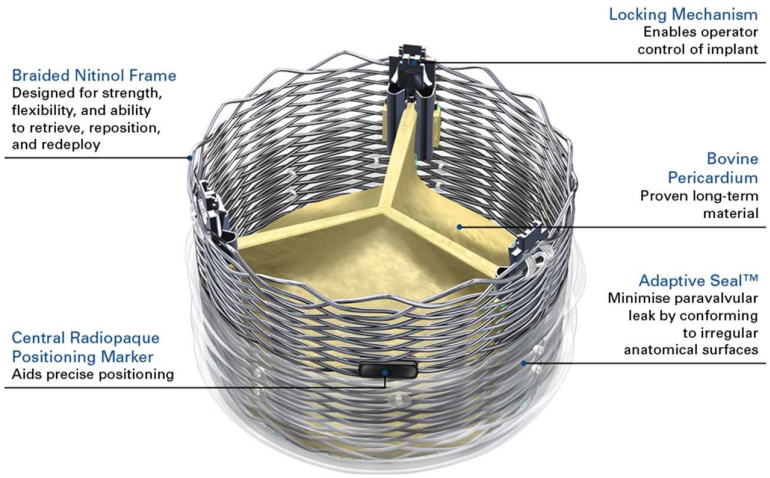

Figure 1-30 The Boston Scientific Lotus valve. From (83)

Direct Flow Medical Valve

Direct Flow Medical developed a very unique valve that contains no metal in the valve frame and is fully repositionable. The Direct Flow Medical TAVI system can be fully deployed and undergo full hemodynamic assessment before final implantation. The

valve comprises bovine pericardial cusps with an expandable Dacron polyester double ring design. The upper and lower ring balloons are interconnected by a tubular bridging system (Figure 1-31). Initially during deployment, the rings are filled with contrast media and saline. Once the optimal position is obtained, a polymer is infused into the PHV replacing the contrast and saline. The polymer then solidifies and the device is no longer retrievable (84).

Figure 1-31 The Direct Flow medical valve. Adapted from (84)

Jena Valve

Jena Valve Technology has developed its version of a PHV valve: the prosthesis comprises of a Nitinol self-expanding stent with porcine root, valve sewn onto it, and a porcine pericardial patch, which functions as a skirt. The unique feature of the JenaValve is the anchoring mechanism, which has 'feelers' that sit in the sinuses of the native valve and thus secures the implant at the site (Figure 1-32). This mechanism of placement ensures that the valve is firmly implanted using active fixation, which is independent of the level of calcification of the native aortic valve. This mechanism of implantation allows the JenaValve to be efficacious in the treatment of severe aortic regurgitation in addition to aortic stenosis. A weak point of the JenaValve is the fact that the delivery system is very large (85). The porcine root determines the french size (32 Fr delivery system for transapical route). The CE mark for this system has not been extended after June 2016.

Figure 1-32 The Jena Valve. Adapted from (85)

Jena Valve Technology is now pursuing its next version of Jena Valve based on porcine pericardium and improved stent frame (Figure 1-33). This system is designed for both transapical and transfemoral implantation routes and it is currently under clinical investigation.

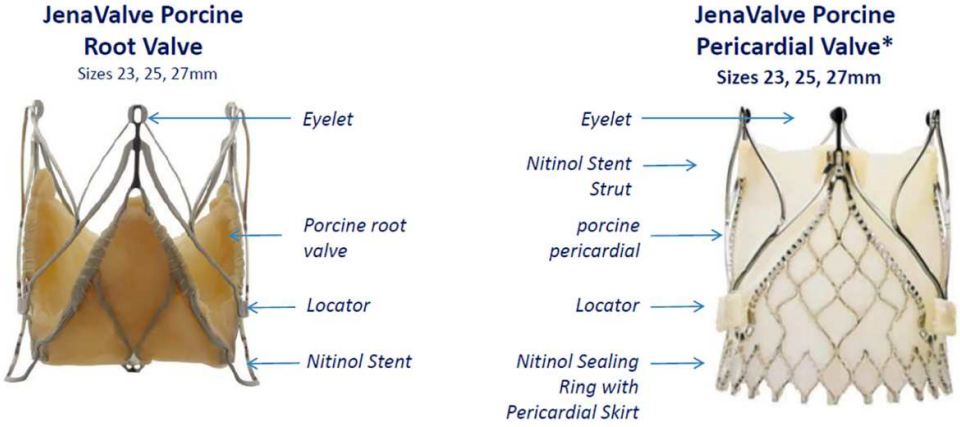

Figure 1-33 A comparison between two versions of Jena Valve. From (86)

Medtronic Engager

Engager was the second product line of Medtronic. It possesses a self-expanding Nitinol frame, a polyester skirt and bovine pericardial cusps. The novelty of this valve is the presence of three control arms, which both guide the operator with tactile feedback and secure the valve during deployment (87).

Figure 1-34 The Medtronic Engager Valve. From (87)

St. Jude Medical Portico

St. Jude Medical developed the Portico valve. It consists of a self-expanding Nitinol stent with bovine pericardial cusps. The valve can be fully repositionable and retrievable *in situ* until fully deployed (88). The size of the valve is 23 mm and is delivered by a 18Fr catheter. The peculiarity of the delivery system is its capability to taper down to 13Fr diameter at the proximal end (89).

Figure 1-35 The St. Jude Portico valve. From (88)

1.4.1 Pericardium as material for PHV cusps

Currently marketed PHVs are prepared from both bovine and porcine pericardia, mainly due to their availability and the rigorous quality control related to intensive battery farming (90). Selecting the most suitable pericardium from animal origin to manufacture PHV requires a detailed comparison of the morphology, biocompatibility and the mechanical characteristics of the pericardium. Table 1-1 gives an overview of the current commercial PHVs and the type of pericardium used in them.

Table 1-1 Commercial PHVs and their cusp material.

Company	Valve name	Cusp material
Edwards Lifesciences	Edwards SAPIEN 3	Bovine Pericardium
Boston Scientific	Lotus Valve	Bovine Pericardium
St. Jude Medical	Portico	Bovine Pericardium
Direct Flow Medical	Direct Flow	Bovine Pericardium
Medtronic	CoreValve	Porcine Pericardium
Symetis	ACURATE neo	Porcine Pericardium
JenaValve Technology	JenaValve TAVR System	Porcine Pericardium

Gauvin *et al.* performed a comparative study of bovine and porcine pericardia, as the most widely used for clinically implantable PHVs. They examined glutaraldehyde-fixed bovine and porcine pericardia by means of histology, scanning and transmission electron microscopy. The mechanical properties of the pericardia were characterised with uniaxial tensile testing. They reported that the fibrocollagenous side is always selected by the valve manufacturers as the inflow and the serous side as the outflow (Figure 1-36). Histologically, as observed under light microscopy, the architecture of the two pericardia were very similar consisting of multiple layers of collagen bundles with some degree of fiber orientation. The *serosa* side had oriented collagen structure while the fibrous side showed poorly aligned and assembled collagen bundles (90). Elastic fibers, nerves, blood and lymphatic vessels were occasionally observed. The morphologies of the serous side of both bovine and porcine pericardia were slightly different as the waviness was more easily recognisable for porcine tissues. In fibrous pericardium, the fibrinocollagenous structure was externally covered by a thin and loose connective tissue layer, for which collagen bundles were oriented in multiple directions. The external surface showed different morphologies according to its adaptation to the various sites of attachment of the pericardium to the surrounding structures. The bovine pericardium showed more loose bundles of collagen than the porcine one. The fibrous surface also incorporated various amounts of blood vessels (capillaries, arterioles) and nerves, depending on the site of harvesting of the pericardium.

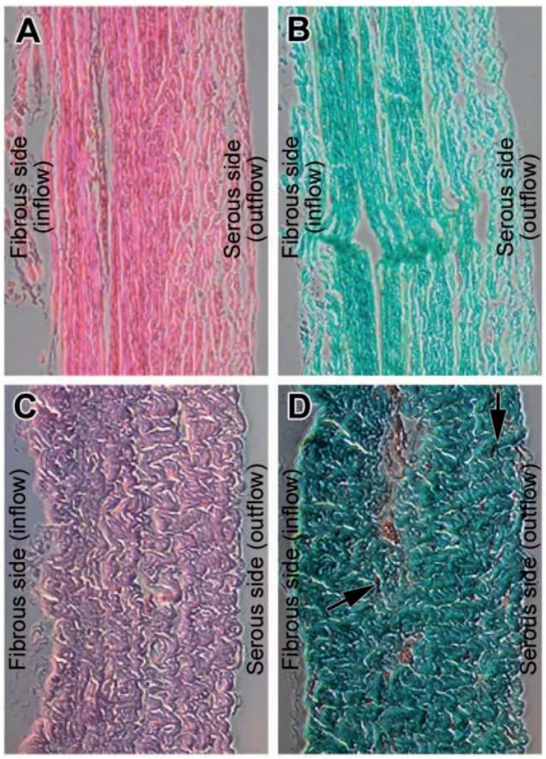

Figure 1-36 Histology of bovine (A, B) and porcine (C, D) pericardia. The sections were stained with hematoxylin-eosin (A, C), Masson's trichrome (B) and Verhoff staining (D). From (90)

Ultimate tensile strength (UTS) and modulus measurement showed that bovine pericardium had significantly higher mechanical strength when compared to porcine pericardium. Tissue morphology analysis showed a preferential alignment of the ECM fibers in both pericardia, suggesting an anisotropic tissue structure. This was confirmed through mechanical testing, as UTS and modulus measured perpendicular to the ECM fibers were significantly lower than the same parameters measured parallel to the ECM fibers.

In terms of thickness, porcine pericardial tissues have approximately half the thickness of bovine ones. One of the study highlighted that this minimal tissue thickness leads to substantial ‘space saving’ for porcine pericardium in the folded configuration, while yielding identical or superior density, elasticity consistency, flexibility, cellular structure and tissue strength characteristics (91). Through magnified imagery, it has been shown that bending induces less buckling in the porcine pericardium than in the bovine counterpart (Figure 1-37).

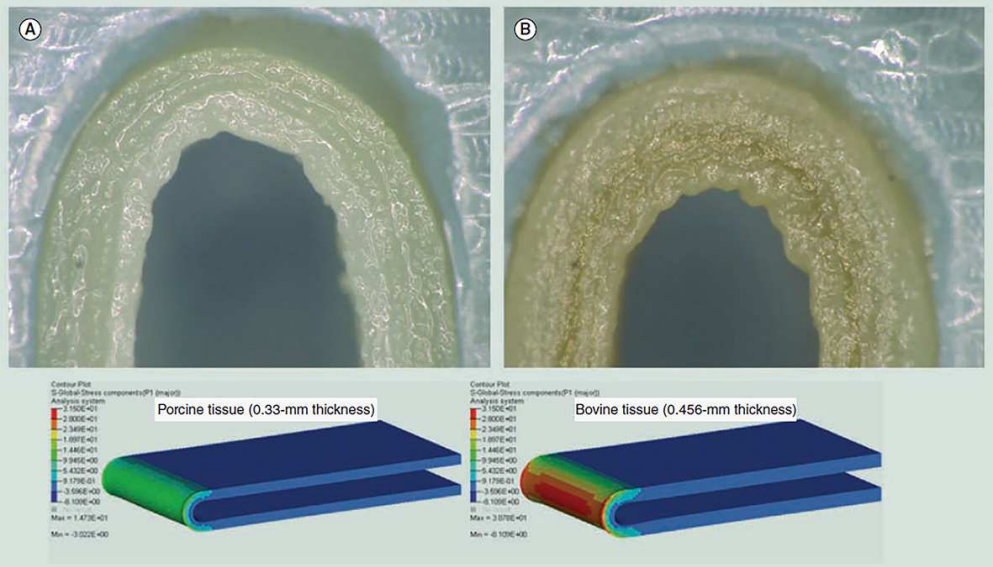

Figure 1-37 Magnified imagery and computer simulation showing effects of buckling in bovine and porcine pericardia. Adopted from (91)

These results suggest that the tissue source, as well as its configurations, can influence the mechanical behaviour of the treated pericardium. Therefore, these parameters should be taken into consideration in the selection and fabrication of prosthetic heart valves.

1.5 Shortcomings of current heart valve substitutes

The currently available mechanical and bioprosthetic heart valves have shown good outcomes and are able to improve the life quality of HVD-suffering patients. However, both of these valve prostheses have limitations. Within 10-15 years after implantation, prosthesis-related defects render necessary to perform reoperation or cause death in at least 50-60% of treated patients (58). The overall complication rates are similar for mechanical and bioprosthetic heart valves, however the frequency and nature of specific valve-related complications may vary with the prosthesis type, model, site of implantation, and patient characteristics (such as age and activity level). The mechanical and bioprosthetic valves do differ in their major causes of failure.

In particular, the mechanical valves are associated with the risk of systemic thromboembolism mainly due to the artificial materials that they employ, and the flow abnormalities generated by the rigid occluders. To minimise this risk, patients are subjected to life-long anticoagulation, which renders them susceptible to potentially

serious haemorrhagic complications. Such a risk constitutes the main disadvantage of mechanical heart valves (58).

The major drawback of BHVs is time-related valve dysfunction leading to regurgitation or stenosis. The pathology and failure mode of BHVs can be influenced by mainly three factors: 1) host metabolic pathways; 2) bioprosthesis engineering and chemistry (e.g. cusp suturing material, stent post flexibility, prosthesis fabric covering, cusp fixation process); and 3) mechanical loading effects (e.g. cusp flexural stress/strain) (92).

The failure modes of bioprosthetic valve failure can be divided into two categories: structural and non-structural degeneration (93). Structural valve degeneration includes intrinsic permanent changes of the prosthetic valve, such as calcification, cusp fibrosis, cusp tear (Figure 1-38), stent fracture and disruption of the seams holding the valve tissue together or the valve tissue to the stent. Non-structural degeneration refers to any abnormality not intrinsic to the prosthetic valve itself, such as cusps thrombosis, endocarditis, pannus ingrowth, patient-prosthetic mismatch and intra- or para-prosthetic regurgitation (Figure 1-39) (94).

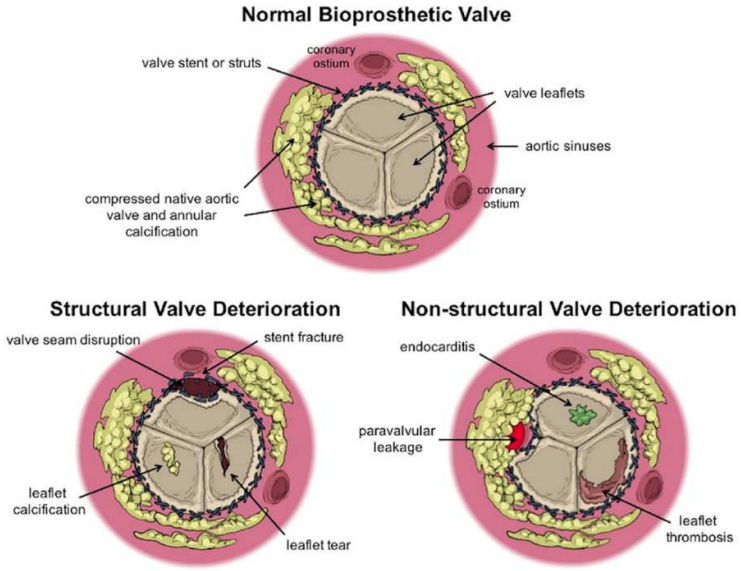

Figure 1-38 Degeneration of bioprosthetic heart valves. From (93)

As stated before, glutaraldehyde fixation of BHV is intended to promote tissue durability by creating stable cross-links between the collagen fibres and to render the xenograft material immunologically inert. However, residual glutaraldehyde-derived

polymers may serve as calcium-binding sites that promote calcium-phosphate deposits. Phospholipids debris released from cell membranes, phosphates from free nucleic acids and mitochondria of dead cells act as source of calcium-binding sites (10). It has also been reported that calcific deposits mainly develop in areas, where cusp flexion and stress are greatest, that is at the basal and commissural attachment points (95).

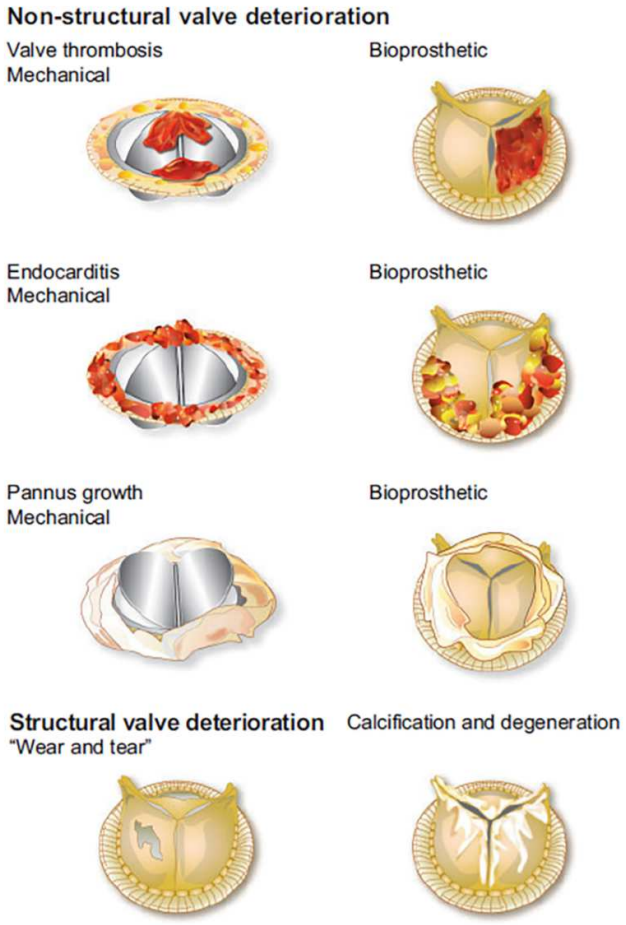

Figure 1-39 Examples of structural and non-structural valve deterioration of current heart valve replacements. From (96)

Pannus ingrowth occurs at the host tissue-prosthesis interface and is result of recipient's response to foreign material/tissue. In early stages, pannus is composed of myofibroblasts, fibroblasts, and capillary endothelial cells. Later, an evolution towards calcification may also occur. Some pannus formation over the suture is normal, as it functions to serve as non-thrombogenic surface. However, when it extends to cusps, it could lead to their stiffening and dysfunction. Figure 1-40 depicts some failed BHVs.

Degenerations similar to BHVs could be hypothesised for PHVs, since the cusps for both are prepared from the same technology. There have already been same cases reported that indicate similar fates for implanted PHVs (Figure 1-41).

Figure 1-40 Pathological specimens showing the most common reasons for bioprosthetic valve failure: (a) Wear and tear; (b) calcific degeneration; (c) pannus; (d) endocarditis; (e) thrombus. From (92)

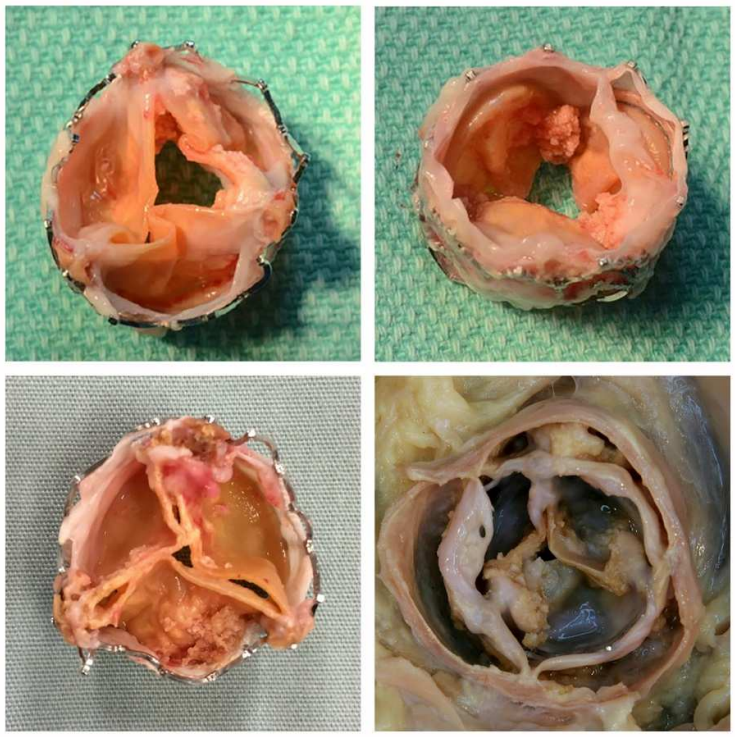

Figure 1-41 Reports of degeneration in PHVs. From (97)

1.6 Heart valve regenerative medicine

In order to address these problems associated with the current valve replacements, there have been considerable attempts to tissue engineer a heart valve. Heart valve regenerative medicine (HVRM) aims to develop a permanent solution for replacement

treatment by biologically engineering a durable living and functional alternative with the capacity to grow, repair and remodel itself (98). This novel valve would be also an ideal solution for the large number of congenital valvular abnormalities in paediatric patients and young adults, for whom currently available valves are poorly suited.

The fundamental principle of regenerative medicine is to combine a suitable scaffold, formed into the shape of the heart valve, onto which appropriate cell repopulation is achieved *in vitro* or *in vivo*, thus transforming it into a viable valve prosthesis.

1.6.1 Scaffolds for HVRM

The initial point for regenerative medicine approach is a starter matrix called scaffolds. Various scaffold materials have been developed and researched for HVRM (Figure 1-42). These scaffolds can be grouped into two broad categories: decellularised native tissue scaffolds and artificial scaffolds fabricated from synthetic or natural polymers (99).

Decellularised scaffolds

Xenogeneic heart valves and pericardium from pigs and cows are the main source of decellularised scaffolds for HVRM. Since xenogeneic cellular antigens induce an immune-mediated rejection of the tissue, decellularisation treatment is applied to render the tissue cell free. The acellular scaffolds thus produced retain the original tissue histoarchitecture and are composed of ECM proteins and molecules, which are generally conserved among species, and hold specific cues for cell attachment, proliferation, and defferentiation.

Allogenic valves, commonly called homografts, have also been used as decellularised scaffolds for HVRM (100, 101). In case of homografts, the endothelium has been considered to behave as antigen presenting cell element to the host's immune system. The presence of human leukocyte antigens (HLA) II has been related to humoral and cellular responses (102). Hence, these theoretically more biocompatible human valve allografts also need to undergo decellularisation, like their xenogeneic counterparts, to render them suitable for HVRM.

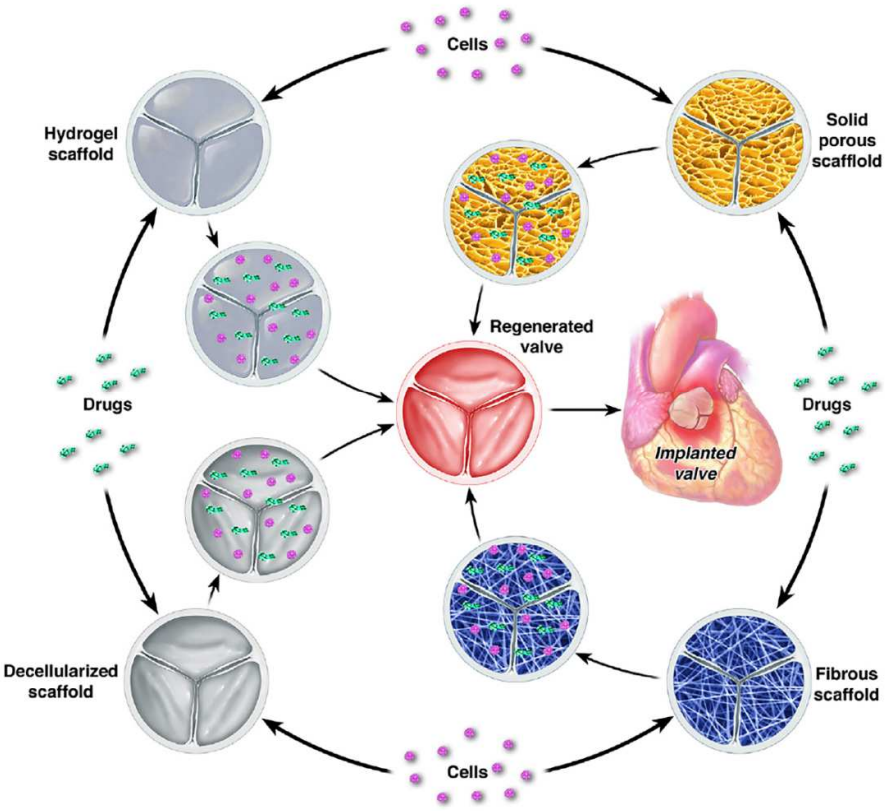

Figure 1-42 Schematic representation of various scaffolds applied for HVRM. From (99)

Polymeric scaffolds

Artificial scaffolds fabricated from synthetic or biological materials, mimicking the structure and function of a heart valve, represent another distinct approach for manufacturing scaffolds for HVRM. An advantage given by the use of these fabricated scaffolds is that their biodegradability, durability, and mechanical properties can be controlled. However, their structure may not completely imitate the complex architecture and function of native tissues.

In general, three types of polymeric scaffolds have been implemented for HVRM: porous scaffolds, fibrous scaffolds, and hydrogels.

Porous 3-D scaffolds with interconnected homogeneous pore network and a large pore size are produced by using natural and synthetic polymeric materials through techniques such as particulate leaching, solvent casting, gas foaming, vacuum drying, melt moulding, high internal phase emulsion and microfabrication (103). The

biomaterial most used to produce solid 3-D scaffolds for HVRM is Polyhydroxyalkanoate (104).

Fibrous materials are another category of scaffolds applied for HVRM. They are created through techniques such as electrospinning, phase separation and self-assembly. They have received greater attention in HVRM since with proper fabrication they have the potential to resemble the structure of native ECM. Fibrous scaffolds are superior to non-fibrous ones in terms of cell adhesion, migration, proliferation, and differentiation. Fibers also have the capability to be loaded with growth factors, which can then be released to specific sites of application. Nanofibrous scaffolds made from polyglycolic acid (PGA) are mostly used for HVRM. Several investigators have moulded PGA meshes into valve-shaped scaffolds by applying polyhydroxibutyrate (P4HB), a homopolymer that has lower degradation rate compared to PGA (105).

Hydrogel scaffolds are synthesised by crosslinking hydrophilic homopolymers, copolymers or macromers through free radical polymerisation or conjugate addition reaction. Poly(vinyl alcohol) (PVA), polyethyleneglycol (PEG) and polyacrylates, such as poly(2-hydroxyethyl methacrylate), are some synthetic monomers used to prepare hydrogels. Biologic hydrogels are formed from collagen, fibrin, hyaluronic acid, alginate or chitosan. The polymer chains in a hydrogel mimic the structure of proteins and other biomolecule chains within the ECM, thus cell encapsulation within hydrogel scaffolds is a standard technique for tissue engineering. PEG-based hydrogels were used as seeding media for bone marrow mesenchymal stromal cells in decellularised porcine aortic valves to improve cell attachment (106). A modified PEG hydrogel – polyethylene glycol diacrylate (PEGDA) - was used to fabricate a sandwiched three-layer construct, with the mechanical anisotropic properties similar to the ones exhibited by the native heart valve cusp. The sandwich remained intact under simulated flow and pressure conditions (107).

1.6.2 *In vitro* tissue engineering

In regard to repopulating the scaffolds with cells, two main approaches are pursued in HVRM: *in vitro* tissue engineering and *in vivo* tissue guided regeneration.

In vitro tissue engineering is the conventional concept, in which scaffolds are seeded with cells prior to implantation. In this approach, cells are ideally harvested from the

patient and expanded to obtain a sufficiently large number of cells for seeding the scaffolds.

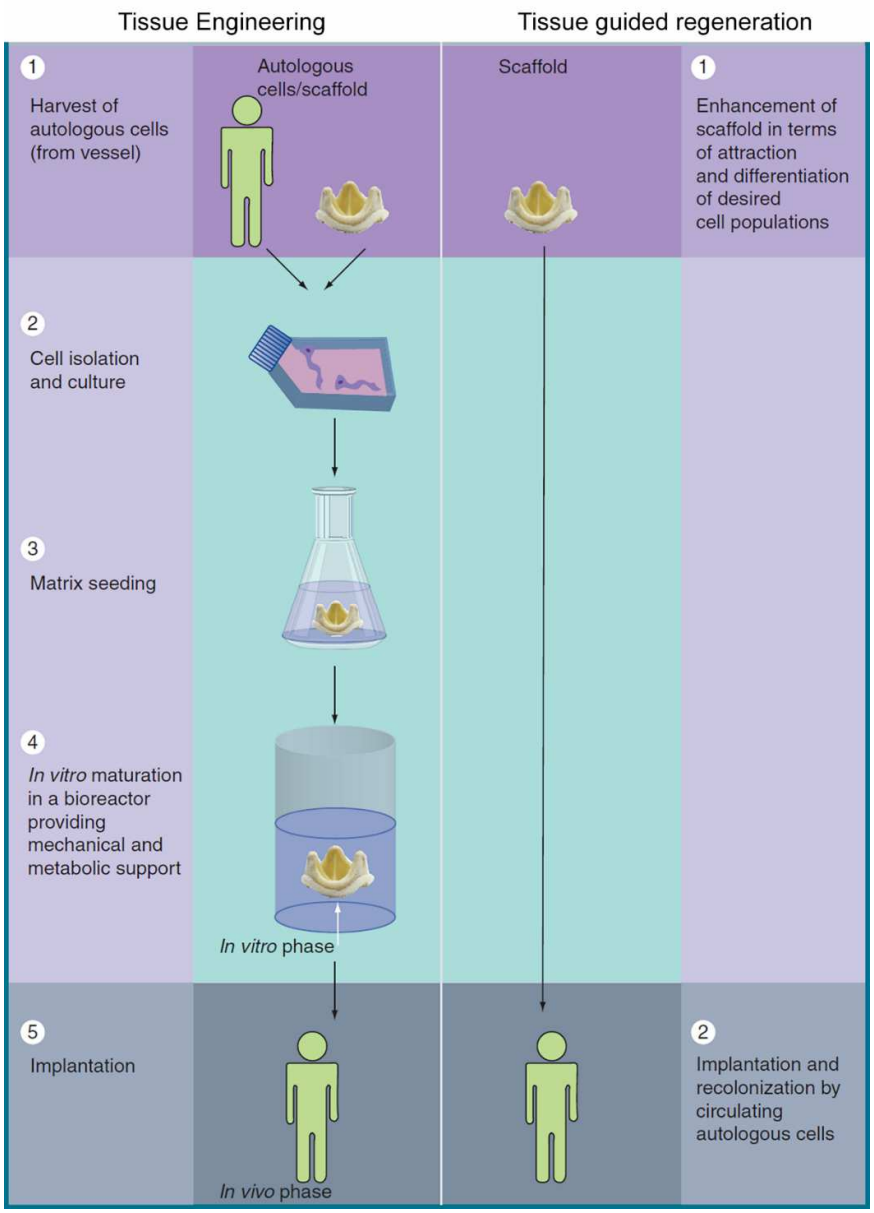

Figure 1-43 Concepts of *in vitro* tissue engineering and *in vivo* tissue guided regeneration applied to HVRM. From (108)

Cells are added to the scaffolds inside a bioreactor, in which the construct is subjected to necessary biochemical and mechanical stimuli. This *in vitro* conditioning is important to induce production of ECM components to create a valve that has sufficient strength to meet *in vivo* hemodynamics once implanted. A large variety of cell types have been investigated for *in vitro* seeding of heart valve scaffolds. Vascular-derived myofibroblasts and endothelial cells, harvested from recipient's saphenous vein, are

one common option because of their ECM production ability (109). Alternative sources are progenitor cells derived from bone marrow, adipose tissue or umbilical cord blood, and circulating endothelial progenitor cells, all of which have shown good potential for *in vitro* heart valve tissue engineering (110). Bone marrow-derived mesenchymal stem cells (MSCs) have been used to seed decellularised matrices showing their ability to differentiate into endothelial cells, fibroblasts or myofibroblasts, and smooth muscle cells (33). In addition to supporting proliferation, differentiation, and ECM production *ex vivo*, MSCs can induce homing and differentiation of autologous host cells through paracrine signalling (111).

Emmert et al. demonstrated the feasibility of a transcatheter, stem cell-based tissue engineered heart valves (TEHV) (Figure 1-44). They constructed trileaflet heart valve scaffolds from non-woven polyglycolic-acid meshes coated with 1.75% poly-4-hydroxybutyrate. The scaffold was seeded with autologous bone marrow mononuclear cells and the TEHVs were crimped and transapically delivered into adult sheep (112). However, 8 weeks post implantation, the line of attachment of leaflets to the wall moved upward with time leading to reduction of leaflet size. Such retraction effect has been one of the main bottle necks holding back the progress of TEHVs based on polymers (113).

The idea of *in vitro* tissue engineering, though promising, has lots of hurdles for successful translation from the preclinical large animal setups to the clinical arena. The first real problem is the difficulty to attain a mature heart valve substitute from an artificial starting matrix. It is important that the scaffolds have proper biomechanical properties. Until now *in vitro* tissue engineering has largely focused on collagen formation to increase the mechanical strength of the valves. However, generation of elastin during *in vitro* condition has been quite challenging (114). This issue need to be properly addressed for increasing the acceptability of artificial scaffolds utilised for *in vitro* tissue engineering.

Another hurdle is the risk of contamination during *in vitro* tissue culture phase (which could take up to 6 weeks from cell harvest to implantation): the potential production facility will have to follow good manufacturing practice standards. Moreover, the extremely time-consuming process would require a challenging infrastructure and enormous costs. These complexities have resulted in a reluctance of all major heart valve manufacturers to invest in the concept of *in vitro* tissue engineering. As a

consequence, HVRM has seen a paradigm shift to the alternative concept of *in vivo* tissue guided regeneration.

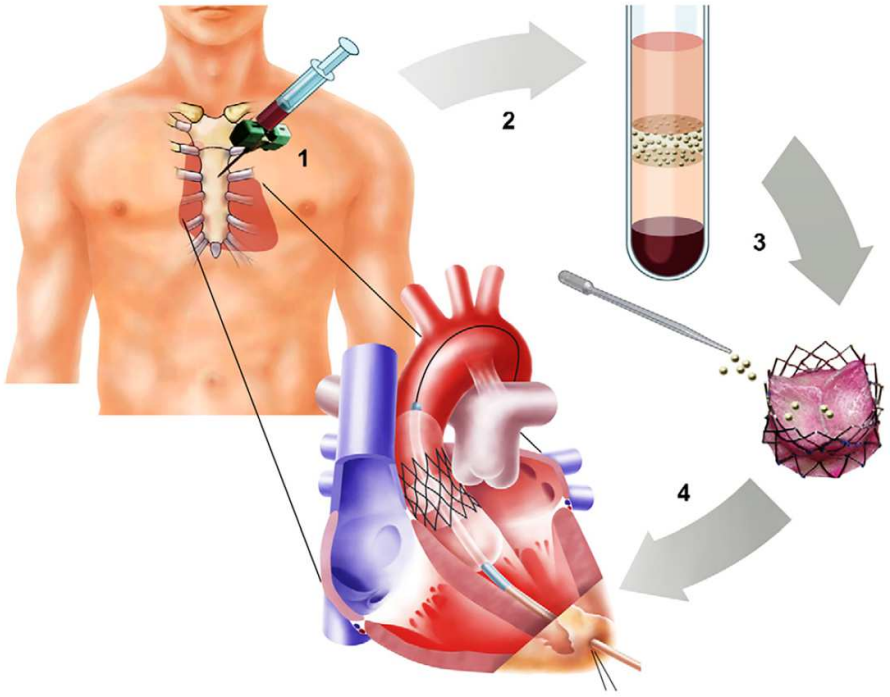

Figure 1-44 Concept of *in vitro* tissue engineering applied to PHVs. From (112)

1.6.3 *In vivo* tissue guided regeneration

In vivo tissue guided regeneration utilises the natural regenerative potential of human body for repopulation of an implanted heart valve scaffold and avoids all cell and tissue culture steps (108). The objective is thus to implant off-the-shelf heart valve scaffolds without any cell seeding prior to implantation.

Various cell populations could contribute to repopulation *in vivo*. In general, it can be hypothesised that the process of cell recruitment will comprise a range of pathophysiological reactions. Recellularisation may involve adhesion of circulating progenitor cells to the luminal surface of the graft in combination with stromal cells migrating from the periadventitial granulation tissue or across the anastomosis site. The large majority of the approaches focused on attracting EPCs circulating in the patient's bloodstream to the surface of heart valve implants. These EPCs possess the ability to differentiate into mature endothelial cells, form mature endothelium and could also transdifferentiate into smooth muscle cells (SMC) upon endothelial-mesenchymal

transition (115). These cells might establish an autologous endothelial cell layer on the surface of the heart valves, achieving a nonthrombogenic blood-tissue interface.

The scaffolds intended for tissue guided regeneration might also undergo specific modifications and surface engineering to prepare them for *in vivo* repopulation. Aptamers, which are single-stranded DNA or RNA molecules folded into 3D structures, combined with star-polyethyleneglycol coating, have been investigated as a promising technique for homing EPCs to graft surfaces (116).

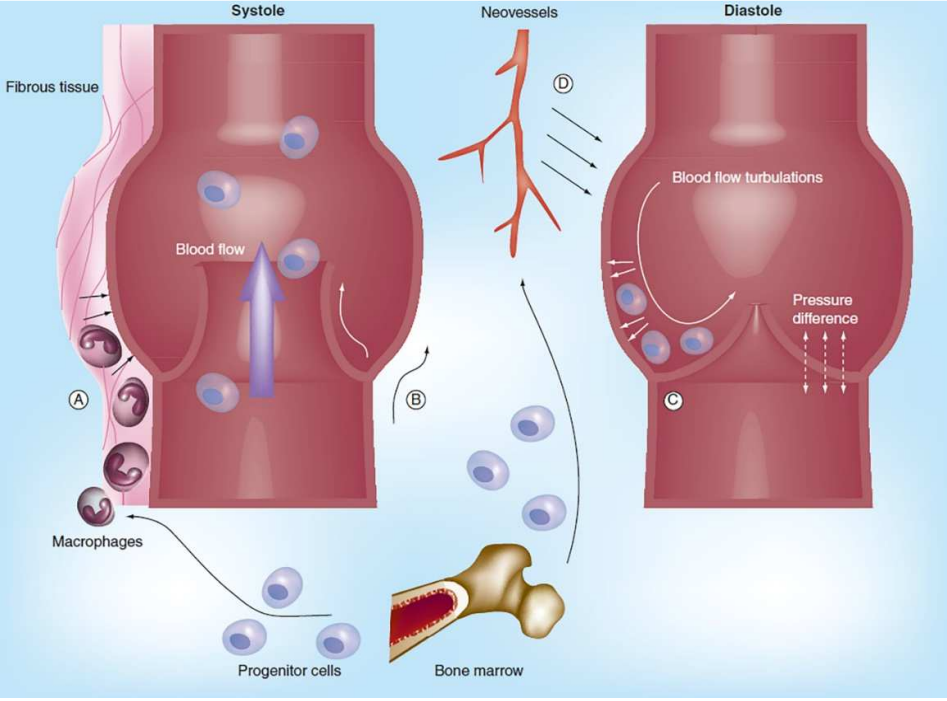

Figure 1-45 Possible cell recruitment process for *in vivo* tissue guided regeneration: (A) Foreign body response, primitive cell types migrate from fibrous tissue encapsulating the implant; (B) Cell in-growth of valve-specific cells from native tissue across the anastomoses; (C) Progenitor cells from blood stream; (D) Circulating progenitor cells recruited from the bone marrow are homed to the implant valve through new vessels. From (114)

These combined effects of natural wound healing response and foreign body reaction holds great promise for the recellularisation potential of heart valve scaffolds (Figure 1-45), confirming to the concept of guided tissue regeneration (114).

Decellularised xenografts or homografts are the most attractive candidates as scaffolds material for guided tissue regeneration of heart valves. Unlike the products of *in vitro* tissue engineering, the scaffolds for tissue guided HVRM have already been translated into clinical use.

CryoLife Inc. (Georgia, USA) has been one of the pioneers in the field of heart valve tissue guided regeneration. Based on patented decellularisation technology, SynerGraft, CryoLife distributed two valve bioprostheses: 500/700 and CryoValve biodevices (117). They suffered an early setback with 500/700 SynerGraft porcine valves, as three out of four paediatric patients receiving the implant died one year post implantation due to hyperacute and acute rejections attributed to xenogeneic ECM (118). However, the other commercial option CryoValve, an allogeneic heart valve substitute, has shown more favourable outcomes. Company data claim that CryoValve has been already implanted in 5,700 patients since 2000 (117). In 2008, the biodevice even received US FDA approval and since then there has been many studies affirming the satisfactory performance of CryoValve (119). A study on the failed SynerGraft disclosed that the failure was due to xenogeneic materials that were not properly removed during decellularisation, which led to such a nightmare for this bioprosthesis (118).

Matrix P, a decellularised porcine pulmonary heart valve, has been another HVRM product with notable clinical applications. Developed and tested by Dohmen and colleagues, Matrix P is commercially distributed by Autotissue Ltd. (Berlin, Germany) (120). Matrix P Plus, a variant of the Matrix P with equine pericardial patch extension, has been conceived for the surgical cases. Both valves received the European CE mark in the 2004-2005. Until now there have been mixed report of success and failures for Matrix P products (121, 122).

In another major development of HVRM, the group of Dr. Haverich (Hannover, Germany) is currently running clinical trials with decellularised fresh human pulmonary and aortic valve allografts (123, 124). Reports from the trials have shown these allogenic valves are characterised by improved freedom from explantation, lower transvalvular gradients, and ability to adaptive growth (100, 125).

In a similar effort, a clinical trial with allogeneic aortic heart valves treated with TRICOL decellularisation technology is now ongoing (126).

1.7 Decellularisation and its application to pericardium

Decellularisation is a modality to render allogenic and xenogeneic matrices immune-privileged and empower them with autologous like regeneration capacity (126). Decellularisation can be defined as a method for producing biological scaffolds

composed of ECM after the removal of all endogenous cell elements including, cell membranes, organelles and nucleic acids, that can prompt adverse inflammatory, immune, and calcific events. The ECM, which is the secreted product of resident cells of any tissue and organ, is generally conserved among species and holds specific cues that affect cell adhesion, proliferation, and differentiation.

1.7.1 Basic principles of decellularisation

The main objective of the decellularisation is to retain the native ultrastructure and composition of ECM while removing the cells. The effectiveness of the agents applied for decellularisation depends upon many factors, such as tissue's cellularity, density, lipid content, and thickness. The chemical agents and methods applied during decellularisation will alter ECM composition and cause some degrees of ultrastructure disruption. Hence, the goal of decellularisation is to minimise these undesirable effects, since complete avoidance would be something ideal to achieve.

Overall, standard decellularisation protocols consist of a multimodal approach starting with the lysis of the cell membrane using either ionic solutions or physical treatments. Subsequently, detergents are used to solubilise the nuclear and cytoplasmic cellular components. At the end of the procedure, all residual cell debris are removed from the remaining ECM. Finally, washing steps are necessary to remove residual chemicals, thus avoiding any host tissue response.

Various chemical, enzymatic agents and physical methods are used for decellularisation (127). Mostly utilised chemical agents include: hypotonic and hypertonic solutions, detergents, and alcohols.

Hypotonic solutions readily cause cell lysis by simple osmotic effects. Hypertonic solutions dissociate DNA from proteins and are also extremely destructive for some proteins, specially those responsible for cell contractility function, by causing their aggregation and misfolding. When used in combination, hypertonic and hypotonic solutions are also able to rinse cell residues from within tissue after lysis.

Detergents are effective in removing cellular material from treated tissues by solubilizing cell membranes and dissociating DNA from proteins. Ionic, non-ionic, and zwitterionic detergents are used for decellularisation. Ionic detergents, such as Sodium dodecyl sulfate (SDS), act strongly on protein-protein interactions and are equally capable of solubilising nuclear membrane (128). Alternatively, other ionic

detergents like sodium cholate do not cause protein denaturation and produce more preservative treatment of ECM (129, 130). Among non-ionic detergents, Triton X-100 is the most widely used and has more delicate mode of action. Triton X-100 mainly targets lipid-lipid and lipid-protein interaction (131). In few cases, zwitterionic detergents, having properties of both ionic and nonionic surfactants, are applied although they generally produce destructive effects (132). The removal of ECM proteins and DNA by detergents increases with exposure time and varies with tissue type and donor age.

Chelating agents such as ethylenediaminetetraacetic acid (EDTA) facilitate cell dissociation from ECM proteins by isolating metal ions and are hence usually added in the initial steps of decellularisation steps to aid the action of subsequent treatments.

Serine protease inhibitors such as phenlymethylsulfonyl fluoride (PMSF) are used to prevent undesirable damage to ECM from the intracellular proteases released during cell lysis. They are normally applied before and during the step that induce cell lysis (12, 132).

Enzymes, are also utilised to disrupt cell-cell binding and proteins, as they provide high specificity for removal of cell residues or undesirable ECM constituents. Enzymes, such as nucleases are mostly used in final step of decellularisation to remove any remnants of nucleic acids released form lysed cells. Nucleases act very efficiently by hydrolysis of the interior or exterior bonds of RNA and DNA chains that generally remain closely attached to the ECM fibers after release in the extracellular space (33). For this purpose, endonucleases are preferred to exonucleases since they cleave nucleotides mid-sequence and are more effective in fragmenting DNA. Trypsin is another commonly used proteolytic enzyme for cleaving the peptide bonds (129).

Alcohols, such as isopropanol, ethanol, and methanol, are applied for removing lipids from treated tissues (12).

Physical processes such as temperature (freeze-thaw process), force and pressure can boost the decellularisation process. Freeze-thaw processing effectively lyses cells within tissues and organs. Multiple freeze-thaw cycles are applied during decellularization and do not significantly increase the loss of ECM proteins from tissue (133). However, freeze-thaw processing does produce minor disruptions of the ECM

ultrastructure and should therefore be used only when such effects are acceptable in the final product (134).

Perfusion and agitation are other physical processes commonly applied for decellularisation. Perfusing a tissue's vascular network has proved to be an efficient approach for decellularisation (135). However, not all tissues have vasculature that allows for straightforward, discrete, complete access and such tissues require other strategies. The most common approach for such tissues is immersion in decellularisation agents while being subjected to agitation. Immersion and agitation methods of tissue decellularisation have been described for a wide variety of tissues, including heart valves, blood vessel, trachea, esophagus and urinary bladder (127). The duration of agitation required for successful decellularisation is a function of the tissue thickness and density, detergent used, and intensity of agitation.

1.7.2 Pericardium decellularisation

Regarding pericardial decellularisation, several protocols have been reported. Courtman et al. proposed the combined use of Triton X-100 and an enzymatic extraction process. After this treatment, the acellular ECM was demonstrated to be composed of collagen, elastin, and glycosaminoglycans while cellular components were removed (136).

Mendoza-Novelo *et al.* performed decellularisation of bovine pericardium with three different protocols and compared them in terms of their effectiveness to extract cellular materials, as well as their effect on GAG content and on tensile biomechanical behavior. The main chemical agents used in three protocols were: Triton X-100, tridecyl polyethoxy ethanol (ATE) and alkaline treatment and subsequent washing with nucleases (DNase/RNase). They reported that the protocols were effective in cell removal. However, GAG content decreased to 61.6 ± 0.6%, 62.7 ± 1.1% and 88.6 ± 0.2% for Triton X-100, ATE and alkaline treatment, respectively. In addition, an alteration in the tissue stress relaxation characteristics was observed after alkaline treatment (137). This indicated that Triton X-100 was the better of the three options.

Other studies have shown that decellularisation of bovine pericardium with SDS causes irreversible denaturation, swelling and decrease in tensile strength compared to the native tissue (138). Conversely, on human pericardial tissue, Mirsadraee *et al.* also applied SDS together with hypotonic buffer, protease inhibitors and nuclease

solution. With this process they showed that glycosaminoglycans and structural proteins, such as collagen, were maintained (139). These contrasting reports suggests the need for more in-depth investigation about appropriate agent for pericardial decellularisation.

Post-decellularisation treatments could be realised on pericardium depending on its final application. Decellularised pericardium could be either coated or biofunctionalised to improve graft integration at the site of implantation as well as decreasing degradation of the pericardial tissue. In their study, Dong *et al*. suggested treating bovine pericardium with acetic acid coupled with RGD polypeptides (Dong et al., 2009). Acetic acid increased pericardial scaffold pore size and porosity while RGD peptides improved cell adhesion and growth (140). However, RGD those have downside. RGD peptides could elicit thrombogenic reactions as it increases platelet adhesion and action. There are also experiments which have shown that the RGA coated on the implants, when combine with adsorbed proteins, such as fibronectin, vitronectin and fibrinogen, has a detrimental effect on MSC adhesion and survival (141). Thus, caution need to be taken as the ultimate effects of RGD will depend upon how signaling from this peptide integrates with endogenous processes such as protein adsorption.

Cross-linking treatments of the pericardial tissues have been performed to enhance their mechanical property and to minimise xenogeneic tissue degradation. Glutaraldehyde is currently the gold standard cross-linking agent, however the drawbacks of such treatments are well known (142), as also previously described. Other alternative cross-linking agents that have been researched are: genipin, penta-golloyl, tannic acid, carbodiimides, and epoxy compound. In particular, penta-golloyl glucose, a collagen-binding polyphenol, has shown to stabilise collagen, prevent its degradation while allowing progressive host cell infiltration as well as ECM remodelling (143).

1.8 Effects of crimping on PHV cusps

With a viable living prosthesis, HVRM provides a valve replacement which will be durable throughout the life-span of the patient. However, in case of PHV a potential hurdle that could compromise the durability of the prosthesis is represented by the

mechanical shocks induced on the cusp tissue by crimping and decrimping process. The unique feature of PHVs is that the valve needs to be crimped to a small diameter before implantation to allow its passage through femoral or apical access routes. Upon reaching the implantation site, the valve is released allowing it to attain the unfolded diameter. In case of a balloon-expandable PHV, the release process also involves the compressing of its cusps against the stent.

Since these manoeuvres are not performed during traditional surgical valve implantation, it is of paramount importance to thoroughly analyse the collateral effects that could be generated by crimping and releasing on the tissue cusps, while characterising the functionality of any PHV. After crimping, the pericardium can alter its structure with fragmentations and disruptions of the collagen and elastic fibers (144). Since collagen fibers provide structural integrity to the tissue to bear enormous loads related to cyclic pressure changes, these traumatic lesions will have an impact on prosthesis durability (145). Materials science has taught us that anytime a structure, such as a heart valve cusp, is altered and exposed to repeated high stress, it will experience increased fatigue that may lead to premature failure.

Zegdi *et al* reported evidence of severity traumatic cusp injury during the use of balloon- and self-expandable PHVs (146, 147). According to their studies, all deployed valves exhibited microscopic lesions of the cusps, observed in the form of transverse fractures and longitudinal cleavages in histological sections (Figure 1-46 and Figure 1-47). Transverse fractures were observed in both balloon- and self-expanding valves, whereas longitudinal cleavages were more frequent in the first ones. The Authors advanced as plausible causes for these damages the crushing and shearing of the pericardium during crimping and deployment procedures.

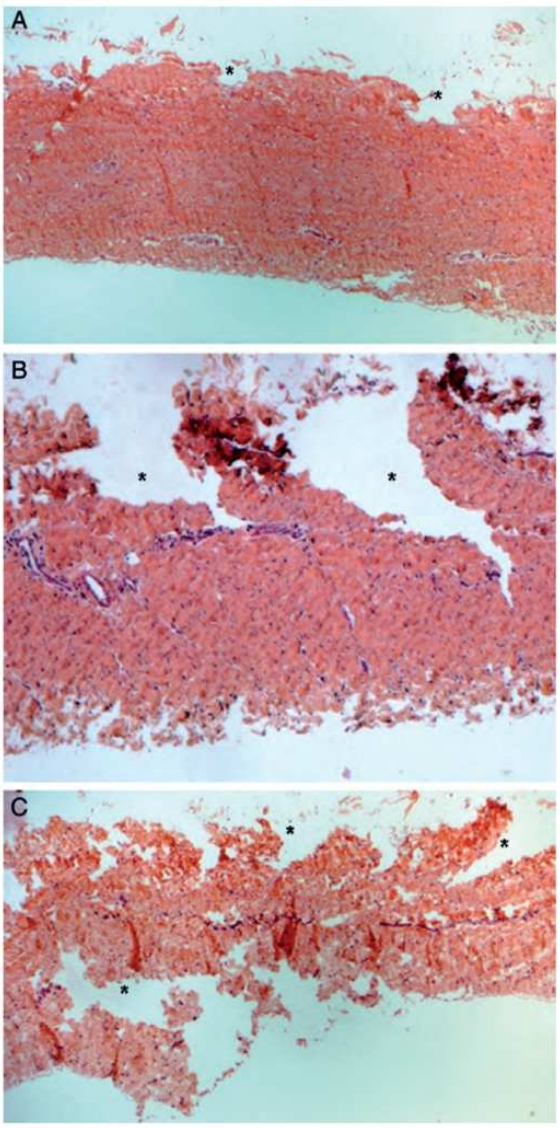

Figure 1-46 H&E staining showing transverse fracture in the bovine pericardium in a control (A), a self-expandable (B) and a balloon-expandable valve (C). The control pericardium has only small (non-significant) aspect of the fracture while large (significant) cracks can be noted in samples from both types of PHVs (asterisks). From (147)

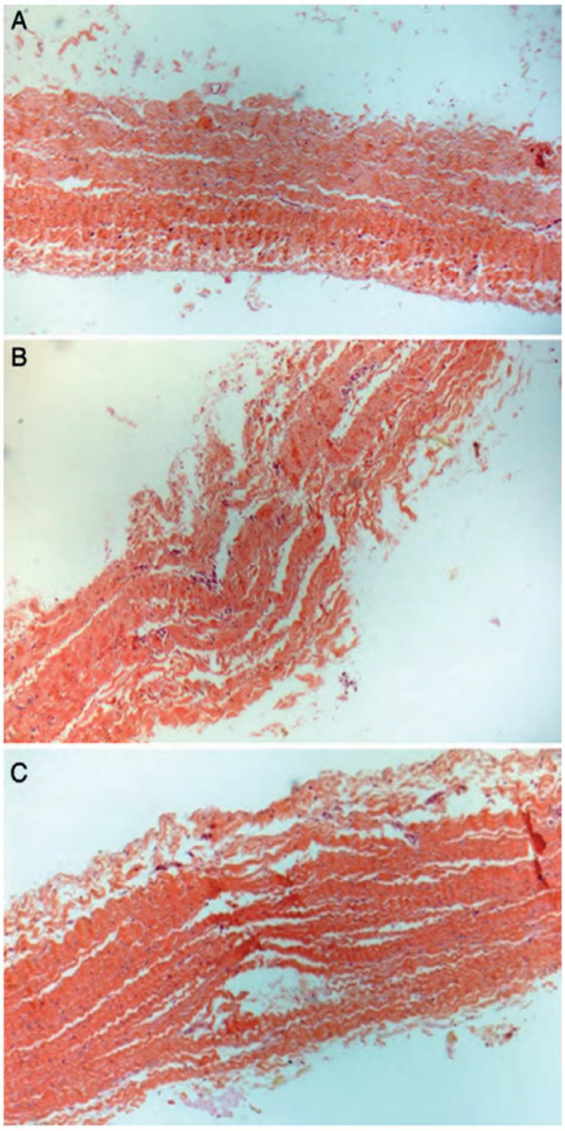

Figure 1-47 H&E staining showing longitudinal cleavages in the bovine pericardium from a control (A), a self-expandable (B) and a balloon-expandable valve (C). Note the thin aspect (when present) of the cleavages in the control pericardium and the large one in both PHVs. From (147)

In case the observations by Zegdi *et al* will be confirmed, then they may cast shadow on the safety of TAVI procedure with regards to tissue integrity, although crimping was proven not to influence the propensity to cusp calcification in the long term (148). However, cautions need to be taken before drawing conclusive remarks just based on these experiments. Concerns have been raised about interpreting these data, due to limitations of technology used in pathological investigations during these studies (149).

Recommendations have been proposed to further widen the area of analysis by employing special histological staining, such as picrosirius red, and scanning electron microscopy, to assess collagen waviness and to exclude any artefacts arising from manipulation at histology (145).

2. AIM OF THE PROJECT

The aim of this PhD project is to develop a novel generation of bioengineered PHVs (bioPHVs) based on decellularised pericardium of porcine and bovine origins, able to meet the requirements of transcatheter heart valve replacements. More specifically, the project is aimed at showing the suitability of decellularised pericardium to perform adequately as cusp material in a PHV setting and hence improve the durability of currently available devices.

In order to realize this main goal, this PhD project has been dedicated to the following objectives:

1. Decellularisation of bovine and porcine pericardia and analysis to test the effectiveness of decellularisation.
2. Fabrication of bioPHVs by combining decellularised pericardia (porcine and bovine) and commercial stent frame.
3. Assessment of hydrodynamic performance of the bioPHVs.
4. Evaluation of the effects of crimping on the pericardial cusps of bioPHVs.

3. MATERIALS AND METHODS

3.1 Preparation of decellularised pericardia and their analyses

3.1.1 Pericardium decellularisation

Porcine and bovine pericardia were decellularised according to the previously established, in-house TRICOL protocol (12). Porcine pericardia were acquired from 9 to 11 months old Duroc pigs weighing between 165 to 175 kg (local slaughterhouse at F.lli Guerriero S.r.l., Villafranca Padovana, Padova). Bovine pericardia were obtained from 7 to 8 months Piebald calves (local abattoir at Bugin S.r.L, Santa Maria di Sala, Venice). Harvested pericardia were transported to the lab in phosphate buffered saline (PBS) solution. Upon arriving in the lab, the pericardia were cleared from fatty tissue and washed in PBS solution at 4 °C for two to three hours to remove blood and dirt. The decellularisation process was then commenced immediately. All reagents used during decellularisation are from Sigma-Aldrich (Saint Louis, MO, USA) unless otherwise stated.

The decellularisation started by placing the pericardia under agitation at 4 °C in hypotonic, ten times diluted, PBS buffer (pH 7.4) containing 10 mM of sodium ascorbate, 5 mM of EDTA, 10% (v/v) DMSO, and protease inhibitors (PI) (2 mM of phenylmethylsulfonyl fluoride, 5 mM of N-ethylmaleimide, 5 mM of benzamidine and 1 mM of iodoacetamide). After 8 hours, the solution was replaced for hypotonic washing solution without DMSO and PI. The pericardia were then washed for 8 hours with 1% (v/v) Triton X-100 in the presence of PI. After a further 8 hours washing without PI in Triton X-100 0.1% (v/v), samples were washed with hypertonic solution of PBS buffer containing NaCl (0.5 M) at 4 °C for two 8 hour-periods. This was followed by hypotonic PBS washing and then Triton X-100 was replaced by 10 mM of sodium cholate, and washing resumed for two 8 hour-periods at room temperature. The pericardia were finally washed in 10% (v/v) isopropanol in saline water. Nucleic acids were removed by Benzonase, a recombinant endonuclease free of proteases that degrades single and double stranded DNA and RNA.

3.1.2 Histological assessment

Histological staining was performed on native and decellularised tissues to verify the success of decellularisation process. The samples for histology were first fixed in 4%

paraformaldehyde in PBS for 20 minutes in darkness at room temperature and then kept in 20% sucrose in PBS overnight at 4 °C. Subsequently, the samples were embedded in 1:1 solution of 20% sucrose and O.C.T™ (Optimal Cutting Temperature compound, Sakura, Japan), snap-frozen in liquid nitrogen, and stored at -80 °C until cryosectioning. The cryosections (5-6 µm) were stained with Hematoxylin and Eosin and Mallory Trichrome (Bioptica, Milan, Italy) and photographed with a Nikon Eclipse 50i light microscope equipped with a NIS-Element D 3.2 Software (Nikon Corporation, Shinagawa, Tokyo, Japan).

3.1.3 Immunofluorescence staining

An indirect immunofluorescence was realised on cryosections of native and decellularised pericardia to evaluate the effectiveness of TRICOL decellularisation protocol in removing cellular components and maintaining ECM structure. Primary antibodies for following markers were used:

- Collagen I (1:100, C2456, Sigma, raised in Mouse)
- Collagen IV (1:100, ab6586, Abcam, raised in Rabbit)
- Elastin (1:100, E4013, Sigma, raised in Mouse)
- Laminin (1:500, Z0097, Dako Cytomation, raised in Rabbit)
- Heparan sulfate (1:100, MAB1948P, Milipore, raised in Rat)

The antibodies were prepared in 1% bovine serum albumin (BSA) in PBS. BSA was used to block potential nonspecific binding sites in the samples to prevent nonspecific antibody binding. Additionally, BSA also served as carrier for the antibodies. Rhodamine (RHOD) or Fluorescein isothiocyanate (FITC)-conjugated anti-mouse, anti-rat and anti-rabbit IgGs (1:100, Millipore, Darmstadt, Germany) were used as secondary antibodies to reveal primary antibody binding. Controls were incubated with 1% BSA without any primary antibodies. Nuclei were detected by counterstaining with 4′,6-diamidino-2-phenylindole (DAPI, Sigma). Photographic observations were recorded with an epifluorescence microscope Leica AF6000, connected to Leica DC300 digital camera, and equipped with LAS AF Software (Leica Micro- systems, Wetzlar, Germany).

3.1.4 Biochemical analyses

Biochemical analyses were performed to quantitatively compare the composition of native and decellularised tissues. The bovine samples for biochemical assays were labelled as native bovine pericardium (NBP) and decellularised bovine pericardium (DBP). Similarly, those for porcine pericardium were labelled as native porcine pericardium (NPP) and decellularised porcine pericardium (DPP).

Water content

Water content was calculated by the difference between wet and dry weights of the pericardium and expressing the difference as percentage of the wet one, following this formula:

$$Water\ content = \frac{wet\ weight - dry\ weight}{wet\ weight} \times 100$$

Samples of about 1 cm^2 were obtained from both the native and decellularised tissues (n=5). In wet state, the samples were gently blotted on filter paper and then weighed to obtain the wet weight after equilibration for 2 minutes. For dry weight, the samples were freeze-dried overnight (Modulyo Freeze Dryer, Edwards) and then weighed following the same procedure described before.

Hydroxyproline assay

Collagen content was determined with a protocol that is based on an amino acid analyser to measure collagen marker hydroxyproline, following acid hydrolysis of the tissues (150).

Samples of about 1 cm^2 from both the native and decellularised tissues (n=5) were lyophilised and hydrolysed with 6 N HCl at 110 °C for 24 hours, evaporated with a rotary evaporator and dissolved in MilliQ water. Each sample and hydroxyproline standards (0.5 - 2.5 µg/ml) were then oxidised by chloramine-T solution and incubated for 20 minutes at room temperature. Then, 19% perchloric acid was used to neutralise the oxidation and the mixture allowed to stand for 5 minutes at room temperature. Finally, Ehrlich reagent (p-dimethylaminobezaldehyde solution) was added and the mixture was incubated again for 20 minutes at 60 °C and then cooled in tap water for 5 minutes. Absorbance of the resulting solution was read at 561 nm in a spectrophotometer (Bibby Scientific Limited, Stone, United Kingdom) and the concentration of hydroxyproline was calculated by interpolation from the standard

curve. Collagen content was then calculated from the hydroxyproline concentration and expressed as µg collagen/mg dry tissue.

Sulfated Glycosaminoglycans (sGAG) assay

sGAG was quantified using Blyscan sulfated glycosaminoglycan assay kit (B1000, Biocolor, Carrickfergus, United Kingdom). The Blyscan assay is a quantitative e dye-binding method, which employs 1, 9-dimethyl-methyene blue as dye label to specifically detect sGAG. Samples with dry weights between 1-2 mg were taken from native and decellularised tissues (n=5) and treated with papain extraction solution (7 U/ml). sGAG quantification was then proceeded following the protocol stated in the kit. Absorbance measurement of the final solution was done at 656 nm in a microplate reader (TECAN Infinite M2, Tecan Trading AG, Männedorf, Switzerland). Standard curves were generated from reference standard solution composed of bovine tracheal chondroitin 4-sulfate (100 µg/ml). sGAG content was reported as µg sGAG/ mg dry tissue weight. The percentage change of sGAG content from native to decellularised tissue was also calculated, as:

$$percentage\ change\ in\ sGAG\ content = \frac{sGAG_{native} - sGAG_{decellularised}}{sGAG_{native}} \times 100$$

Elastin assay

Elastin content was quantified using Fastin Elastin assay kit (F2000, Biocolor, Carrickfergus, United Kingdom). The kit applies 5, 10, 15, 20-tetraphenyl-21H,23H-porphine tetrasulfonate (TPPS) a dye label to detect elastin. Samples with 2-3 mg dry weight were taken from native and decellularised tissues (n=5). 0.25 M oxalic acid treatment was using to extract α-elastin from the sample and quantification was conducted following the steps of the kit. The absorbance of final solution was read at 513 nm in a microplate reader (TECAN Infinite M2, Tecan Trading AG, Männedorf, Switzerland). Standard curves were generated from a reference standard solution composed of high molecular weight fraction of α-elastin standard prepared from bovine neck ligament elastin (1 mg/ml), in 0.25 M oxalic acid. Elastin content was reported as µg elastin/ mg dry tissue weight.

3.1.5 DNA quantification

Total DNA content was quantified in samples of native and decellularised pericardia. Samples of 5-10 mg wet weight (n=3) were minced and DNA was extracted with the

spin-column protocol of the DNeasy Blood & Tissue Kit (Qiagen, Valencia, CA, USA). The concentration of DNA in final elution buffer was measured at 260 nm with a NanoDrop 2000 spectrophotometer (ThermoFisher Scientific, Wilmington, Delaware, USA). The DNA content was expressed as µg DNA/mg dry tissue weight.

3.2 PHVs and delivery system

3.2.1 ACURATE neo™ TF stents

Six self-expanding stents of diameter 27 mm (Figure 3-1) used for ACURATE neo™ TF transfemoral TAVI system were obtained from Symetis (Ecublens, Switzerland).

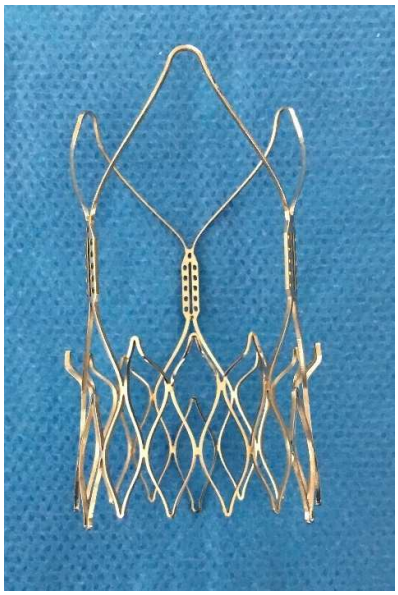

Figure 3-1 An ACURATE neo TF stent obtained from Symetis.

Composed of nitinol, the stent architecture has several unique features: 1) flexible stabilisation arches, which are responsible for the self-aligning properties of the valve; 2) upper crown, ensures stable positioning and supra-annular anchoring of the valve and caps the native cusps, reducing the risk of coronary obstruction and paravalvular leak; and 3) lower crown, which opens upon full deployment and protrudes just minimally toward left ventricular outflow tract (Figure 3-2).

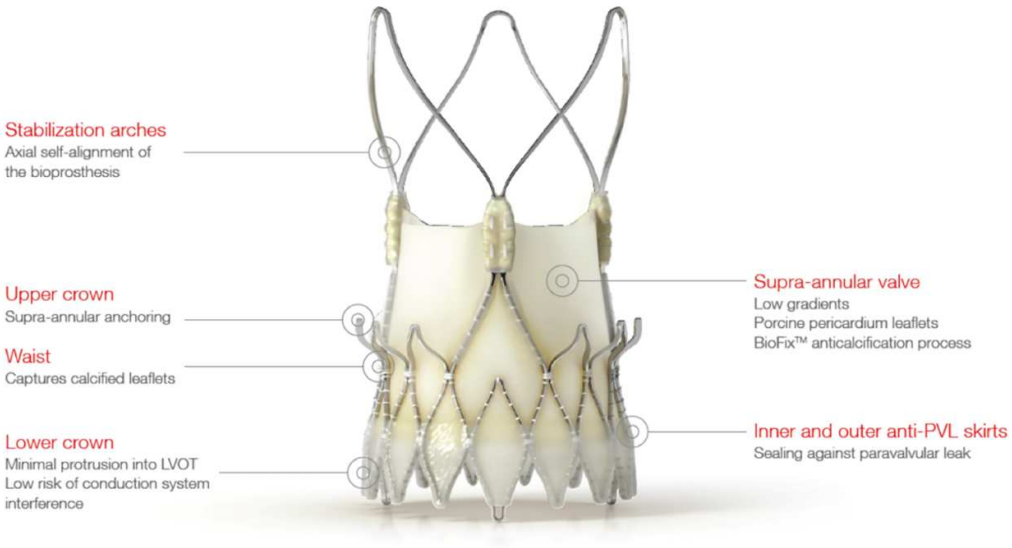

Figure 3-2 Different features of ACURATE neo TF stent. From (151)

3.2.2 bioPHVs fabrication

bioPHVs were fabricated by mounting TRICOL decellularised pericardium onto ACURATE neo™ TF stent. The fabrication was based on the tubular leaflet design, where the function of the cusps is carried out by opportune shaping of a simple tubular construct. This latter is sutured along a circumferential line at the annulus and at three single points at the sino-tubular junction following the single point attached commissures (SPAC) technique (Figure 3-3) (152, 153). The suture lines used during valve fabrication are listed in Table 3-1.

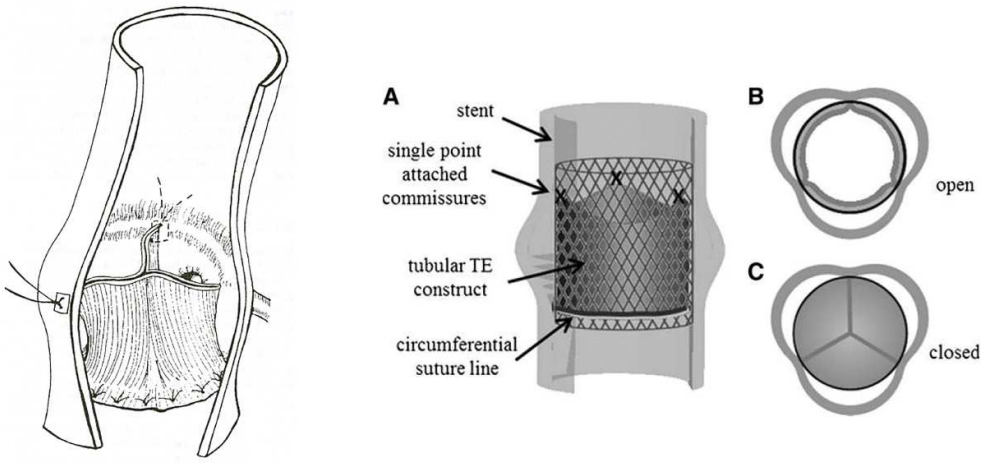

Figure 3-3 Principle of the tubular valve design. *Right:* Concept proposed by Goetz, *Left:* Sketch of Stented valve based on this principle. From (152, 154)

Table 3-1 Sutures used during valve fabrication.

Suture size (USP)	Material	Company
6-0	Polyester, white braided, Non Absorbable	Assut Medical Sàrl, Switzerland
5-0	Polyester, white braided Non Absorbable	Assut Medical Sàrl, Switzerland
6-0	PROLENE Polypropylen	Ethicon US, LLC
5-0	PROLENE Polypropylen	Ethicon US, LLC

The steps followed during valve fabrication are illustrated in Figure 3-4. Firstly, a trapezoidal strip of pericardium was isolated. The pericardial patches were selected from area with uniform thickness, preferably from anterior-left region. The patches were then oriented in such a way that the majority of collagen fiber orientation are aligned along the circumferential direction. The two shorter sides of the trapezoid were then joined with continuous suture to form a tube. Three commissural attachment points were marked on one end of the tube by tying sutures 120° apart. Then, following the SPAC technique, these three points were attached to the three commissural posts of the stent while at the annular level the pericardium was tied to the stent struts with interrupted sutures throughout a circumferential line. The extra length of the pericardium was flipped over and stitched to the struts with another interrupted circumferential suturing to create a pericardial skirt at the annular level. One additional interrupted circumferential suturing was done at the waist level of the stent so that the part of the pericardial tube between the lower crown and the waist was completely affixed to the stent struts. As last step of fabrication, pinching was performed by tying a knot at the commissural attachment point across two corresponding cusps (Figure 3-5).

The bioPHVs fabricated with decellularised bovine pericardium were labelled as bovine bioPHVs (B-bioPHVs), while those with decellularised porcine tissue were labelled as porcine bioPHVs (P-bioPHVs).

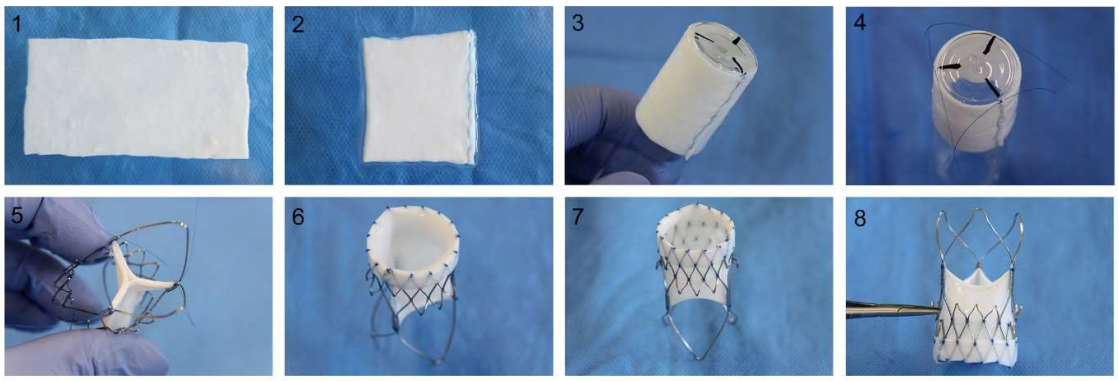

Figure 3-4 bioPHV fabrication: 1) Pericardial strip, 2) Two ends of strip sutured, 3) Pericardial tube, 4) Three commissural point marked, 5) Commissural points tied to stent, (6-8) Interrupted circumferential sutures at annular side.

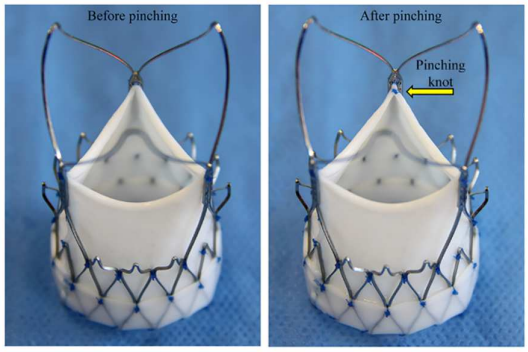

Figure 3-5 Pinching at the commissures.

3.2.3 ACURATE TA™ Transapical TAVI valves

ACURATE TA™ Transapical TAVI (Ref no. SYM-SV27-001) valves were obtained from Symetis (Ecublens, Switzerland) and acted as controls in the study. Each bioprosthesis is comprised of a radiopaque, nitinol self-expanding support structure (stent), an integrated tri-leaflet biological tissue valve and a polyethylene terephthalate (PET) fabric skirt (155). The biological valve is manufactured from three non-coronary native porcine cusps (Figure 3-6) that have been preserved in low concentration solutions of buffered glutaraldehyde and chemically sterilised through heat treatment in sterilant solution containing glutaraldehyde and ethanol. Each bioprosthesis is packaged and stored in low concentration solution of buffered glutaraldehyde. The storage temperature for this PHV is in the range of 5 and 25 °C.

Figure 3-6 A Symetis ACURATE TA bioprosthesis obtained from Symetis.

3.2.4 ACURATE TA™ Transapical delivery system

One ACURATE TA™ transapical delivery system (Ref no. SYM-DS-001) together with a specially designed bioprosthesis loading tool was obtained from Symetis. The ACURATE TA™ transapical delivery system is designed for positioning and deploying the ACURATE TA™ transapical aortic bioprosthesis over patient's native stenotic aortic valve via transapical access. This transapical delivery system is compatible also with the stent of ACURATE neo™ TF system, which are originally for use with transfemoral system. Hence, for this study the transapical delivery system was applied for crimping and delivery of the ACURATE neo™ TF stent.

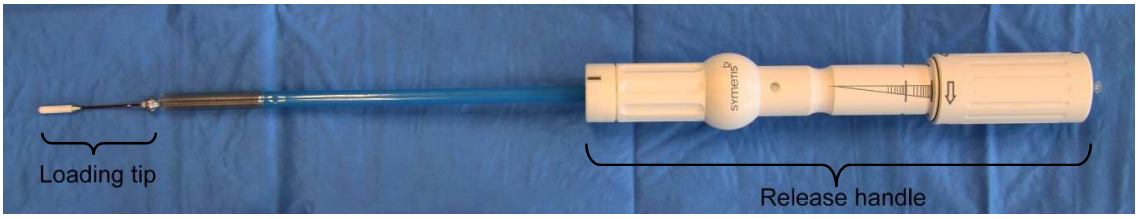

Figure 3-7 ACURATE TA™ transapical delivery system

The delivery system (Figure 3-7) has a crossing profile of 33 F and a usable length of 340 mm. The system is compatible with all three sizes of the ACURATE TA bioprosthesis. The delivery system is comprised of the following components:

1) A release handle for deployment of the bioprosthesis. The handle comprises of:
    - A rotating ring with markings to indicate the position of the three commissures of the bioprosthesis when loaded onto the delivery system.

- A rotating knob for the two-step controlled release of the bioprosthesis from the delivery system.
- Markings to gradually indicate the position of the rotating knob during the two-step release procedure ("partial release" and "full release").
- A safety button to avoid premature release of the partially expanded bioprosthesis.

2) A flexible inner membrane that contains a guide wire lumen. Distally, the membrane has a radio-opaque atraumatic loading tip, a stent holder, and a radio-opaque marker band for correct positioning of the bioprosthesis. The membrane is proximally fixed to the release handle.
3) A flexible outer membrane, which distally contains the compressed, or crimped, bioprosthesis and is fixed proximally to the release handle.

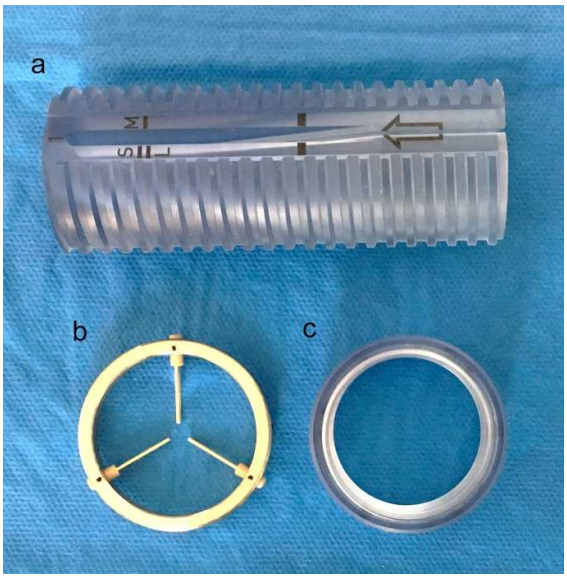

Figure 3-8 Loading tool.

The specially designed loading tool consists of three parts: a cylinder (Figure 3-8a) whose outer surface has threads while the inner part is formed into a conical hole, a circular metallic frame (Figure 3-8b) with three spokes 120° apart and a nut (Figure 3-8c) with threads in its inner surface.

3.2.5 Loading and simulation of crimping

Loading and crimping of the valves, either commercial PHVs or bioPHVs, were performed with an ACURATE TA™ transapical delivery system and a specially designed loading tool in accordance with the manufacturer's Instructions for use (IFU).

As first step, each valve was gradually pushed down the conical hole of the loading cylinder, as visible in Figure 3-9 and Figure 3-10. The lower crown was inserted onto the wider end of the cylinder ensuring proper alignment of the commissures (see image 1 in Figure 3-10). Next, the circular frame was placed over the valve with its spokes aligned to the commissures (see image 2 in Figure 3-10. Then, the nut was placed on top of both the valve and the frame (see image 3 in Figure 3-10). The nut was then slowly screwed down, pushing the valve towards the narrower end of the cone until the stent hooks appeared from the bottom hole of the cylinder, thus crimping it to a smaller diameter.

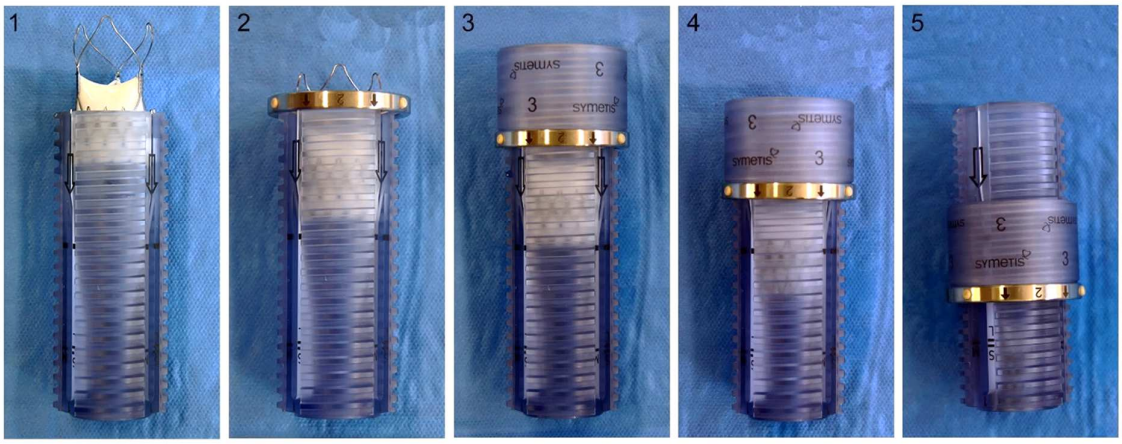

Figure 3-9 Loading of the valve into the loading tool. (Side view)

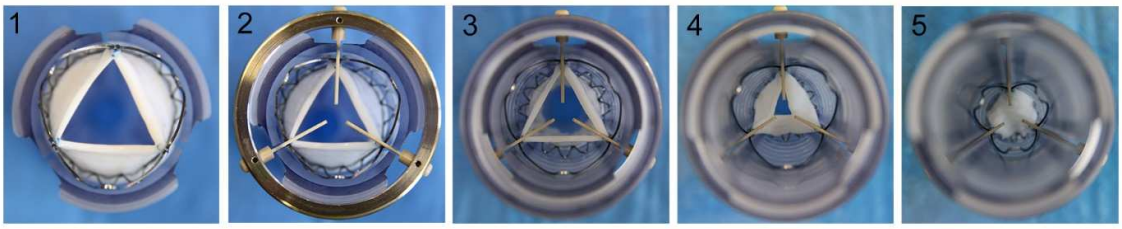

Figure 3-10 Loading of the valve into the loading tool. (Top view)

As next step of loading, each crimped valve was transferred from the loading tool into the delivery system (Figure 3-11). For this, the loading-tip of the delivery system was inserted through the crimped valve and the three stent holder pins were locked into the three stent hooks. Then, by using the rotating handle, the folded valve was slowly pulled until the valve was fully inside and covered by the outer membrane of the delivery system. Each PHV was then left in crimped state until the required duration. While in crimped state, every valve was continuously flushed with saline solution to prevent dehydration.

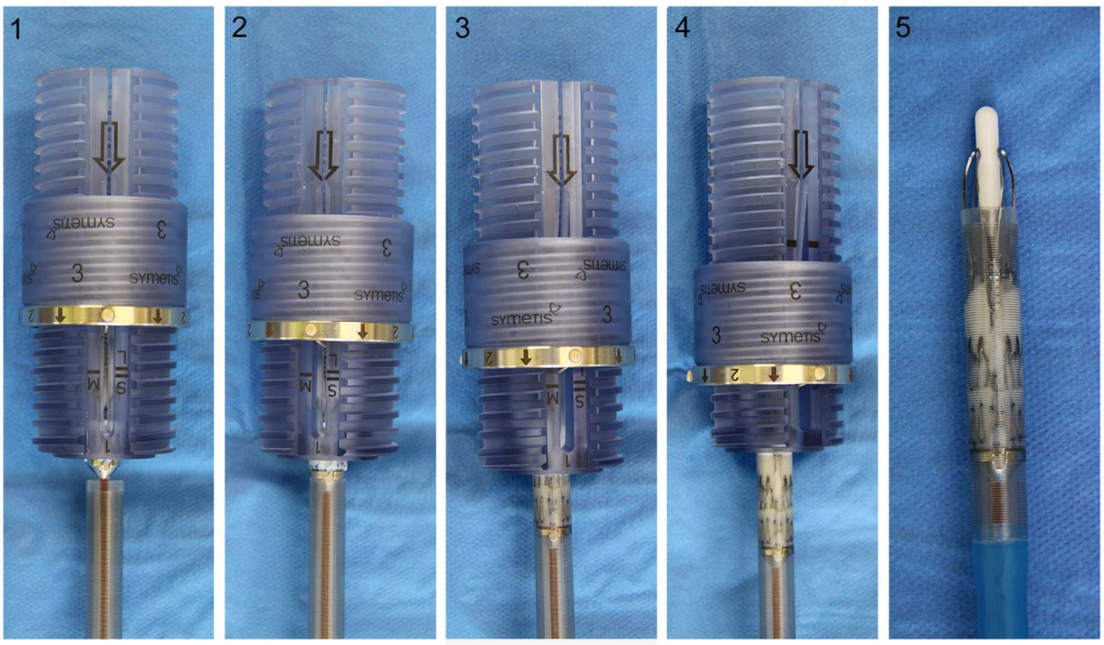

Figure 3-11 Transferring crimped valve from loading tool to delivery system.

3.3 Hydrodynamic characterisation

BioPHVs (n=3 for each pericardial type) were tested in a home-made flow-loop system (152) in order to evaluate their hydrodynamic performance, in collaboration with the Department of Tissue Engineering and Textile Implants, Helmholtz Institute for Biomedical Engineering (University Hospital RWTH Aachen, Aachen, Germany). The valves were placed in a silicone tube (diameter = 25 mm) featuring the sinuses of Valsalva, produced by moulding technique (Figure 3-12) (153). The valves were left in the crimped configuration for 20 minutes to simulate the scenario the valve would go through during an actual implantation procedure. Two ACURATE TA™ transapical valves (diameter = 27 mm) were utilised as controls.

BioPHVs and control valves were tested at seven different conditions (Table 3-2) following ISO 5840-3 guidelines (156).

In the first set of conditions, the valves were evaluated at four different cardiac outputs (CO) of 2, 4, 5 and 7 l/min, identified as conditions A, B, C, and D respectively (157-159) at a fixed heart rate of 70 cycles/minute and mean aortic pressure of 100 mmHg.

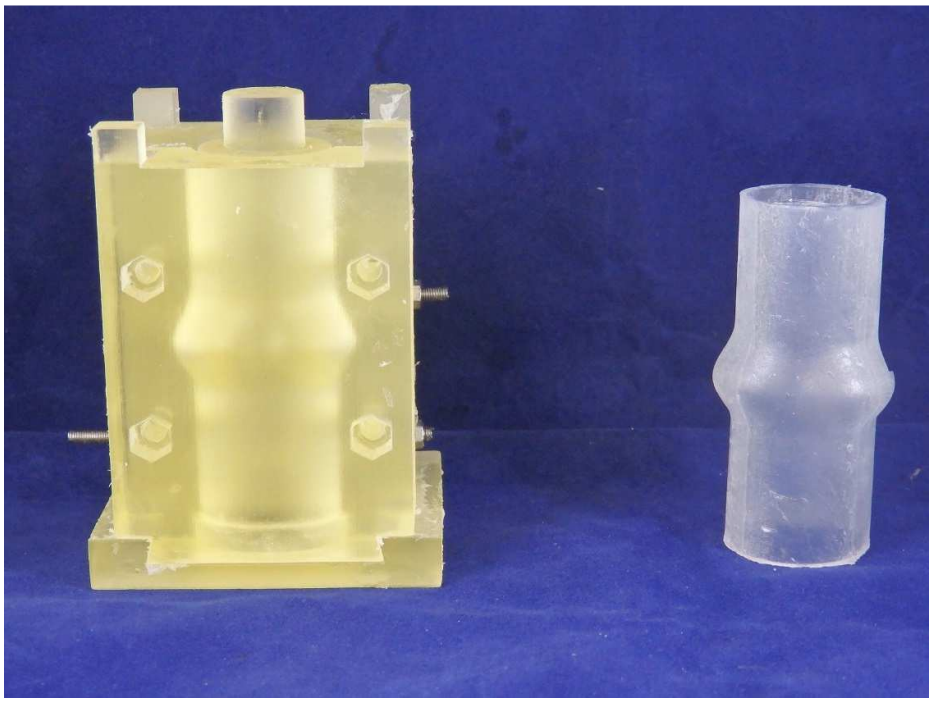

Figure 3-12 Mould (left) and the silicon tube with sinuses of Valsalva (right).

For the second set of conditions, the valves were tested at three different back pressures of 80, 120 and 160 mmHg, identified as condition E, F, and G while the heart rate was 70 cycles/minutes and cardiac output 5 l/min. Tests were performed in saline solution (0.9 % w/v NaCl, Sigma-Aldrich) at room temperature. In all tested conditions, the systolic duration occupied 35% of the cardiac cycle, as recommended in ISO 5840-3 (156).

Table 3-2 Test conditions at four different cardiac outputs (A-D) and at three different mean back pressures (E-G)

Condition	**Heart Rate (cycles/minute)**	**Cardiac Output (l/min)**	**Mean aortic pressure (mmHg)**
A	70	2	100
B	70	4	100
C	70	5	100
D	70	7	100
Condition	**Heart Rate (cycles/minute)**	**Cardiac Output (l/min)**	**Mean back pressure (mmHg)**
E	70	5	80
F	70	5	120
G	70	5	160

Pressure values were measured by transducers positioned immediately upstream and downstream the valve to be tested. The instantaneous flow of the valve was measured at its downstream by a flow meter (sonoTT, em-tec GmbH, Finning, Germany). Upon stabilisation of the test conditions, pressure and flow values were recorded by a LabVIEW application (National Instruments, Texas, USA).

Based on these recordings, effective orifice area (EOA), regurgitant fractions, mean systolic transvalvular pressure drop (Δp) and energy losses were calculated and averaged over ten consecutive cycles.

The EOA, which indicates the smallest cross-sectional area of the flow at the aortic valve orifice during the positive differential pressure period, was determined with following equation, as stated in ISO (156).

$$EOA = \frac{q_{v\,RMS}}{51.6\sqrt{\frac{\Delta p}{\rho}}}$$

Where,

$q_{v\ RMS}$ → is the root mean square forward flow (ml/s) during the positive differential pressure period;

ρ → is the density of the test fluid (g/cm^3).

The Mean systolic transvalvular pressure drop (Δp) was measured as the mean pressure difference during the positive differential pressure period.

The Regurgitant fraction was given by the total regurgitant volume expressed as a percentage of the total forward flow volume. The total regurgitant volume included closing volume, transvalvular leakage volume and paravalvular leakage volume.

Additionally, the energy loss, a parameter which indicates workload on the left ventricular myocardium, was calculated as the time integral of the product of the pressure drop and flow, over different phases of the cardiac cycle, as indicated in following formula (160).

$$Energy\ loss = \int \Delta p(t) q_{v\,RMS}(t) dt$$

For the conditions E, F, and G only the regurgitation was evaluated as required by the ISO. These represent the extreme conditions that could be generated during hypertensive states of the patient to be treated.

Videos of the valve performance were taken at normal and high speed (240 frames per second) with camera.

3.4 Evaluation of effects of crimping

For the realization of the experiments to study the effects of crimping, the valves, either, commercial PHVs or bioPHVs, were divided into three groups (Table 3-3). The first group did not undergo loading and crimping process after fabrication and were used as control. These set of valves were termed as 'uncrimped'. The second group of valves remained crimped for 20 minutes, simulating the average time a TAVI valve stays crimped during a usual valve implantation operation. The third group of valves were kept crimped for 60 minutes to simulate an extended duration of force generated during crimping. Patches of decellularised pericardium (about 2 cm^2), labelled as 'unmounted' samples, were used as extra control. The comparison between the unmounted and uncrimped groups was used to study the effect on the pericardial matrix solely due to the valve fabrication procedure.

Table 3-3 Samples number for crimping effects evaluation

Valve type / Crimping duration	B-bioPHV	P-bioPHV
Uncrimped	3	3
20 minutes	3	3
60 minutes	3	3

In total, nine valves were fabricated for each species, i.e. porcine and bovine. Pictures of each valve were taken before crimping and after crimping to evaluate any macroscopic changes. The pictures were taken from five different views: 1) First cusp, 2) Second cusp, 3) Third cusp, 4) Aortic side and 5) Ventricular side.

After the completion of the required crimping duration, three samples were isolated from two different cusps of each tested valve according to the scheme shown in Figure 3-13. The samples were labelled as 1, 3A and 3B. Sutures were made on samples 1

and 3B to mark the area closer to the waist of the stent. The samples were stored in formalin until further analysis in collaboration with the group of Cardiovascular Pathology in the Department of Cardiac, Thoracic and Vascular Sciences (University of Padova).

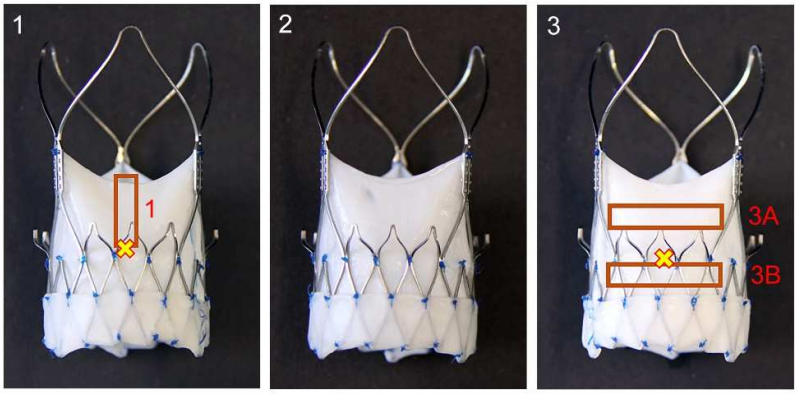

Figure 3-13 Samples for histology, indicated by orange rectangle. The yellow cross are the locations of suture marker.

3.4.1 Processing for histological analysis

Pericardium samples, after fixation in 4% formaldeyde in phosphate buffer 0.1 M pH 7.2, and dehydration in ethanol crescent series, were embedded in paraffin, and 3-4 µm thick sections were stained with hematoxylin–eosin (HE) to detect cells extracellular matrix and Picrosirius red (PSR) to visualise collagen fibers waviness at polarized lens, and were observed at the microscope Zeiss Axioplan 2 (Carl Zeiss, Oberkochen, Germany).

3.4.2 Morphometrical Analysis

To assess a potential deformation of collagen after crimping procedures, collagen fibers wave periodicity was measured (161, 162). Picrosirius red stained sections were analyzed: five random not overlapping fields under polarized lens were acquired at 200x magnification by using an image analysis system constituted by optical microscope Zeiss Axioplan 2 (Carl Zeiss, Oberkochen, Germany) equipped with the digital photocamera AxioVision, (Carl Zeiss, Oberkochen, Germany) and the morphometrical imaging analyzer software Image PRO-Plus 5.1 (Media Cybernetics, Silver Spring, MA, USA). Collagen fiber periodicity was measured with the modality *measurement/length*, based on the length of the period of the collagen (Figure 3-14).

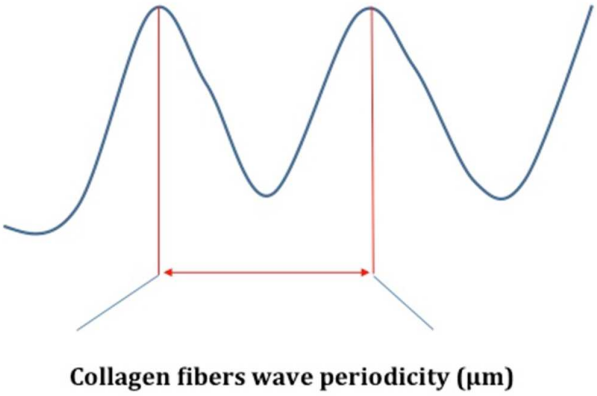

Figure 3-14 Schematic representation of collagen period length measurement.

3.5 Statistical analyses

For descriptive analysis all the data were expressed as mean ± standard deviation (SD). Data were analysed in Microsoft Excel, MATLAB R2017a (MathWorks Inc, Massachusetts) and GraphPad Prism 7 for Windows, Version 7.03 (GraphPad Software Inc., California). Two-sided unpaired t-test and one-way ANOVA followed by comparisons using Tukey post hoc test were applied to evaluate any significant difference between groups. Statistical tests were indicated in figure legends and $P<0.05$ was considered to be statistically significant at the 5% confidence level.

Regarding the sampling number, at least three samples were tested for the biochemical, DNA quantification and hydrodynamic tests. In case of control valves for hydrodynamic test, only two samples were used since these were commercial valves, which are already standardised. Even if the sampling number adopted for each assay may not be sufficient for a high statistical power, it was chosen following the principle of reproducibility.

4. RESULTS

4.1 Assessments of decellularised pericardia

4.1.1 Histological assessment

In the native pericardium, mesothelium (M), *fibrosa* (F) and epipericardium (E) appeared to be well populated, as it is possible to appreciate by Hematoxylin - Eosin in bovine and porcine tissues (Figure 4-1a and Figure 4-2a respectively). As observable by Mallory trichrome, the ECM structure was mainly composed by collagen fibers with their peculiar wavy appearance (Figure 4-1b and Figure 4-2b for bovine and porcine tissues respectively).

After TRICOL decellularization, both bovine and porcine pericardia resulted acellular. Particularly, cellular fragments and nuclear residues were absent while the overall ECM architecture and components were maintained, as visible in Hematoxylin - Eosin (Figure 4-1c and Figure 4-2c respectively) and Mallory trichrome (Figure 4-1d and Figure 4-2d respectively) performed on TRICOL samples.

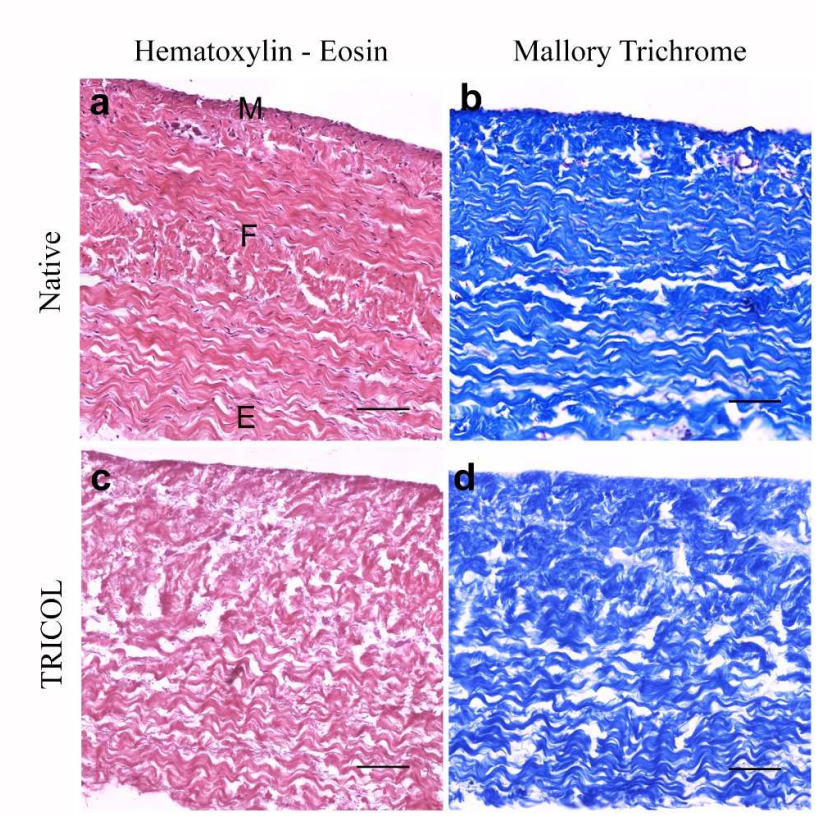

Figure 4-1 Histology of bovine pericardium. (a, c) Hematoxylin - Eosin (b, d) Mallory Trichrome. *M = Mesothelium, F = Fibrosa, E = Epipericardium*, Scale bar = 100 µm

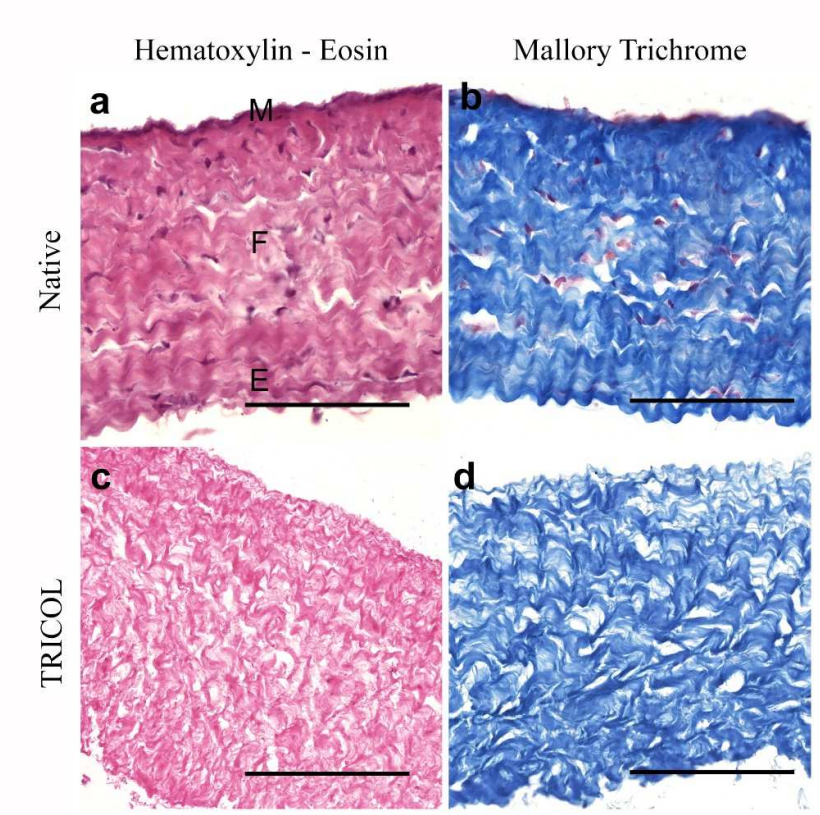

Figure 4-2 Histology of porcine pericardium. (a, c) Hematoxylin - Eosin (b, d) Mallory Trichrome. *M = Mesothelium, F = Fibrosa, E = Epipericardium*, Scale bar = 100 µm

4.1.2 Immunofluorescence staining

To evaluate the effectiveness of TRICOL decellularisation protocol, an immunofluorescence for the typical components of the pericardial extracellular matrix was performed. Collagen I fibers with their peculiar wavy appearance could be observed in both native and decellularised tissues (Figure 4-3 a, f and Figure 4-4 a, f), meaning that collagen I fibers remained intact after the decellularisation process. The elastin fiber network was also well preserved in TRICOL-treated pericardium compared to that of the native counterpart (Figure 4-3 b, g and Figure 4-4 b, g). The decellularisation procedure also did not affect collagen IV, laminin and heparan sulfate (Figure 4-3 c-e, h-j and Figure 4-4 c-e, h-j). These are the main components of the basal lamina of the submesothelium and of small-caliber vessels found in *fibrosa* layer, and are particularly important to guarantee cell adhesion. DAPI staining reconfirmed the removal of nuclear components (Figure 4-3 and Figure 4-4).

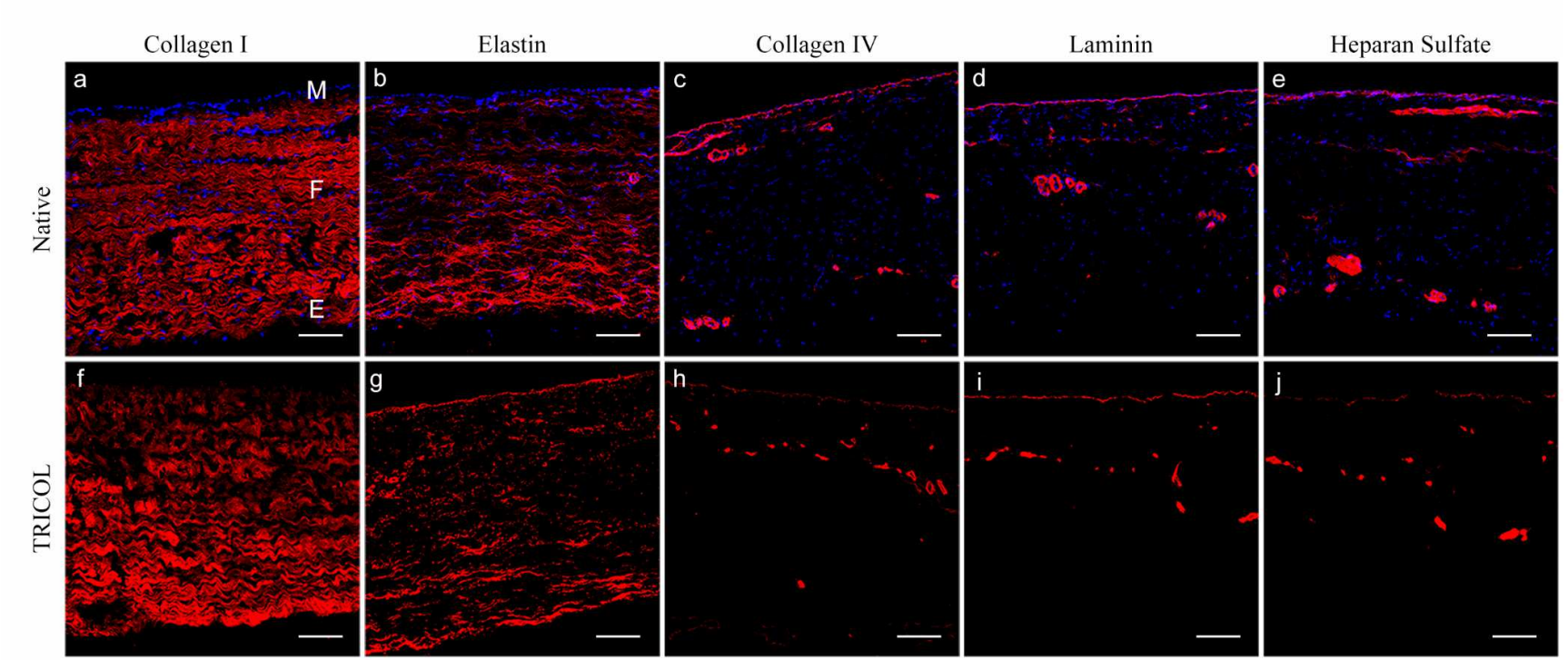

Figure 4-3 Immunofluorescence on native (a-e) and TRICOL (f-j) bovine pericardium: General histoarchitecture was preserved after TRICOL decellularisation (red; f,g) with respect to native tissues (a,b). The basal lamina elements were not removed in TRICOL treated tissues (red; h-j) when compared to native ones (a,b). Nuclei that were clearly visible with DAPI in native tissues (blue; a-e) were absent after decellularisation (f-j). *M = Mesothelium, F = Fibrosa, E = Epipericardium*. Scale bar: 100 µm

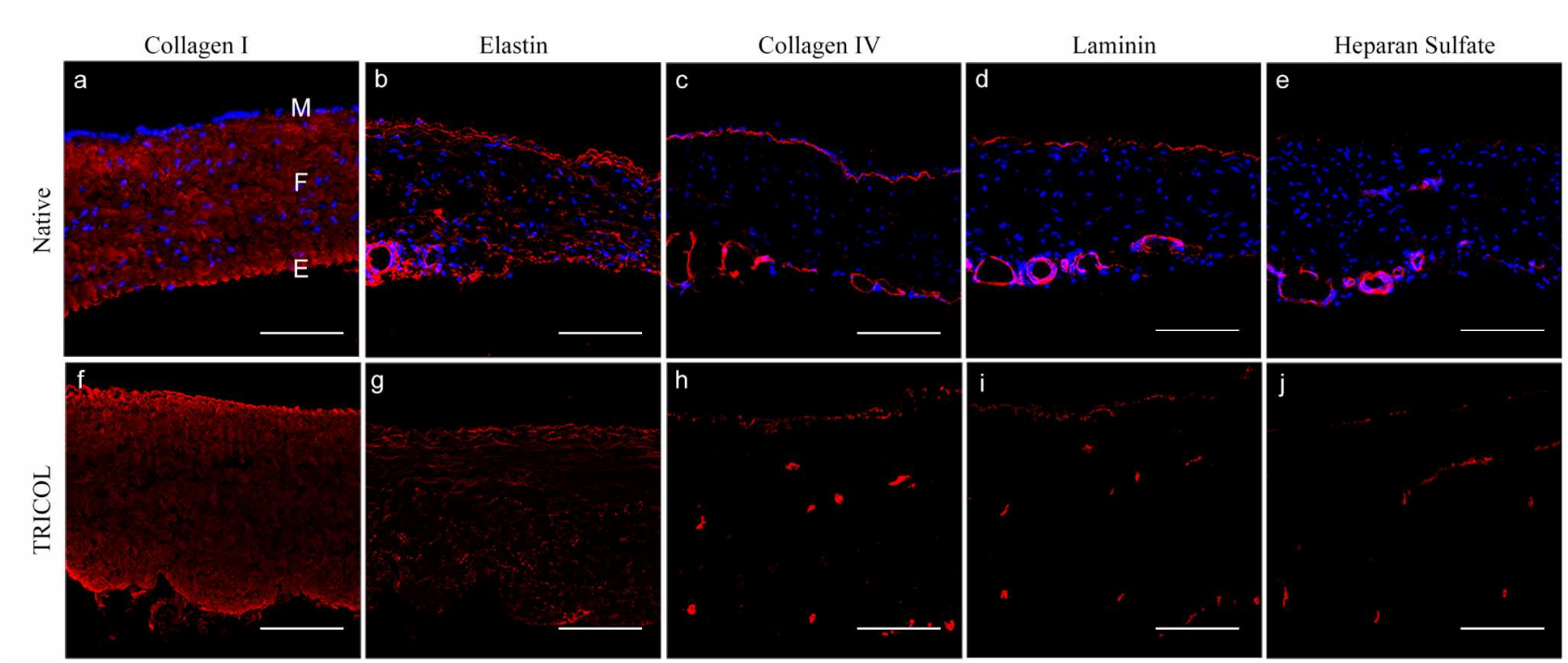

Figure 4-4 Immunofluorescence of native (a-e) and decellularised (f-j) porcine pericardium: General histoarchitecture remained intact after TRICOL decellularisation (red; f,g) with respect to native tissues (a,b). The basal lamina elements were not removed in TRICOL treated tissue (red; h-j) when compared to native ones (a,b). Nuclei present in native tissues (blue; a-e) were completely removed after decellularisation (f-j). *M = Mesothelium, F = Fibrosa, E = Epipericardium*. Scale bar: 100 µm

4.1.3 Biochemical analyses

Biochemical analyses confirmed the maintenance of ECM after decellularisation as observed with the histological and immunofluorescence assessment.

After decellularisation, due to the loss of cells and soluble proteins, the collagen amount in the tissue was determined to be higher, the difference being statistically significant in the case of the bovine tissue ($P<0.01$) (Figure 4-5a).

However, TRICOL procedure resulted in loss of sGAG (Figure 4-5b). The percentage decrease in sGAG content for bovine and porcine tissues was respectively 54.33% and 24.54%. The difference was again statistically significant for the bovine pericardium ($P<0.005$).

Elastin content was not affected by decellularisation. There was no statistically significant difference between elastin content values in native and decellularised pericardia (Figure 4-5c).

The composition of the different ECM components in native and decellularised pericardia are enlisted in Table 4-1.

Table 4-1 Quantification of the composition of different ECM components in native and decellularised pericardia. Data are expressed as mean ± SD. All the contents have been expressed as µg/mg dry tissue.

	Bovine		P values
	Native	TRICOL	
Collagen	761.42 ± 22.24	809.00 ± 14.00	0.0076
sGAG	12.59 ± 4.10	5.75 ± 1.01	0.0027
Elastin	44.95 ± 11.12	48.88 ± 18.36	0.6634
	Porcine		
	Native	TRICOL	
Collagen	817.70 ± 79.82	866.44 ± 81.62	0.3667
sGAG	8.15 ± 2.49	6.15 ± 1.01	0.0991
Elastin	49.55 ± 6.58	46.42 ± 11.78	0.5828

In bovine pericardium the water quantity increased (P<0.005) after decellularisation. This could be probably because water would fill in the cell-depleted volume of the decellularised matrix. In the opposite, for the porcine pericardium there was slight decrease (P<0.05) of water content post decellularisation (Figure 4-5d) (Table 4-2).

Interestingly, for all the other three components analysed, porcine tissues showed no significant change after treatment.

All these data indicated that the TRICOL has different effects on bovine and porcine tissue while viewed in term of quantitative composition of ECM components.

Table 4-2 Quantification of the water content in native and decellularised pericardia. *Data are expressed as mean ± SD. All the contents have been expressed as % of wet weight.*

	Native	TRICOL	P values
Bovine	81.01 ± 0.87	83.00 ± 00.00	0.0002
Porcine	78.36 ± 2.67	75.26 ± 0.95	0.0249

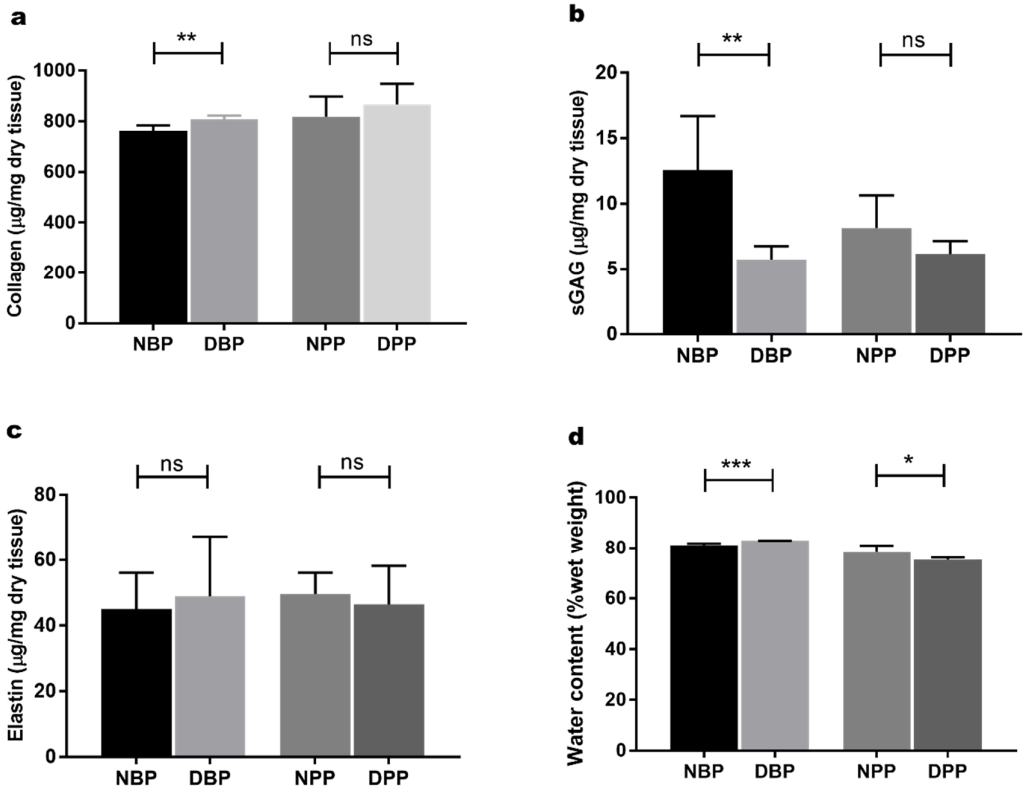

Figure 4-5 ECM content of bovine and porcine pericardia: a) Collagen, b) sGAG, c) Elastin, and d) Water.

4.1.4 DNA content

The DNA content of NBP and NPP was respectively 1777.18 ± 763.84 and 1962.59 ± 448.34 ng DNA/mg of dry tissue.

After decellularization, the DNA amount in DBP and DPP was respectively 44.80 ± 7.77 and 30.76 ± 14.95 ng DNA/mg of dry tissue (Figure 4-6). These values are inferior to the threshold of 50 ng/mg per dry tissue, set as objective criteria for assessing the efficacy of decellularisation protocols (13). Percentagewise, the DNA content was reduced by 97.48% and 98.43% in bovine and porcine TRICOL samples relative to the native ones, showing the effectiveness of the decellularisation protocol.

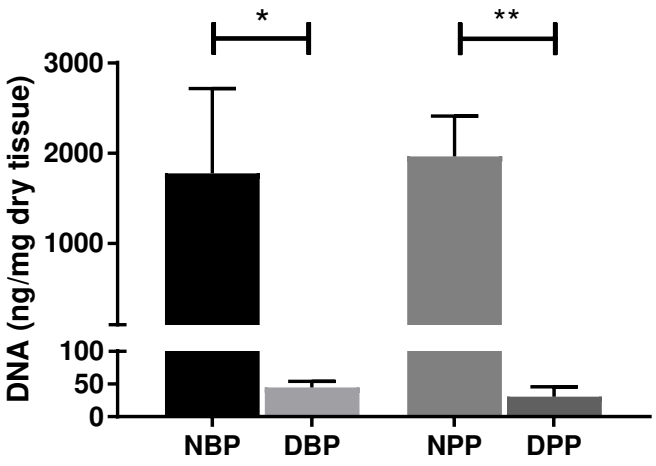

Figure 4-6 DNA content of bovine and porcine pericardia.

4.2 Fabricated bioPHV

Following the SPAC technique, a simple tubular construct of pericardial tissue was transformed to function as cusps. BioPHVs fabricated with decellularised bovine and porcine pericardia are shown in Figure 4-7 and Figure 4-8 respectively. By this modelling, in fact, the parts of the tube between the commissure points and the waist of the stent formed the cusps. After the fabrication, the cusps of the bioPHVs appear shorter than what would be normally expected using SPAC technique, as it can be observed in the figures. In reality, this appearance was only derived from the slackened behaviour of the tubular shape-fashioned decellularised tissue when in open air. As an apparent result, the cusps would seem to undergo some shrinkage.

However, when placed in a physiological solution, the cusps stretch and co-apt efficiently according to the principle of SPAC.

In addition, a pericardial skirt was formed at the annular level with the aim to prevent paravalvular leakage events.

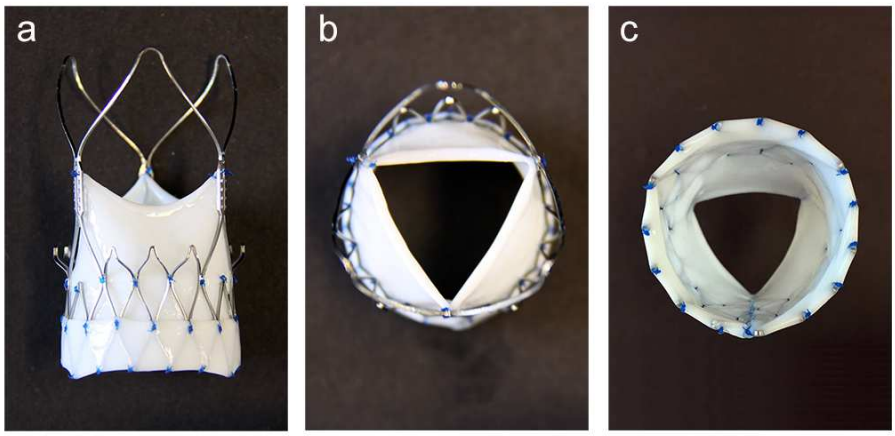

Figure 4-7 A bioPHV with decellularised bovine pericardium, B-bioPHV.

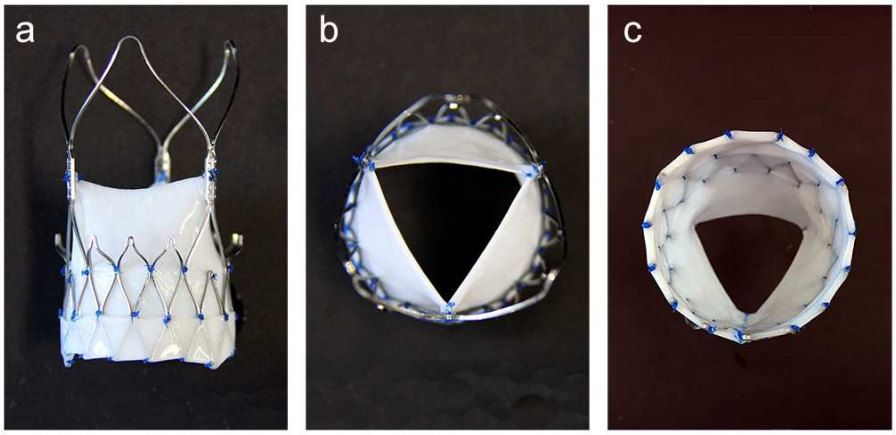

Figure 4-8 A bioPHV with decellularised porcine pericardium, P-bioPHV.

4.3 Hydrodynamic Performance

Appropriate flow and pressure were generated to properly simulate the physiologic condition the valves would encounter while implanted *in vivo*. Specially for COs of 4 and 5 l/min, dicrotic notch could also be observed in the aortic pressure curve. Representative pressure and flow waveforms generated for all the conditions are shown in Figure 4-9 and Figure 4-10.

A. B-bioPHV

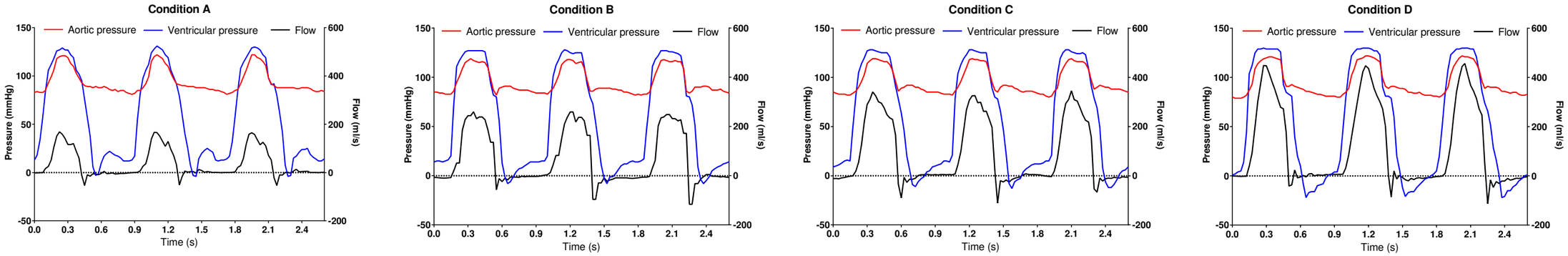

B. P-bioPHV

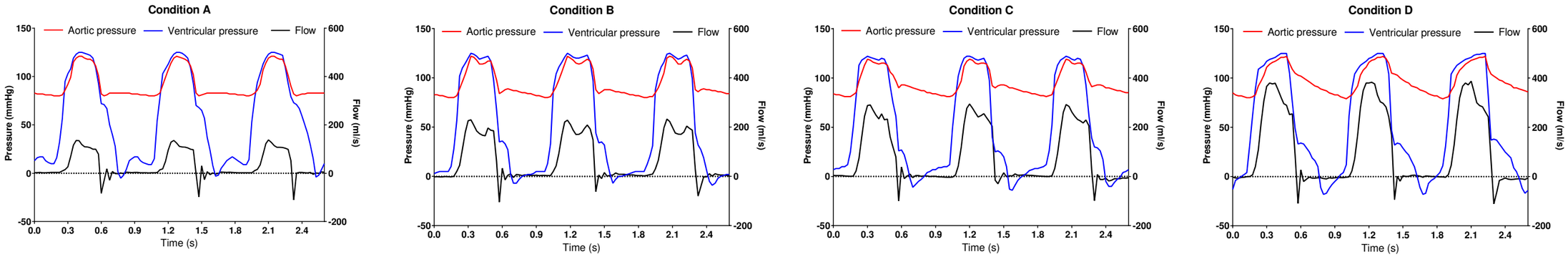

C. Control

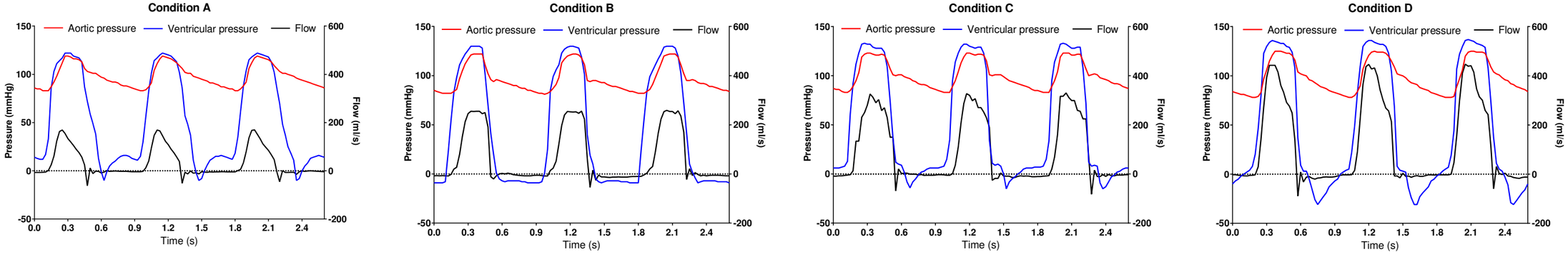

Figure 4-9 Pressure and flow curves for conditions A-D. The mean aortic and ventricular pressure remains same while the flow increases from condition A to D.

A. B-bioPHV

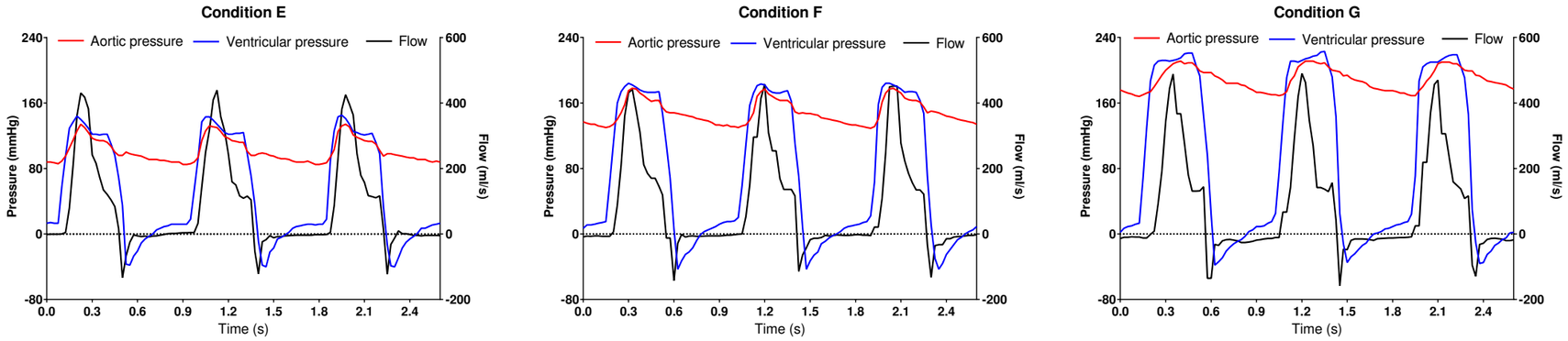

B. P-bioPHV

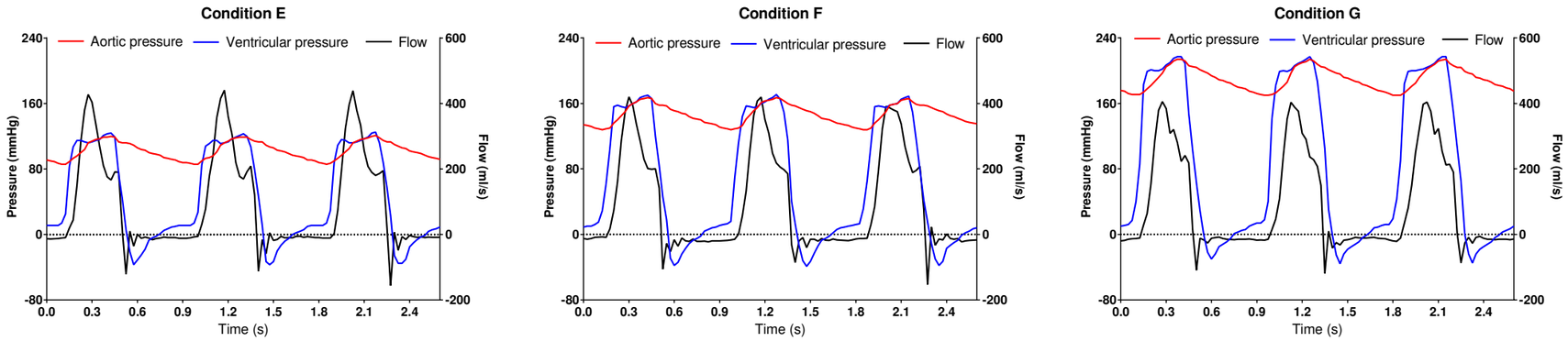

C. Control

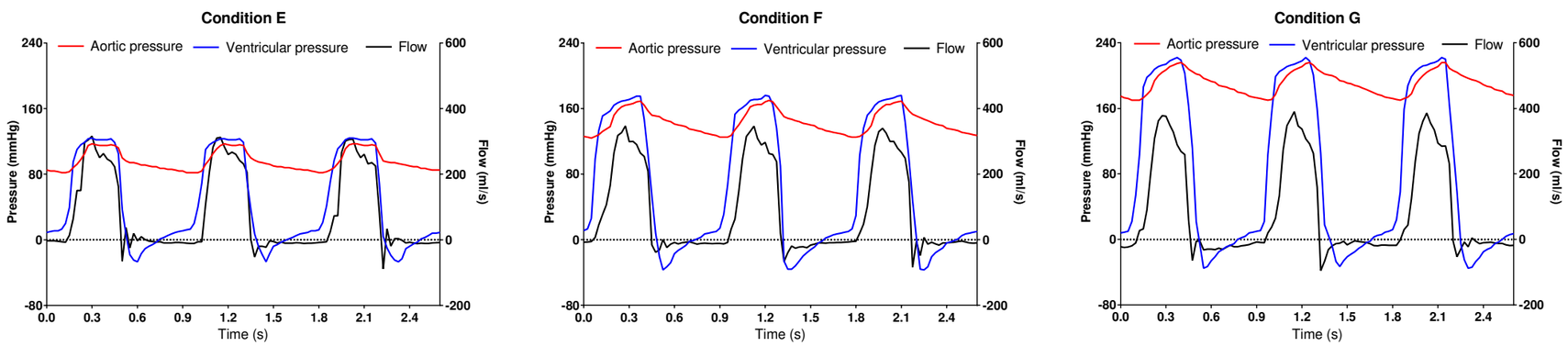

Figure 4-10 Pressure and flow curve for condition E-G. Flow remains same as the pressure increases from condition E to G

4.3.1 Minimum requirement condition

The ISO 5840-3 standard defines the minimum performance requirements for PHVs at beat rate of 70 cycles/min, cardiac output of 5 l/min and mean aortic pressure of 100 mmHg. This corresponds to condition C applied in the test. The EOA and regurgitant fractions of all tested valves fulfilled the criteria at the minimum requirement performance condition (Figure 4-11), as evidenced by the values listed in Table 4-3.

Table 4-3 Performance of the valves at minimum performance requirement condition. Data are expressed as mean ± SD. P values show statistical difference compared to ISO requirement.

	Bovine	**Porcine**	**Control**	**ISO requirement**	P values
EOA (cm^2)	1.65 ± 0.07	1.99 ± 0.13	1.58 ± 0.08	> 1.45	B < 0.0001 P < 0.0001 C < 0.0001
Regurgitation (% of forward flow)	7.38 ± 2.71	3.61 ± 1.38	6.66 ± 2.15	< 20	B < 0.0001 P < 0.0001 C < 0.0001

Legend: B: B-bioPHVs; P: P-bioPHVs; C: Control valves

The EOA and regurgitation values of P-bioPHVs were statistically different (P<0.0001) compared to both B-bioPHVs and control valves. On the other hand, there was no statistically significant difference (P>0.05) between the values of the B-bioPHVs and the controls (Figure 4-11).

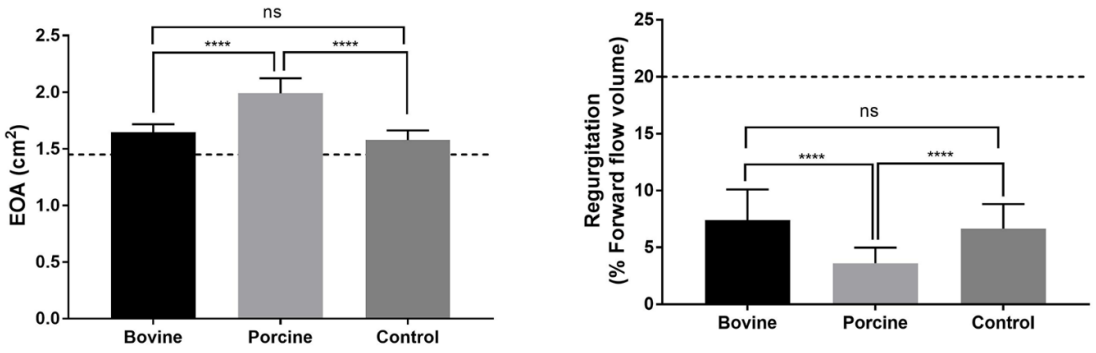

Figure 4-11 EOA and regurgitation values of all tested valves compared to the standard values. The ISO requirements are indicated with the dotted line: EOA should be greater than 1.45 cm^2 and regurgitation needs to be less than 20 %

Still video frames of the manufactured bioPHVs and control valves over one cardiac cycle showed proper opening and closing of the valve cusps during systolic and

diastolic phases (Figure 4-12). Hence, the bioPHVs, either of porcine or bovine tissue, met the performance standard set by ISO 5840-3 (163).

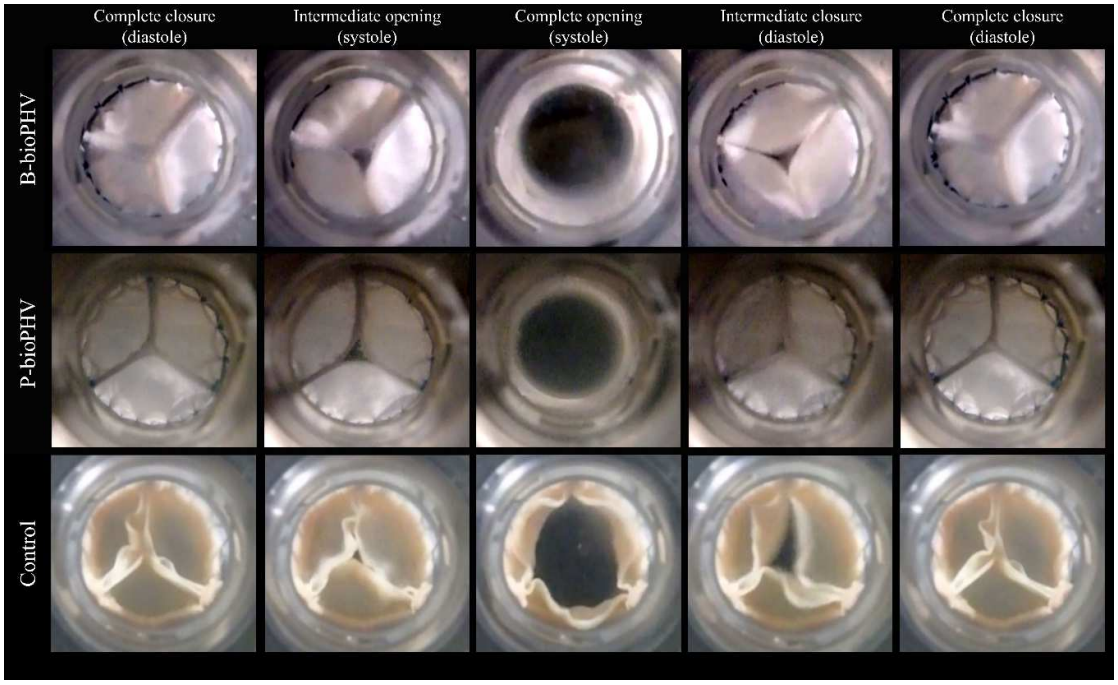

Figure 4-12 Video frames of different phases of the cardiac cycle for bioPHVs and control valve.

4.3.2 Condition A – D

Mean pressure difference (MPD)

The MPD was less than 20 mmHg in all the cases. The pressure drop for the P-bioPHVs was significantly lower ($P < 0.0001$) than for the B-bioPHVs and the control valves (Table 4-4). For conditions B and C, the MPD of the B-bioPHVs and the control valves were similar and showed no statistically significant difference. (Figure 4-13a).

Table 4-4 MPD at the four cardiac outputs. All values are expressed in mmHg. Data are expressed as mean ± SD. P values compared different types of valves for a given condition.

	A	B	C	D
Bovine	8.16 ± 0.91	9.51 ± 1.05	9.91 ± 1.01	10.62 ± 1.02
Porcine	5.21 ± 042	5.71 ± 0.55	6.02 ± 0.46	6.63 ± 0.58
Control	5.22 ± 0.34	9.31 ± 0.38	10.29 ± 0.70	12.67 ± 0.59
P values	B vs P < 0.0001 B vs C < 0.0001 P vs C > 0.9999	B vs P < 0.0001 B vs C = 0.6250 P vs C < 0.0001	B vs P < 0.0001 B vs C < 0.2149 P vs C < 0.0001	B vs P < 0.0001 B vs C < 0.0001 P vs C < 0.0001

Legend: B: B-bioPHVs; P: P-bioPHVs; C: Control valves

Effective Orifice Area (EOA)

The EOAs increased concurrently as the CO was raised from 2 to 7 l/min. The P-bioPHVs had an efficient performance among the three types of valve, as the EOA were significantly higher ($P < 0.0001$) in comparison to the B-bioPHVs and the control valves (Table 4-5). Similar to MPD, for condition B and C, the EOA of the B-bioPHVs and the control valves were similar and showed no statistically significant difference (Figure 4-13b).

Table 4-5 EOA over all four cardiac output conditions. All values are expressed in cm^2. Data are expressed as mean ± SD. P values compared different types of valves for a given condition.

	A	B	C	D
Bovine	0.83 ± 006	1.36 ± 0.09	1.65 ± 0.07	2.18 ± 0.20
Porcine	0.95 ± 0.07	1.62 ± 0.14	1.99 ± 0.13	2.45 ± 0.15
Control	1.04 ± 0.11	1.41 ± 0.05	1.58 ± 0.08	1.92 ± 0.19
P values	B vs P < 0.0001 B vs C < 0.0001 P vs C = 0.0005	B vs P < 0.0001 B vs C = 0.2491 P vs C < 0.0001	B vs P < 0.0001 B vs C = 0.0648 P vs C < 0.0001	B vs P < 0.0001 B vs C < 0.0001 P vs C < 0.0001

Legend: B: B-bioPHVs; P: P-bioPHVs; C: Control valves

Regurgitant fraction

For all three tested valves, the highest regurgitation was observed for the lowest CO of 2 l/min (condition A). The regurgitation then decreased by increasing the CO. In case of the P-bioPHVs, the regurgitation remained steady from condition B to D (Figure 4-13c) with no statistically significant difference ($P>0.05$) between the three conditions (Table 4-6)

Table 4-6 Regurgitant fraction values over all four cardiac output conditions. All values are expressed as percentage of forward flow volume. Data are expressed as mean ± SD. P values compared different types of valves for a given condition

	A	B	C	D
Bovine	10.47 ± 3.97	8.52 ± 3.40	7.38 ± 2.71	4.15 ± 1.72
Porcine	7.91 ± 2.56	4.50 ± 3.19	3.61 ± 1.38	3.06 ± 1.27
Control	11.54 ± 3.23	8.16 ± 3.79	6.66 ± 2.15	5.41 ± 1.59
P values	B vs P = 0.0104 B vs C = 0.5042 P vs C = 0.0008	B vs P < 0.0001 B vs C = 0.9310 P vs C = 0.0012	B vs P < 0.0001 B vs C = 0.4828 P vs C < 0.0001	B vs P = 0.0200 B vs C = 0.0151 P vs C < 0.0001

Legend: B: B-bioPHVs; P: P-bioPHVs; C: Control valves

Closing and leakage volumes

In most of the cases, the closing volume within a test valve did not show statistically significant variation (P>0.05) with the increase in CO. The closing volumes of the control valves were significantly lower than those of the bioPHVs for all four CO conditions. On the other hand, the leakage volumes of the control valves were higher (P<0.0001) than those of all bioPHVs (Table 4-7). The P-bioPHVs had the smallest leakage volume for all tested conditions (Figure 4-14A).

Table 4-7 Regurgitation volumes over all the cardiac output conditions. All values are in ml. Data are expressed as mean ± SD. P values compared different types of valves for a given condition.

	CO (l/min)	Bovine	Porcine	Control	P values
Closing	2	1.72 ± 0.78	1.94 ± 0.53	0.99 ± 0.22	B vs P = 0.3515 B vs C = 0.0001 P vs C < 0.0001
	4	2.28 ± 1.28	1.82 ± 1.40	0.55 ± 0.38	B vs P = 0.2977 B vs C < 0.0001 P vs C = 0.0010
	5	2.34 ± 1.01	1.48 ± 0.59	0.95 ± 0.51	B vs P = 0.0001 B vs C < 0.0001 P vs C = 0.0471
	7	1.46 ± 0.67	1.61 ± 0.94	0.92 ± 0.49	B vs P = 0.6943 B vs C = 0.0424 P vs C = 0.0058
Leakage	2	1.73 ± 0.98	0.60 ± 0.38	2.89 ± 1.22	B vs P < 0.0001 B vs C < 0.0001 P vs C < 0.0001
	4	3.17 ± 2.10	0.92 ± 1.10	4.67 ± 2.30	B vs P < 0.0001 B vs C = 0.0173 P vs C < 0.0001
	5	3.36 ± 1.74	1.28 ± 0.69	4.27 ± 1.48	B vs P < 0.0001 B vs C = 0.0602 P vs C < 0.0001
	7	2.88 ± 1.42	1.51 ± 0.94	4.81 ± 1.44	B vs P = 0.0002 B vs C < 0.0001 P vs C < 0.0001

Legend: B: B-bioPHVs; P: P-bioPHVs; C: Control valves

Energy losses

The energy loss during forward flow phase accounted for the majority of the total loss. The control valves had the highest forward and closed energy loss values for all the COs, while the P-bioPHVs had the least ones. The closing energy formed the smallest share of the total loss for all the valves. The forward energy loss increased with higher CO for all the three types of tested valves (Table 4-8). However, the closing and closed energies did not vary significantly, specially for COs 4 to 7 l/min (Figure 4-14 B).

Table 4-8 Energy losses over different cardiac cycles. All values are in mJ. Data are expressed as mean ± SD. P values compared different types of valves for a given condition

	CO (l/min)	Bovine	Porcine	Control	P values
Forward	2	34.01 ± 4.10	21.59 ± 2.87	25.31 ± 4.08	B vs P < 0.0001 B vs C < 0.0001 P vs C = 0.0022
	4	71.58 ± 11.01	50.71 ± 7.44	87.38 ± 10.09	B vs P < 0.0001 B vs C < 0.0001 P vs C < 0.0001
	5	93.62 ± 9.95	72.01 ± 10.09	134.10 ± 9.97	B vs P < 0.0001 B vs C < 0.0001 P vs C < 0.0001
	7	131.67 ± 10.75	95.23 ± 12.19	189.87 ± 17.75	B vs P < 0.0001 B vs C < 0.0001 P vs C < 0.0001
Closing	2	4.87 ± 5.33	5.91 ± 1.58	9.71 ± 4.40	B vs P = 0.5796 B vs C = 0.0003 P vs C = 0.0049
	4	11.27 ± 7.90	19.78 ± 8.64	14.72 ± 4.86	B vs P = 0.0001 B vs C = 0.2615 P vs C = 0.0601
	5	9.82 ± 6.87	22.91 ± 6.12	21.50 ± 7.39	B vs P < 0.0001 B vs C < 0.0001 P vs C = 0.7499
	7	11.18 ± 3.85	24.13 ± 8.35	19.10 ± 6.43	B vs P < 0.0001 B vs C = 0.0002 P vs C = 0.0238
Closed	2	20.00 ± 7.41	16.21 ± 5.19	31.15 ± 12.38	B vs P = 0.1868 B vs C < 0.0001 P vs C < 0.0001
	4	36.27 ± 18.37	24.09 ± 9.72	56.59 ± 22.22	B vs P = 0.0177 B vs C = 0.0002 P vs C < 0.0001
	5	39.88 ± 16.15	24.64 ± 7.98	48.76 ± 15.53	B vs P = 0.0001 B vs C = 0.0648 P vs C < 0.0001
	7	38.81 ± 12.60	24.62 ± 8.73	61.01 ± 16.31	B vs P < 0.0001 B vs C < 0.0001 P vs C < 0.0001

Legend: B: B-bioPHVs; P: P-bioPHVs; C: Control valves

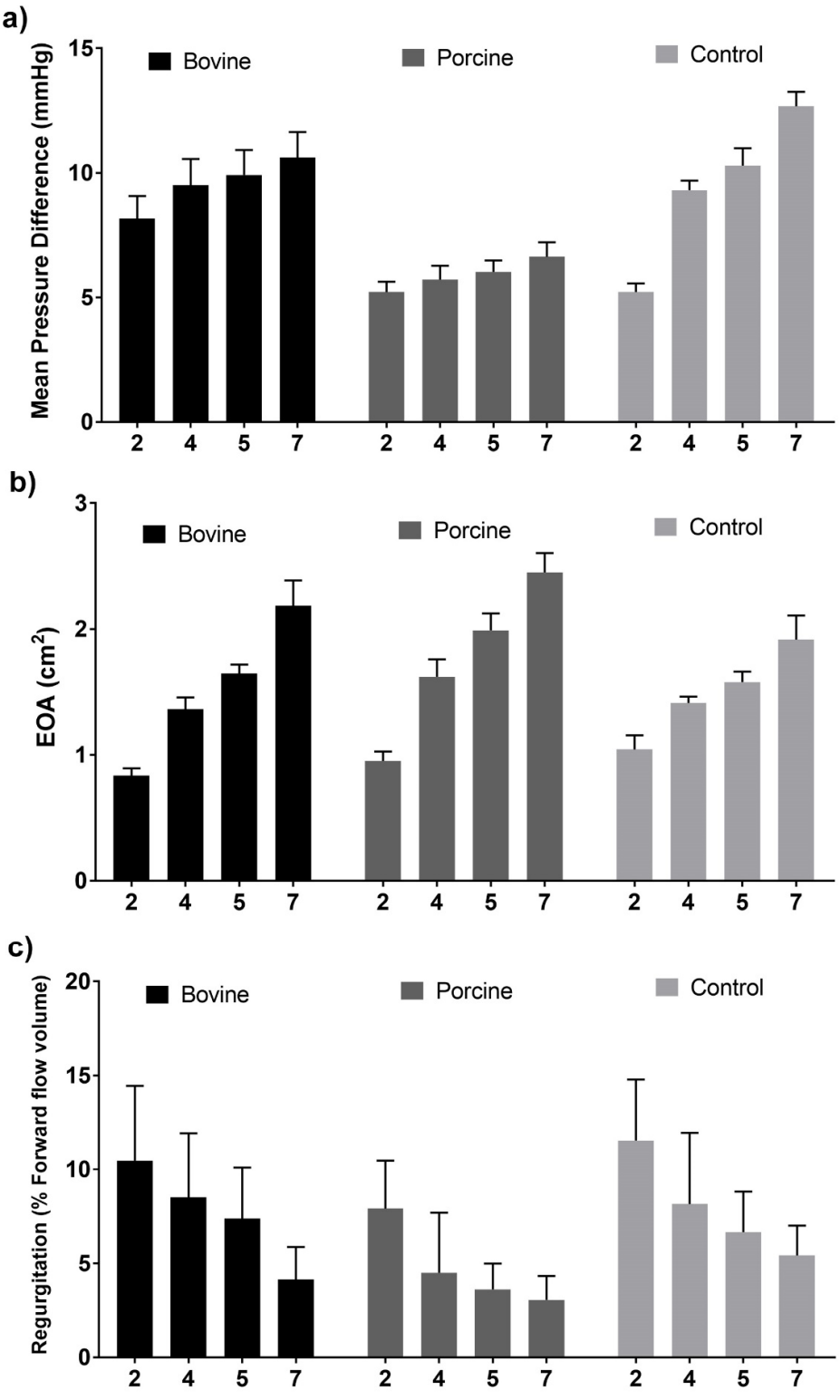

Figure 4-13 Hydrodynamic parameters over all the cardiac outputs. a) MPD, b) EOA, c) Regurgitant fraction. Note that all MPD are inferior to 20 mmHg. EOAs increased concurrently with COs, on the contrary regurgitation fraction decreased. *Data are expressed as mean ± SD, n = 30 for B-bioPHVs and P-bioPHVs (three valves, each tested over 10 cycles) and n = 20 for control valves (two valves tested over 10 cycles).*

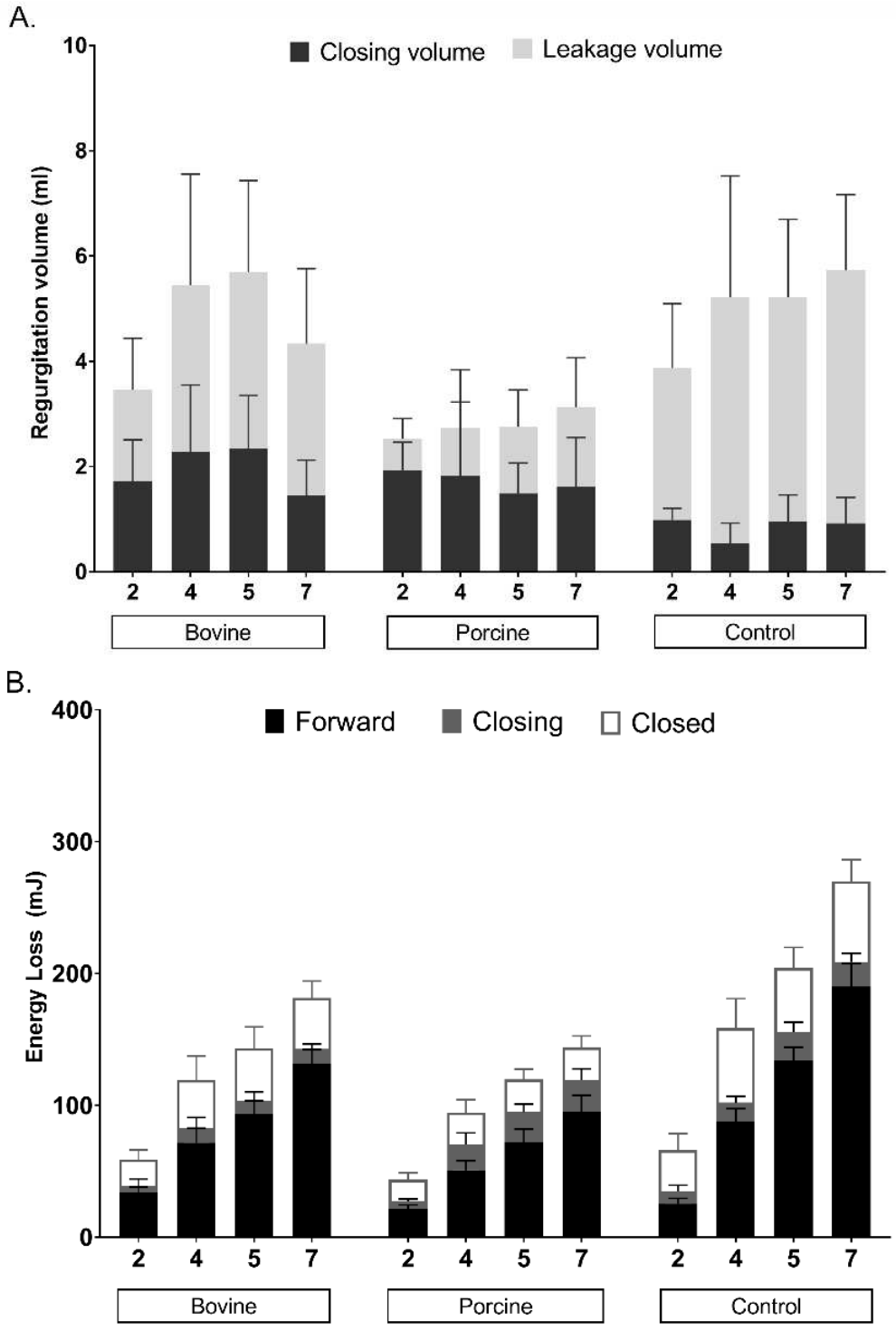

Figure 4-14 Breakdown of regurgitant volumes and energy losses over the different cardiac outputs. A) Closing and leakage volumes B) Energy losses during forward, closing and closed phases of the cardiac cycle. It can be appreciated that P-bioPHVs had the lowest leakage volumes. On the other hand, for all the tested valves the energy losses increased with CO increase. *Data are expressed as mean ± SD, n = 30 for the B-bioPHVs and the P-bioPHVs (three valves, each tested over 10 cycles) and n = 20 for the control valves (two valves tested over 10 cycles).*

4.3.3 Condition E - G

The regurgitation fraction remained below 20 % for all the back-pressure conditions. The P-bioPHVs had the smallest values (P<0.01), while the B-bioPHVs and the control valves had statistically similar regurgitation values (Table 4-9 and Figure 4-15 A).

For each type of valve, there was no variation between the closing volumes at the three different back pressure conditions. This implied that closing volume mainly depends on CO since the flow rate was analogous for the conditions E-G (Figure 4-15 B). Similar to conditions A-D, the control valves had the lowest closing volume and largest leakage volumes in all conditions (Table 4-10).

Table 4-9 Regurgitation fractions at back pressure conditions. All values are in % of forward flow volume. *Data are expressed as mean ± SD. P values compared different types of valves for a given condition.*

	E	F	G
Bovine	8.61 ± 3.42	9.32 ± 2.80	16.26 ± 2.43
Porcine	5.56 ± 2.74	8.14 ± 4.01	8.08 ± 3.40
Control	8.28 ± 3.42	11.11 ± 3.11	15.03 ± 4.10
P values	B vs P = 0.0011 B vs C = 0.9327 P vs C = 0.0113	B vs P = 0.3682 B vs C = 0.1634 P vs C = 0.0086	B vs P < 0.0001 B vs C = 0.4031 P vs C < 0.0001

Legend: B: B-bioPHVs; P: P-bioPHVs; C: Control valves

Table 4-10 Regurgitation volumes at back pressure conditions. All values are in ml. *Data are expressed as mean ± SD. P values compared different types of valves for a given condition.*

	Closing volume			Leakage volume		
	E	**F**	**G**	**E**	**F**	**G**
Bovine	3.63 ± 1.29	3.69 ± 1.71	4.08 ± 2.10	3.22 ± 3.17	3.80 ± 2.04	9.72 ± 3.27
Porcine	2.15 ± 0.78	2.59 ± 0.91	2.53 ± 0.82	2.27 ± 1.96	3.98 ± 3.22	4.03 ± 2.92
Control	1.14 ± 0.86	1.64 ± 0.65	2.03 ± 1.14	5.57 ± 2.77	7.49 ± 2.67	10.28 ± 3.34
P values	B vs P < 0.0001 B vs C < 0.0001 P vs C = 0.0009	B vs P = 0.0030 B vs C < 0.0001 P vs C < 0.0001	B vs P = 0.0003 B vs C < 0.0001 P vs C = 0.0211	B vs P = 0.3645 B vs C = 0.0086 P vs C = 0.0002	B vs P = 0.9623 B vs C < 0.0001 P vs C < 0.0001	B vs P < 0.0001 B vs C = 0.8113 P vs C < 0.0001

Legend: B: B-bioPHVs; P: P-bioPHVs; C: Control valves

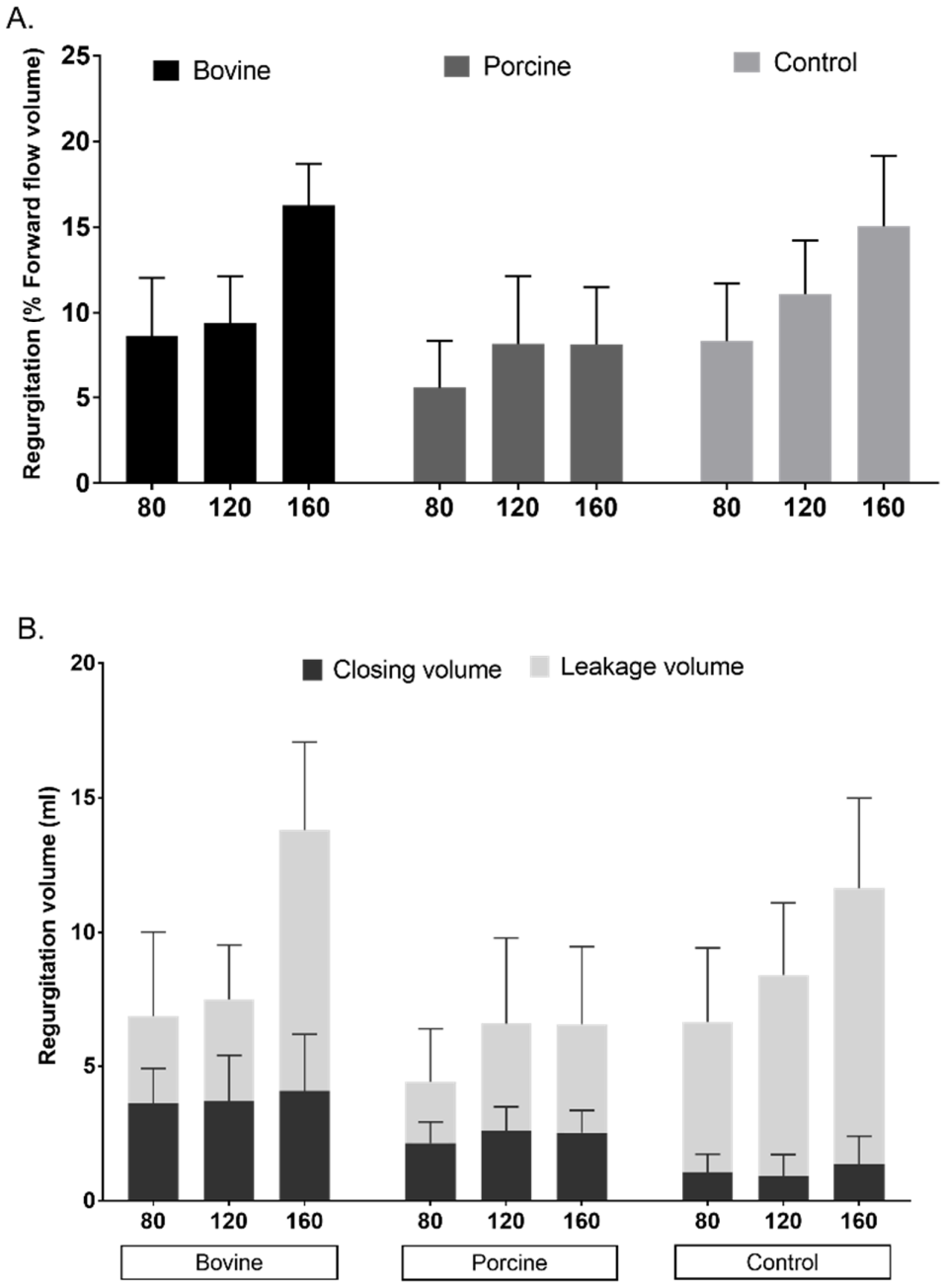

Figure 4-15 Valve performance at back pressure conditions. A) Regurgitation fractions B) Regurgitation volumes. These values demonstrated that the bioPHVs functioned equally well also in back pressure conditions. *Data are expressed as mean ± SD, n = 30 for the B-bioPHVs and the P-bioPHVs (three valves, each tested over 10 cycles) and n = 20 for the control valves (two valves tested over 10 cycles).*

4.4 Effects of crimping

4.4.1 Gross examination

The B-bioPHVs and the P-bioPHVs, after crimping, revealed no macroscopic evidence of traumatic injury to the pericardial cusps. There were optimal pericardial cusp coaptation in the absence of tears, perforations or folding (Figure 4-16 and Figure 4-17). The prosthetic frame showed a preserved shape without distortion.

A. 20 minutes crimping

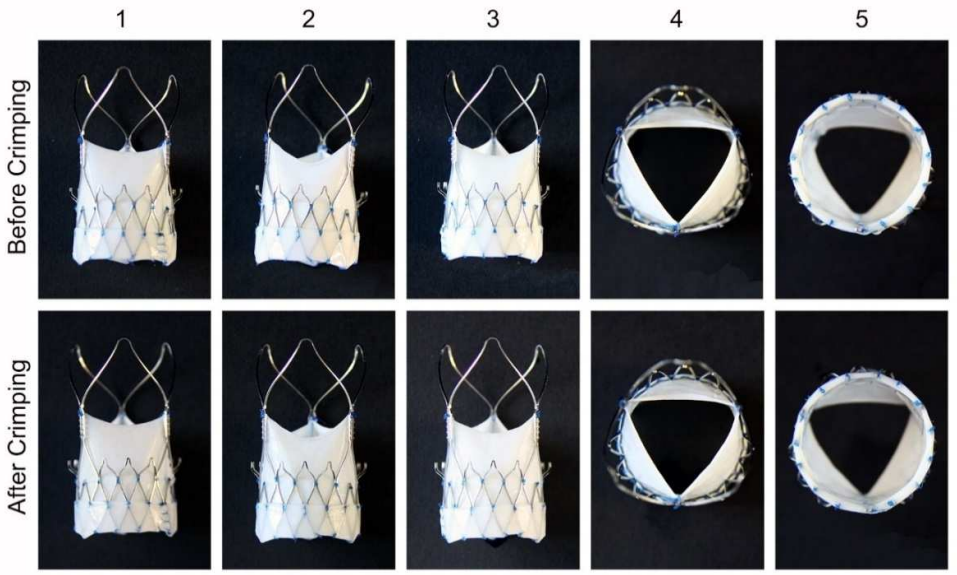

B. 60 minutes crimping

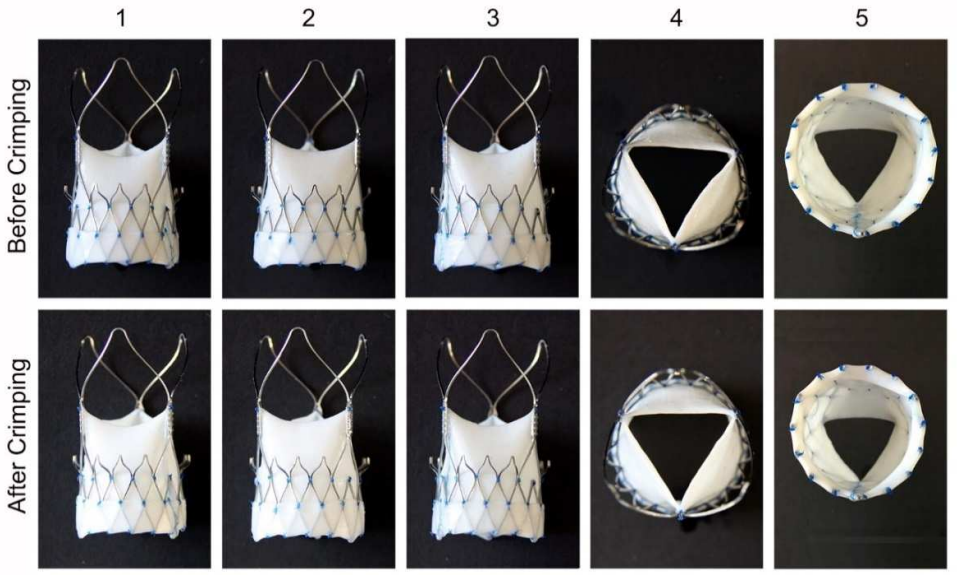

Figure 4-16 Gross images of the B-bioPHVs before crimping and after crimping for 20 and 60 minutes. 1-3) Side views; 4) aortic view; 5) ventricular view

A. 20 minutes crimping

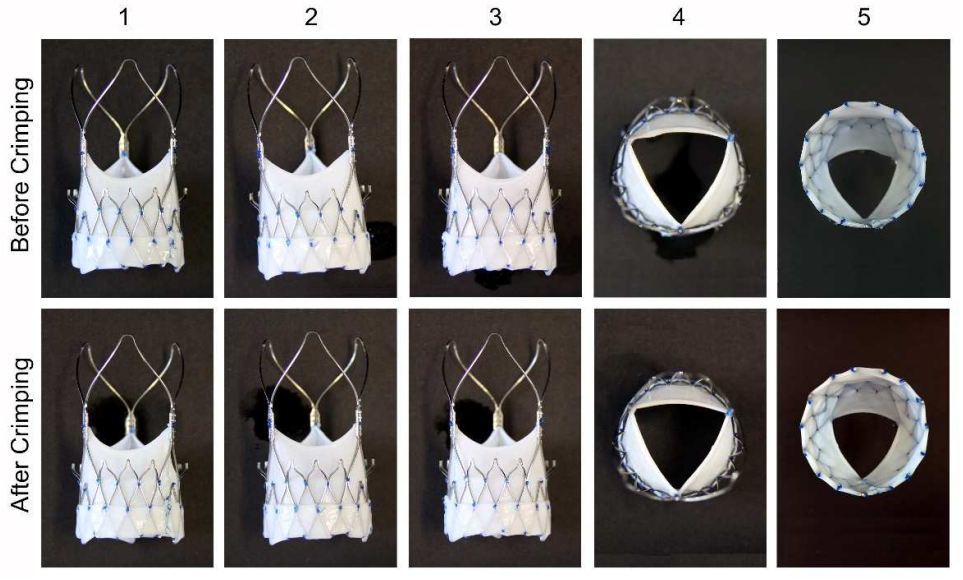

B. 60 minutes crimping

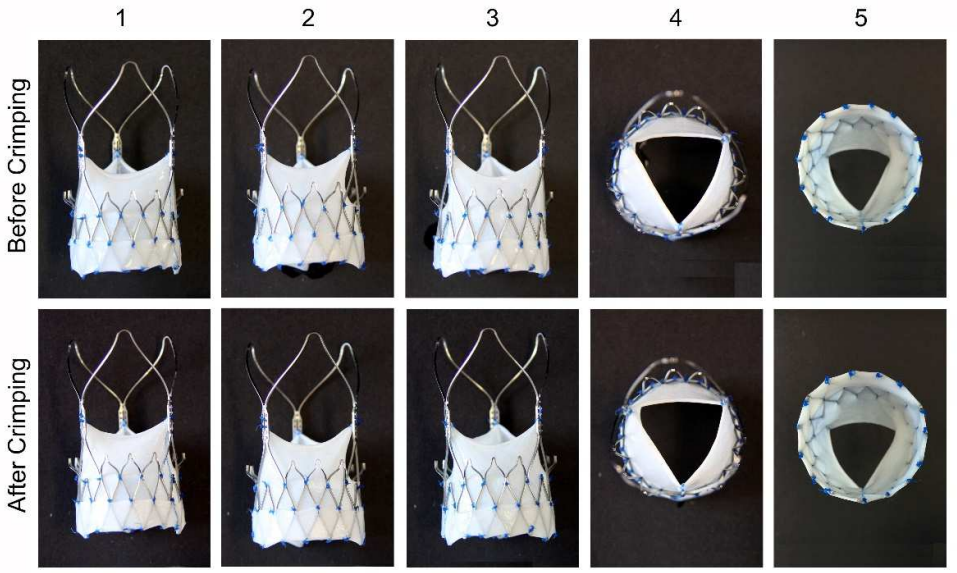

Figure 4-17 Gross images of the P-bioPHVs before crimping and after crimping for 20 and 60 minutes. 1-3) Side views; 4) aortic view; 5) ventricular view

4.4.2 Microscopic evaluation

Histological analyses showed fair preservation of the pericardial tissue, intact preservation of the collagen bundles with neither disruptions, interruptions nor fragmentations in both bioPHVs. No distortion was detected also in depth of collagen fibers (Figure 4-18 and Figure 4-19).

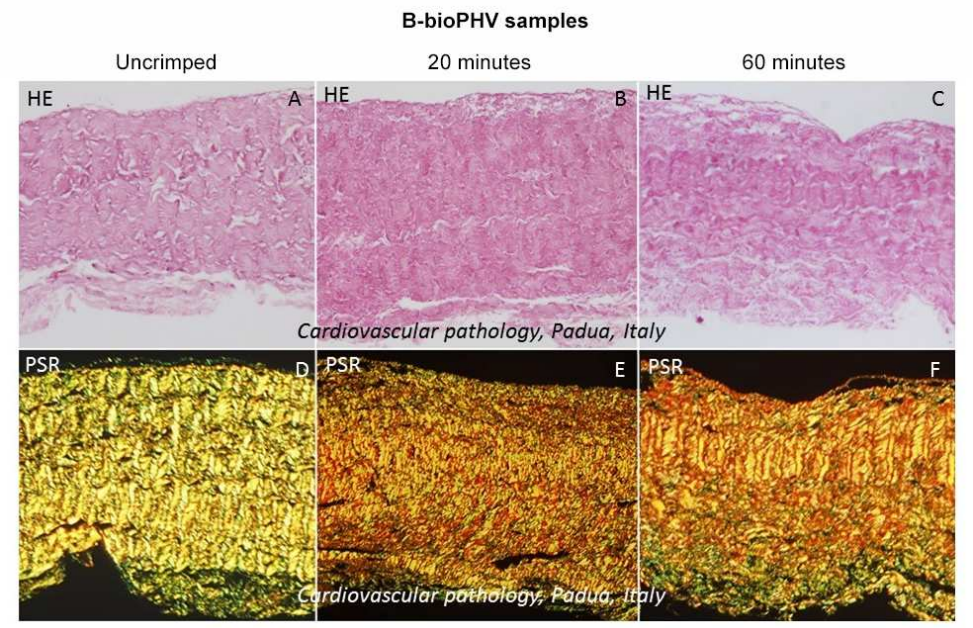

Figure 4-18 Histology of samples from the B-bioPHVs. Collagen fibers waviness of pericardial cusps in control and at different times of crimping. A-C) hematoxylin-eosin, D-F) Picrosirius Red stain at polarized light. A-F) 50x, original magnification.

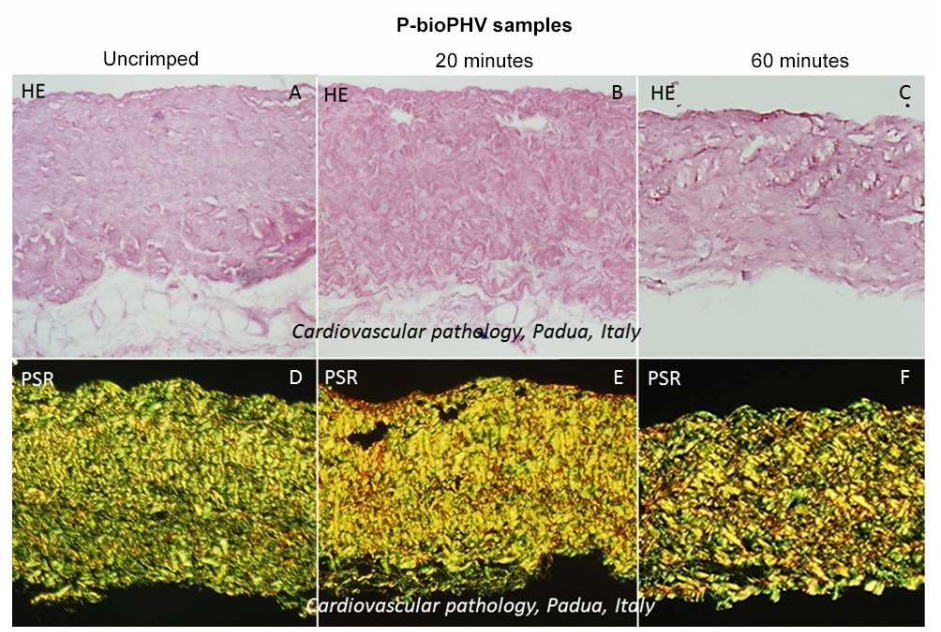

Figure 4-19 Histology of samples from the P-bioPHVs. Collagen fibers waviness of pericardial cusps in control and at different times of crimping. A-C) hematoxylin-eosin, D-F) Picrosirius Red stain at polarized light. A-F) 50x, original magnification.

4.4.3 Morphometrical analysis

The measurements of *fibrosa* collagen wavelength periodicity were 8.54 ± 2.22 µm and 9.36 ± 2.43 µm in the B-bioPHVs submitted to 20 and 60 minutes crimping, respectively, and 9.39 ± 2.20 µm in the uncrimped controls (P=NS). In the native and decellularised unmounted pericardium collagen wavelength periodicity was 7.69 ± 2.72 µm and 8.72 ± 2.05 µm (P<0.05), respectively (Table 4-11). Statistically significant differences were observed in the comparison among uncrimped, 20 minutes, 60 minutes crimped B-bioPHVs and native bovine pericardium (Table 4-11).

Table 4-11 B-bioPHVs. Histogram displaying collagen wavelength at different crimping duration in comparison with controls (native, decellularised unmounted pericardium and uncrimped valves). All values are expressed as mean ± SD. The measurements are in µm.

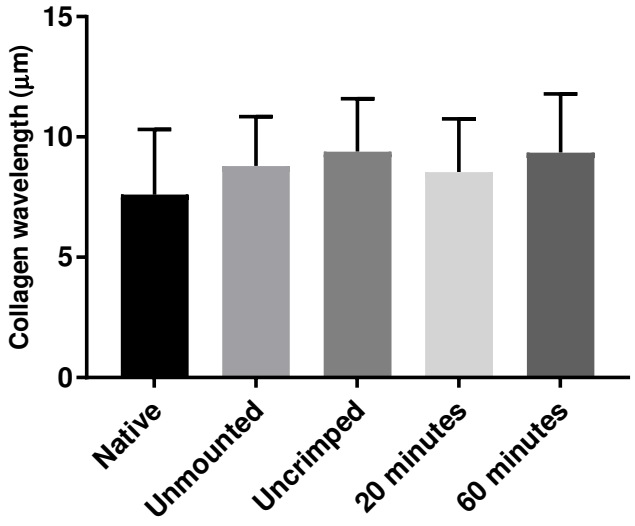

Native	Unmounted	Uncrimped	20 minutes	60 minutes
7.61 ± 2.71	8.79 ± 2.05	9.39 ± 2.20	8.54 ± 2.22	9.36 ± 2.43

Regarding the P-bioPHVs, the measurements of *fibrosa* collagen wavelength periodicity did not reveal any statistically significant differences among the study groups (20 minutes: 8.30 ± 1.30 µm; 60 minutes: 7.97 ± 1.58 µm) and the uncrimped controls (7.78 ± 1.70 µm), as well as the native and the decellularised unmounted pericardium (7.37 ± 2.51 µm and 8.63 ± 1.98) (P=NS) (Table 4-12).

Table 4-12 P-bioPHVs. Histogram displaying collagen wavelength at different crimping duration in comparison with controls (native and decellularised unmounted pericardium and uncrimped valves). All values are expressed as mean ± SD. The measurements are in µm. No statistical differences were observed among the groups.

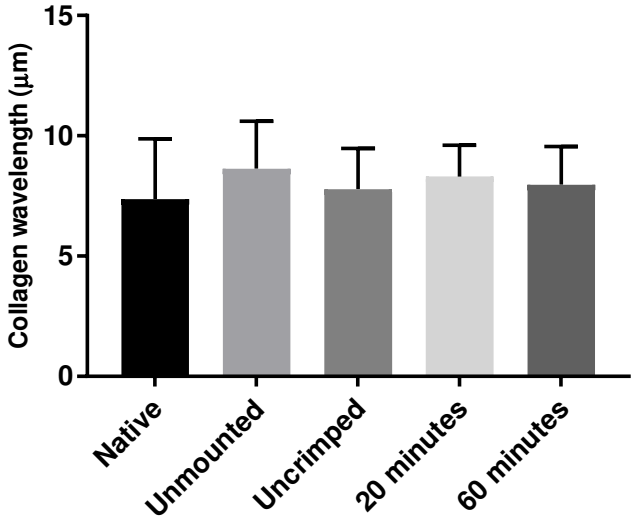

Native	Unmounted	Uncrimped	20 minutes	60 minutes
7.37 ± 2.51	8.63 ± 1.98	7.78 ± 1.70	8.30 ± 1.30	7.97 ± 1.58

5. DISCUSSION AND FUTURE OUTLOOK

TAVI has now been established as a formidable treatment modality for HVD, specially in high risk patients. It emerged in 2002 as an expansion of the cardiology field of transcatheter interventions (164). Since then, during this 15-year period, TAVI technology has seen lot of developments, especially in the design of its replacements, i.e. the PHVs, and is still in course of improvement and enhancement.

In this project, a novel generation of PHVs has been realised with cusps based on decellularised scaffolds. These advanced PHVs, i.e. the bioPHVs, have been envisioned with the aim at addressing the issue of limited durability, associated with the current replacements, whose cusps are made with chemically treated tissues.

Bovine and porcine pericardia were decellularised with the well-established TRICOL decellularisation protocol, which has already been successfully applied on pulmonary and aortic heart valves (12).

As demonstrated by histology, immunofluorescence, and biochemical analysis, TRICOL revealed to be equally successful for the decellularisation of both porcine and bovine pericardia. In fact, after decellularisation the general histoarchitecture of the original ECM demonstrated to be well preserved while cell components, included nuclei, were removed. Moreover, the immunodetection of specific components of the ECM revealed the preservation of main fibers, collagen I and elastin, as well as of collagen IV, laminin and heparan sulfate in both bovine and porcine TRICOL pericardia. This is of major significance as the basal membrane plays an important role for cell adhesion, as initial step for the development of regenerating tissues after implantation.

Quantitative biochemical assessments showed there was an apparent increase of collagen content in the decellularised tissues, with the difference being statistically significant in the case of the bovine pericardium. The increase of collagen content is due to the loss of cells and soluble proteins, which causes the decrease of weight. Since the collagen content is normalized to the dry weight, it appears that the decellularization introduced a gain of collagen content. This is in line with the theory of conservation of collagen reported by Courtman *et al.* (136).

A decrease of sGAG content was revealed after decellularisation with statistically significant difference only for bovine pericardium, as our group already reported for

both valves and pericardial tissues (11). Similar findings of loss of GAGs during decellularisation of bovine pericardium with Triton X-100, ATE and alkaline treatments have been reported by Wong *et al.* and Mendoza-Novelo *et al.* (137, 165) and they suggested that the removal of GAG facilitates decellularisation processing by increasing the access of the decellularisation reagents to diffuse into the tissue. Roosens *et al.* and Dong *et al.*, applying Triton X-100, sodium deoxycholate and trypsin, also reported similar loss for decellularised porcine pericardium (166). The most probable reason for GAGs removal is the fact that they are linked to the ECM with weaker chemical binding than collagen or elastin and this induces them to be washed away more easily. An emerging hypothesis argues that the loss of GAGs in decellularized tissues could be protective from the onset of calcification (167). However, it is also necessary for successful HVRM approaches to consider the natural role of GAGs. In the native heart valve, GAGs play an important activity in maintaining its proper biomechanical properties, since they participate to the cushioning of mechanical stresses in the *spongiosa* of the heart valve cusps during the opening and closure cycle. Hence, while it is inevitable that some amount of GAGs gets removed during decellularisation, it is necessary that the degree of loss does not have detrimental effects. Further studies should be performed to evaluate the positive and negative effects associated to GAGs content.

Publications by Dong *et al*. and Roosens *et al*. about decellularisation, based on Triton X-100 and sodium deoxycholate, reported that also elastin content was decreased following decellularisation process. This led to suggestions that detergents could have more impact on elastin of pericardial tissues and that elastic fibers with low levels of organisation could be more susceptible to degradation or solubilisation by the decellularisation agents. By contrast, our study showed that the elastin content was preserved after decellularisation, as also observed in the immunofluorescence staining.

All the outcomes of this project revealed that TRICOL exerts a more preservative effect on the ECM components, in respect to the methods described before for pericardium decellularization. This is particularly pivotal in heart valve tissue engineering and regeneration.

In HVRM, in fact, it is fundamental to rely on an original, mature, and well-preserved ECM scaffolding, as a functional starter matrix. This ideal property might be difficultly replicated by the use of other synthetic polymeric scaffolds.

Another key aspect in decellularization is the removal of cellular material, which should reach the highest yield in order to prevent inflammatory, immunologic and calcific events once the decellularized scaffold is implanted in the patient. In this context, Crapo *et al.* defined in 2011 the minimal criteria to satisfy the intent of decellularisation as (127):

- less than 50 ng dsDNA per mg ECM dry weight;
- lack of visible nuclear material in tissue stained with DAPI or H&E

Histological and DNA content analysis of TRICOL decellularised bovine and porcine pericardium fulfilled these criteria.

In the evaluation of DNA residues, it appears more and more important to identify if remaining sequences might have coding ability. It is highly probable that DNA sequences longer than 200 base pairs (bp) might have this capability. Ongoing experiments in our lab are evaluating whether TRICOL-treated tissues could still possess >200 bp DNA of the donor, i.e. porcine and bovine coding nuclear material.

Additionally, TRICOL is all effective in removal of α-gal xenoantigen a powerful trigger of hyperacute rejection in xenotransplantation (33, 168) thus rendering available tissues with high biocompatibility.

In addition to the characterisations mentioned, mechanical tests on native and decellularised pericardium (unpublished internal data) demonstrated that after decellularisation there was a tendency towards a decrease of elastic modulus, which is statistically significant for porcine pericardium. However, there was no change in terms of ultimate tensile strength before and after decellularisation.

Under the profile of decellularization effectiveness, TRICOL pericardia of bovine and porcine origins are, therefore, suitable materials for cardiovascular applications and, in particular, we tested them as biomaterials for the manufacturing of bioengineered PHVs.

The two main components of a PHV are the stent and the cusp material. As generously provided by Symetis, commercial stents currently applied in the clinical setting in the

ACURATE neo™ TF TAVI system, were utilised to fabricate the bioPHVs. The use of these CE-marked stents created a solid basis for achieving the aim of this study, i.e. the evaluation of the potential of decellularised pericardium to perform adequately as cusp biomaterial for novel bioPHVs.

Decellularised pericardia, either bovine or porcine, were mounted onto these stents following a simple but efficient technique based on the concept of tubular cusps design. A single patch of pericardium was converted into a tube, which was then transformed to function as three cusps through attachment of the tube to the stent with the SPAC method. In the currently available bioprosthetic heart valves and PHVs, the cusps are formed by joining together three separate sheets of pericardium, a procedure which requires lots of suturing and stitches. However, it is desirable to have as less sutures as possible since the stitch holes are the focal points susceptible to tissue tear in the region of flexion (169). Through the implementation of a the SPAC technique, it was possible to reduce the amount of sutures to the minimum required, demonstrating that this simple method might be equally competent to realize the cuspal function.

ISO 5840-3 defines the guidelines for the hydrodynamic testing of heart valve substitutes intended for implantation by transcatheter technique (163).

In order to verify if the developed bioPHVs fulfilled the minimal requirements, we performed their validation by assessment at 5 l/min cardiac output (condition C applied in this study), as required for all transcatheter devices following the ISO 5840-3.

The MPD, EOA and regurgitation values that we determined during this study for both bioPHVs and control valves are comparable to the corresponding ones reported in the literature in the *in vitro* tests of Medtronic CoreValve, Edwards SAPIEN XT and other new transcatheter heart valves (169, 170).

MPD values above 20 mmHg are considered as indicative of valve stenosis (171). All tested valves demonstrated MPD below this threshold for all the conditions. In particular, the P-bioPHVs always displayed lower MPDs, with the highest pressure drop being 6.63 mmHg. As a general observation, the MPD values tended to increase as the CO was raised. The B-bioPHVs and the P-bioPHVs showed a slow rate of increment in MPD, while for the control valves a sharp rise of MPD was documented from 2 to 7 l/min.

Altogether, the EOA varied from the smallest value of 0.83 cm^2 to the largest one of 2.45 cm^2 for the CO range from 2 to 7 l/min. Similar to MDP, also EOA increased concurrently with rising CO, but in this case linearly. Contrary to MPD values, a faster increment rate was appreciated for the B-bioPHVs and the P-bioPHVs with changing CO, while the change remained more restrained for the control valves. This large variation in EOA of the bioPHVs compared to control valves is related to the different mechanical properties of their composing tissues. In fact, the decellularised tissue is more flexible than the glutaraldehyde-fixed one of the control valves. Uniaxial tensile loading to failure test (unpublished internal data) showed that compared to both bovine and porcine pericardia, glutaraldehyde-treated tissues have higher elastic modulus than the decellularised counterparts. This likely indicates that following glutaraldehyde fixation the tissue, independently on the species considered, becomes less compliant and loses flexibility. As a result, with increasing CO the opening of control valves does not change so much, while in case of bioPHVs the opening of the valve increases drastically with CO due to the more flexible tissue. Such outcomes are also confirmed from the still video frames captured during the hydrodynamic tests, which show that the control valves have smaller opening than the bioPHVs for corresponding CO during systole (Figure 4-12).This wider opening of bioPHVs means they will offer lesser resistance to blood flow through heart and thus reduced workload on the heart muscle. This would be a clear advantage over the current commercial valves.

The total regurgitation fraction remained always below 20% for all types of valves. Further analysis revealed that the bioPHVs had significantly lower leakage volume compared to the control valves. This suggests that the pericardium skirt in the bioPHVs is effective in preventing possible paravalvular leakage. On the other hand, the control valves always had smaller closing volume than the bioPHVs, implying they needed less volume of fluid to force their closure. This is expected since as mentioned earlier the control valves open less and therefore also need small volume of back-flowing fluid to close them. On the contrary, the bioPHVs have wider opening during systole, thus implying they require bigger closing volumes.

In addition to regurgitation, another indicator providing a more comprehensive idea of the hydrodynamic performance is the energy loss. The lower energy loss incurred in the bioPHVs compared to the control valves showed that the first ones might impose less workload on heart muscles, in accordance to what was indicated through the

results of EOA. These data, taken together, might be suggestive of a superior hydrodynamic performance of the bioPHVs in respect to the control valves. Moreover, the P-bioPHVs showed lower energy loss among the two bioengineered valves, thus indicating their possible hemodynamical advantage over the B-bioPHVs.

The back-pressure conditions simulated during the hydrodynamic test represent the extreme circumstances that are often observed in the high risk patients who receive a TAVI treatment. In fact, patients with a diagnose of severe aortic stenosis present systolic blood pressure reaching to values of 200 mmHg (172). For these reasons, ISO 5840-3 recommends checking regurgitant volumes at these back pressure conditions (163). All three types of valves performed optimally at these pressure settings, as no events of severe regurgitation were reported. This also suggests that the developed bioPHVs are able to withstand these extreme conditions and that the suturing technique used to fabricate the bioPHVs is qualified for resistant PHV manufacturing.

Following the positive outcomes from hydrodynamic test, decellularised pericardial tissue also did not show any lacerations of disruption and comparable collagen wave period length measurements after crimping. Both macroscopic and microscopic examination revealed that the pericardial tissue remained free of severe damage or fracture, after different durations of crimping. This is in contrast to the reported cases of traumatic injury and fragmentation on pericardial cusps in the literature (146, 147). In particular, for the decellularised porcine pericardial cusps, *fibrosa* collagen wavelength periodicity did not reveal any statistically significant differences among groups. Only in the case of decellularised bovine pericardial cusps, comparison among the native and study groups showed statistically significant differences in terms of collagen wavelength periodicity. The significant loss of GAGs observed in bovine pericardium after decellularisation might be the basis of the quantitative modifications of collagen waviness. Apart from this possible explanation, further causes should be evaluated, also in relationship to the differential cell/ECM ratio displayed by the pericardial tissues of the two species and hence to the effects that their cell loss could exert in the dynamically reciprocal ECMs. In any case, since the results demonstrated that collagen tissue natural waviness is maintained, even after crimping procedure, we can conclude that the choice of decellularised pericardium is safe for PHV.

In general, a limitation in this study could be related to the lack of enough statistical power due to the small sampling number adopted. A large sample size would be possibly needed to increase the statistical power. Nevertheless, the confidence on the likelihood of achieved results has been obtained by the homogeneous representation observed during *in vitro* sample studies.

Overall, P-bioPHVs performed better in terms of the hydrodynamic parameters. Moreover, since porcine pericardium is thinner than bovine, it would allow to achieve smaller crimped profile, as desired for PHV valves. These outcomes provide an indication that the porcine pericardium might be a better option for PHV fabrication than the bovine counterpart. However, the development of a novel PHV is a challenging and lengthy process and needs to take into account other aspects to ascertain its durability. In order to further establish this, the next step in the development of these bioPHV prototypes will be to conduct fatigue test following the guidelines of ISO 5840-3. The fatigue test performed on unseeded bioPHVs will give an idea about the long-term stability of the stented decellularised scaffold. This crucial assay will give a clearer insight on which decellularised tissue exhibits superior properties for the realisation of durable bioPHVs. However, since the conditions simulated during the standard durability test are not physiological, it would not be suitable to test the durability of cell-seeded bioPHVs *in vitro*. Thus, the next logical step will be the assessment of valve performance through *in vivo* validation in a large animal model. As previously demonstrated by our group, the minipig represents the ideal model for testing heart valve substitutes due to its similarities to a human being (blood coagulation, growth rate, etc.) (173). Following an approach of tissue guided regeneration, the bioPHVs could be implanted without previous cell conditioning. In order to facilitate the fast re-endothelialisation in the recipient, the decellularised pericardium might be processed through some surface treatments or modifications to enhance its homing of circulating cells (142). To sum up, this study is an important stepping stone for shifting the field of transcatheter valve replacement from current degenerative PHVs to a new generation of regenerative PHVs.

6. REFERENCES

1. Brinkley DM, Gelfand EV. Valvular Heart Disease: Classic Teaching and Emerging Paradigms. The American Journal of Medicine. 2013;126(12):1035-42.

2. Korossis SA, Fisher J, Ingham E. Cardiac valve replacement: a bioengineering approach. Bio-Medical Materials and Engineering. 2000;10(2):83-124.

3. Ismail M, Kim Fatt Hon J, Wei Chan Z, Liang Leo H. Recent Advances in Transcatheter Heart Valve Replacement: A Review on Aortic and Mitral Implantation. Recent Patents on Biomedical Engineering. 2012;5(3):235-52.

4. Toggweiler S, Humphries KH, Lee M, Binder RK, Moss RR, Freeman M, et al. 5-year outcome after transcatheter aortic valve implantation. Journal of the American College of Cardiology. 2013;61(4):413-9.

5. Sawaya F, Kappetein AP, Wisser W, Nataf P, Thomas M, Schachinger V, et al. Five-year haemodynamic outcomes of the first-generation SAPIEN balloon-expandable transcatheter heart valve. EuroIntervention. 2016;12(6):775-82.

6. Gilard M, Eltchaninoff H, Iung B, Donzeau-Gouge P, Chevreul K, Fajadet J, et al. Registry of Transcatheter Aortic-Valve Implantation in High-Risk Patients. New England Journal of Medicine. 2012;366(18):1705-15.

7. Blumenstein J, Liebetrau C, Linden AV, Moellmann H, Walther T, Kempfert J. Recent Advances in Transcatheter Aortic Valve Implantation: Novel Devices and Potential Shortcomings. Current Cardiology Reviews. 2013;9(4):274-80.

8. Stoeckel D, Bonsignore C, Duda S. A survey of stent designs. Minimally Invasive Therapy & Allied Technologies. 2002;11(4):137-47.

9. Fernandez D, Cevallos J, Brugaletta S, Martin-Yuste V, Freixa X, Andrea R, et al. Percutaneous transcatheter aortic valve implantation: present and future perspective. Expert Review of Medical Devices. 2013;10(2):185-99.

10. Thiene G, Valente M. Calcification of valve bioprostheses: the cardiac surgeon's nightmare. European Journal of Cardio-Thoracic Surgery. 1994;8(9):476.

11. Cigliano A, Gandaglia A, Lepedda AJ, Zinellu E, Naso F, Gastaldello A, et al. Fine structure of glycosaminoglycans from fresh and decellularized porcine cardiac valves and pericardium. Biochemistry Research International. 2012;2012:979351.

12. Spina M, Ortolani F, El Messlemani A, Gandaglia A, Bujan J, Garcia-Honduvilla N, et al. Isolation of intact aortic valve scaffolds for heart-valve bioprostheses:

extracellular matrix structure, prevention from calcification, and cell repopulation features. Journal of Biomedical Materials Research, Part A. 2003;67(4):1338-50.

13. Gilbert TW. Strategies for tissue and organ decellularization. Journal of Cellular Biochemistry. 2012;113(7):2217-22.

14. Breuer CK, Mettler BA, Anthony T, Sales VL, Schoen FJ, Mayer JE. Application of Tissue-Engineering Principles toward the Development of a Semilunar Heart Valve Substitute. Tissue Engineering. 2004;10(11-12):1725-36.

15. Barron V, Lyons E, Stenson-Cox C, McHugh PE, Pandit A. Bioreactors for cardiovascular cell and tissue growth: a review. Annals of Biomedical Engineering. 2003;31(9):1017-30.

16. Marieb EN, Hoehn K. Human anatomy & physiology. 9th ed. Boston: Pearson; 2013.

17. Iaizzo PA. Handbook of cardiac anatomy, physiology, and devices. Totowa, N.J.: Humana Press; 2005.

18. Levick JR. An introduction to cardiovascular physiology. 4th ed. London; New York: Arnold; Oxford University Press; 2003.

19. Schoen FJ. Evolving Concepts of Cardiac Valve Dynamics: The Continuum of Development, Functional Structure, Pathobiology, and Tissue Engineering. Circulation. 2008;118(18):1864-80.

20. Misfeld M, Sievers H-H. Heart valve macro- and microstructure. Philosophical Transactions of the Royal Society B: Biological Sciences. 2007;362(1484):1421-36.

21. Iaizzo PA, Bianco RW, Hill AJ, Louis JDS. Heart Valves: From Design to Clinical Implantation: Springer; 2013.

22. Akay M. Wiley encyclopedia of biomedical engineering. Hoboken, N.J.: Wiley-Interscience; 2006.

23. Kline J. Handbook of biomedical engineering. San Diego: Academic Press; 1988.

24. Rajamannan NM, Evans FJ, Aikawa E, Grande-Allen KJ, Demer LL, Heistad DD, et al. Calcific Aortic Valve Disease: Not Simply a Degenerative Process A Review and Agenda for Research From the National Heart and Lung and Blood Institute Aortic Stenosis Working GroupExecutive Summary: Calcific Aortic Valve Disease – 2011 Update. Circulation. 2011;124(16):1783-91.

25. Butcher JT, Mahler GJ, Hockaday LA. Aortic valve disease and treatment: The need for naturally engineered solutions. Advanced Drug Delivery Reviews. 2011;63(4-5):242-68.

26. Christie GW. Anatomy of aortic heart valve leaflets: the influence of glutaraldehyde fixation on function. European Journal of Cardio-Thoracic Surgery: Official Journal of the European Association for Cardio-Thoracic Surgery. 1992;6 Suppl 1:S25-32; discussion S3.

27. Vesely I. The role of elastin in aortic valve mechanics. Journal of Biomechanics. 1998;31(2):115-23.

28. Weind KL, Boughner DR, Rigutto L, Ellis CG. Oxygen diffusion and consumption of aortic valve cusps. American Journal of Physiology Heart and Circulatory Physiology. 2001;281(6):H2604-11.

29. Thubrikar M, Piepgrass WC, Deck JD, Nolan SP. Stresses of natural versus prosthetic aortic valve leaflets in vivo. The Annals of Thoracic Surgery. 1980;30(3):230-9.

30. Lee JM, Boughner DR, Courtman DW. The glutaraldehyde-stabilized porcine aortic valve xenograft. II. Effect of fixation with or without pressure on the tensile viscoelastic properties of the leaflet material. Journal of Biomedical Materials Research. 1984;18(1):79-98.

31. Frater RWM, Gong G, Hoffman D, Liao K. Endothelial covering of biological artificial heart valves. The Annals of Thoracic Surgery. 1992;53(3):371-2.

32. Deck JD. Endothelial cell orientation on aortic valve leaflets. Cardiovascular Research. 1986;20(10):760-7.

33. Iop L, Renier V, Naso F, Piccoli M, Bonetti A, Gandaglia A, et al. The influence of heart valve leaflet matrix characteristics on the interaction between human mesenchymal stem cells and decellularized scaffolds. Biomaterials. 2009;30(25):4104-16.

34. Liu AC, Joag VR, Gotlieb AI. The Emerging Role of Valve Interstitial Cell Phenotypes in Regulating Heart Valve Pathobiology. The American Journal of Pathology. 2007;171(5):1407-18.

35. Dreger SA, Taylor PM, Allen SP, Yacoub MH. Profile and localization of matrix metalloproteinases (MMPs) and their tissue inhibitors (TIMPs) in human heart valves. The Journal of Heart Valve Disease. 2002;11(6):875-80; discussion 80.

36. Schneider PJ, Deck JD. Tissue and cell renewal in the natural aortic valve of rats: an autoradiographic study. Cardiovascular Research. 1981;15(4):181-9.

37. Cimini M, Rogers KA, Boughner DR. Smoothelin-positive cells in human and porcine semilunar valves. Histochemistry and Cell Biology. 2003;120(4):307-17.

38. Marron K, Yacoub MH, Polak JM, Sheppard MN, Fagan D, Whitehead BF, et al. Innervation of human atrioventricular and arterial valves. Circulation. 1996;94(3):368-75.

39. Nkomo VT, Gardin JM, Skelton TN, Gottdiener JS, Scott CG, Enriquez-Sarano M. Burden of valvular heart diseases: a population-based study. Lancet. 2006;368(9540):1005-11.

40. Schoen FJ. Mechanisms of Function and Disease of Natural and Replacement Heart Valves. Annual Review of Pathology: Mechanisms of Disease. 2012;7(1):161-83.

41. City IHI-SL. Aortic Valve Stenosis - Intermountain Heart Institute - Salt Lake City, UT 2016 [Available from: http://intermountainhealthcare.org/hospitals/imed/services/heart-institute/heart-health-a-z/Pages/condition-aortic-valve-stenosis.aspx.

42. Kim KM. Calcification of matrix vesicles in human aortic valve and aortic media. Federation Proceedings. 1976;35(2):156-62.

43. Lincoln J, Lange AW, Yutzey KE. Hearts and bones: Shared regulatory mechanisms in heart valve, cartilage, tendon, and bone development. Developmental Biology. 2006;294(2):292-302.

44. Thiene G, Frescura C. Anatomical and pathophysiological classification of congenital heart disease. Cardiovascular Pathology.19(5):259-74.

45. Harb SC, Griffin BP. Mitral Valve Disease: a Comprehensive Review. Current Cardiology Reports. 2017;19(8):73.

46. Holt JP. The normal pericardium. American Journal of Cardiology. 1970;26(5):455-65.

47. Kenhub. Pericardium 2017 [Available from: https://www.kenhub.com/en/library/anatomy/the-pericardium.

48. Aboutdotcom. What Is the Pericardium? : @aboutdotcom; 2017 [Available from: http://biology.about.com/od/anatomy/a/aa050407a.htm.

49. Ishihara T, Ferrans VJ, Jones M, Boyce SW, Kawanami O, Roberts WC. Histologic and ultrastructural features of normal human parietal pericardium. The American Journal of Cardiology. 1980;46(5):744-53.

50. Kheradvar A, Groves EM, Dasi LP, Alavi SH, Tranquillo R, Grande-Allen KJ, et al. Emerging Trends in Heart Valve Engineering: Part I. Solutions for Future. Annals of Biomedical Engineering. 2014:1-11.

51. Yacoub MH, Takkenberg JJM. Will heart valve tissue engineering change the world? Nature Clinical Practice Cardiovascular Medicine. 2005;2(2):60-1.

52. Kheradvar A, Groves EM, Goergen CJ, Alavi SH, Tranquillo R, Simmons CA, et al. Emerging Trends in Heart Valve Engineering: Part II. Novel and Standard Technologies for Aortic Valve Replacement. Annals of Biomedical Engineering. 2014:1-14.

53. Akay M, Wiley I. Wiley encyclopedia of biomedical engineering. Hoboken, N.J.: Wiley-InterScience; 2006 2006.

54. Blog AsHVS. Miles Edwards' First Mechanical Heart Valve Replacement 2014 [Available from: http://www.heart-valve-surgery.com/heart-surgery-blog/2008/02/24/first-mechanical-heart-valve-replacement/.

55. HeartValveSurgery. First Mechanical Heart Valve Replacement Surgery 2016 [Available from: http://www.heart-valve-surgery.com/heart-surgery-blog/2008/05/30/first-mechanical-heart-valve-keeps-tickin-38-years-later/.

56. Medtronic. Artificial Heart Valves: Medtronic Open Pivot™ Bileaflet Mechanical Heart Valves. 2014.

57. Medical S. Bicarbon Fitline Aortic 2014 [Available from: http://www.sorin.com/products/cardiac-surgery/aortic/bicarbon-fitline.

58. Schoen FJ, Levy RJ. Tissue heart valves: Current challenges and future research perspectives. Journal of Biomedical Materials Research. 1999;47(4):439-65.

59. Carpentier A, Lemaigre G, Robert L, Carpentier S, Dubost C. Biological factors affecting long-term results of valvular heterografts. Journal of Thoracic and Cardiovascular Surgery. 1969;58(4):467-83.

60. O'Brien MF, Clarebrough JK. Preliminary communication heterograft aortic valve transplantation for human valve disease. The Medical Journal of Australia. 1966;2(5):228-30.

61. CThSurgery. BIOPROSTHESIS - CThSurgery.com 2017 [Available from: http://www.cthsurgery.com/bioprosthesis.html.

62. Bapat VN, Attia R, Thomas M. Effect of valve design on the stent internal diameter of a bioprosthetic valve: a concept of true internal diameter and its implications for the valve-in-valve procedure. JACC Cardiovascular interventions. 2014;7(2):115-27.

63. Ciubotaru A, Cebotari S, Tudorache I, Beckmann E, Hilfiker A, Haverich A. Biological heart valves. Biomedizinische Technik. 2013;58(5):389-97.

64. Heimbecker RO, Baird RJ, Lajos TZ, Varga AT, Greenwood WF. Homograft Replacement of the Human Mitral Valve: A Preliminary Report. Canadian Medical Association Journal. 1962;86(18):805-9.

65. Ross D. Homograft replacement of the aortic valve. British Journal of Surgery. 1967;54(10):842-5.

66. Yacoub M, Rasmi NR, Sundt TM, Lund O, Boyland E, Radley-Smith R, et al. Fourteen-year experience with homovital homografts for aortic valve replacement. Journal of Thoracic and Cardiovascular Surgery. 1995;110(1):186-93; discussion 93-4.

67. Gulbins H, Kreuzer E, Reichart B. Homografts: a review. Expert Review of Cardiovascular Therapy. 2003;1(4):533-9.

68. Ross DN. Replacement of aortic and mitral valves with a pulmonary autograft. Lancet. 1967;2(7523):956-8.

69. Melbourne TRCsH. Cardiology : Aortic Stenosis AS 2017 [Available from: http://www.rch.org.au/cardiology/heart_defects/Aortic_Stenosis_AS/.

70. Andersen HR, Knudsen LL, Hasenkam JM. Transluminal implantation of artificial heart valves. Description of a new expandable aortic valve and initial results with implantation by catheter technique in closed chest pigs. European Heart Journal. 1992;13(5):704-8.

71. Bonhoeffer P, Boudjemline Y, Saliba Z, Hausse AO, Aggoun Y, Bonnet D, et al. Transcatheter Implantation of a Bovine Valve in Pulmonary Position. A Lamb Study. 2000;102(7):813-6.

72. Bonhoeffer P, Boudjemline Y, Saliba Z, Merckx J, Aggoun Y, Bonnet D, et al. Percutaneous replacement of pulmonary valve in a right-ventricle to pulmonary-artery prosthetic conduit with valve dysfunction. The Lancet. 2000;356(9239):1403-5.

73. Cribier A, Eltchaninoff H, Bash A, Borenstein N, Tron C, Bauer F, et al. Percutaneous transcatheter implantation of an aortic valve prosthesis for calcific aortic stenosis: first human case description. Circulation. 2002;106(24):3006-8.

74. Rozeik MM, Wheatley DJ, Gourlay T. Percutaneous heart valves; past, present and future. Perfusion. 2014;29(5):397-410.

75. Lifesciences E. Transcatheter Heart Valves 2013 [Available from: http://www.edwards.com/Products/transcathetervalve/Pages/THVcategory.aspx.

76. Binder RK, Rodés-Cabau J, Wood DA, Mok M, Leipsic J, De Larochellière R, et al. Transcatheter Aortic Valve Replacement With the SAPIEN 3. JACC: Cardiovascular Interventions. 2013;6(3):293-300.

77. Kodali S, editor The SAPIEN 3 TAVR System: Design Features, "Special" Attributes, and Brief Clinical Trial Status. TVT 2016; 2016; Chicago.

78. Medtronic. Transcatheter Aortic Valve Replacement - CoreValve US | Medtronic 2016 [Available from: http://www.corevalve.com/us/index.htm.

79. Hermiller J, editor The EVOLUT R TAVR System: Design Features, "Special" Attributes, and Brief Clinical Trial Status. TVT 2016; 2016; Chicago.

80. SYMETIS. ACURATE TA | Symetis 2017 [Available from: https://www.symetis.com/products/acurate-ta.

81. Huber C, Wenaweser P, Windecker S, Carrel T. Transapical transcatheter aortic valve implantation using the second-generation self-expanding Symetis ACURATE TA valve. Multimed Man Cardiothorac Surg. 2014;2014.

82. Mollmann H, Diemert P, Grube E, Baldus S, Kempfert J, Abizaid A. Symetis ACURATE TF aortic bioprosthesis. EuroIntervention. 2013;9 Suppl:S107-10.

83. Scientific B. The Power of Control | Boston Scientific 2015 [Available from: http://www.bostonscientific.com/en-EU/products/transcatheter-heart-valve/lotus-heart-valve/the-power-to-control.html.

84. Medical DF. Our Technology (new) | Direct Flow Medical 2012 [Available from: http://directflowmedical.com/our-technology-new.

85. JenaValve. JenaValve Technology : Home 2016 [Available from: http://www.jenavalve.com/.

86. Treede H, editor The JenaValve TAVR System: Status Updates. TVT 2016; 2016; Chicago.

87. Medtronic. Transcatheter Aortic Valve Replacement – TAVR | Medtronic Engager 2016 [Available from: http://www.medtronic-engager.com/home/transcatheter-aortic-valve-replacement/index.htm.

88. Medical SJ. Home | Portico™ Transcatheter Aortic Valve Implantation System 2015 [Available from: http://professional-intl.sjm.com/therapies/portico-transcatheter-aortic-valve/home.

89. Willson AB, Rodès-Cabau J, Wood DA, Leipsic J, Cheung A, Toggweiler S, et al. Transcatheter Aortic Valve Replacement With the St. Jude Medical Portico Valve: First-in-Human Experience. Journal of the American College of Cardiology. 2012;60(7):581-6.

90. Gauvin R, Marinov G, Mehri Y, Klein J, Li B, Larouche D, et al. A comparative study of bovine and porcine pericardium to highlight their potential advantages to manufacture percutaneous cardiovascular implants. Journal of Biomaterials Applications. 2013;28(4):552-65.

91. Bruschi G, De Marco F, Martinelli L, Klugmann S. CoreValve® transcatheter self-expandable aortic bioprosthesis. Expert Review of Medical Devices. 2013;10(1):15-26.

92. Piazza N, Bleiziffer S, Brockmann G, Hendrick R, Deutsch M-A, Opitz A, et al. Transcatheter aortic valve implantation for failing surgical aortic bioprosthetic valve: from concept to clinical application and evaluation (part 1). JACC Cardiovascular interventions. 2011;4(7):721-32.

93. Bagur R, Pibarot P, Otto CM. Importance of the valve durability-life expectancy ratio in selection of a prosthetic aortic valve. Heart. 2017.

94. Capodanno D, Petronio AS, Prendergast B, Eltchaninoff H, Vahanian A, Modine T, et al. Standardized definitions of structural deterioration and valve failure in assessing long-term durability of transcatheter and surgical aortic bioprosthetic valves: a consensus statement from the European Association of Percutaneous Cardiovascular Interventions (EAPCI) endorsed by the European Society of Cardiology (ESC) and the European Association for Cardio-Thoracic Surgery (EACTS). European Journal of Cardio-Thoracic Surgery. 2017;52(3):408-17.

95. Butany J, Nair V, Leong SW, Soor GS, Feindel C. Carpentier-Edwards Perimount valves--morphological findings in surgical explants. Journal of Cardiac Surgery. 2007;22(1):7-12.

96. Head SJ, Celik M, Kappetein AP. Mechanical versus bioprosthetic aortic valve replacement. European Heart Journal. 2017;38(28):2183-91.

97. Dvir D, editor First look at long-term durability of transcatheter heart valves: Assessment of valve function up to 10-years after implantation. EuroPCR 2016; 2016 2016; Paris, France. Paris, France2016.

98. Sacks MS, Schoen FJ, Mayer JE. Bioengineering challenges for heart valve tissue engineering. Annual Review of Biomedical Engineering. 2009;11:289-313.

99. Jana S, Tefft BJ, Spoon DB, Simari RD. Scaffolds for tissue engineering of cardiac valves. Acta Biomaterialia. 2014;10(7):2877-93.

100. Tudorache I, Horke A, Cebotari S, Sarikouch S, Boethig D, Breymann T, et al. Decellularized aortic homografts for aortic valve and aorta ascendens replacement. European Journal of Cardio-Thoracic Surgery. 2016;50(1):89-97.

101. Cebotari S, Tudorache I, Ciubotaru A, Boethig D, Sarikouch S, Goerler A, et al. Use of fresh decellularized allografts for pulmonary valve replacement may reduce the reoperation rate in children and young adults: early report. Circulation. 2011;124(11 Suppl):S115-23.

102. Lupinetti FM, Tsai TT, Kneebone JM, Bove EL. Effect of cryopreservation on the presence of endothelial cells on human valve allografts. Journal of Thoracic and Cardiovascular Surgery. 1993;106(5):912-7.

103. Carletti E, Motta A, Migliaresi C. Scaffolds for tissue engineering and 3D cell culture. Methods in Molecular Biology. 2011;695:17-39.

104. Chen G-Q, Wu Q. The application of polyhydroxyalkanoates as tissue engineering materials. Biomaterials. 2005;26(33):6565-78.

105. Hoerstrup SP, Sodian R, Daebritz S, Wang J, Bacha EA, Martin DP, et al. Functional Living Trileaflet Heart Valves Grown In Vitro. Circulation. 2000;102(suppl 3):Iii-44-Iii-9.

106. Ouyang H, Zhang JB, Liu Y, Li Q, Peng YH, Kang XJ, et al. [Research on application of modified polyethylene glycol hydrogels in the construction of tissue engineered heart valve]. Zhonghua Wai Ke Za Zhi Chinese Journal of Surgery. 2008;46(22):1723-6.

107. Tseng H, Cuchiara ML, Durst CA, Cuchiara MP, Lin CJ, West JL, et al. Fabrication and mechanical evaluation of anatomically-inspired quasilaminate hydrogel structures with layer-specific formulations. Annals of Biomedical Engineering. 2013;41(2):398-407.

108. Schleicher M, Wendel HP, Fritze O, Stock UA. In vivo tissue engineering of heart valves: evolution of a novel concept. Regenerative Medicine. 2009;4(4):613-9.

109. MacGrogan D, Luxán G, Driessen-Mol A, Bouten C, Baaijens F, Pompa JLdl. How to Make a Heart Valve: From Embryonic Development to Bioengineering of Living Valve Substitutes. Cold Spring Harbor Perspectives in Medicine. 2014;4(11):a013912.

110. Schmidt D, Stock UA, Hoerstrup SP. Tissue engineering of heart valves using decellularized xenogeneic or polymeric starter matrices. Philosophical Transactions of the Royal Society B: Biological Sciences. 2007;362(1484):1505-12.

111. Roh JD, Sawh-Martinez R, Brennan MP, Jay SM, Devine L, Rao DA, et al. Tissue-engineered vascular grafts transform into mature blood vessels via an inflammation-mediated process of vascular remodeling. Proceedings of the National Academy of Sciences. 2010;107(10):4669-74.

112. Emmert MY, Weber B, Wolint P, Behr L, Sammut S, Frauenfelder T, et al. Stem Cell–Based Transcatheter Aortic Valve Implantation: First Experiences in a Pre-Clinical Model. JACC: Cardiovascular Interventions. 2012;5(8):874-83.

113. Driessen-Mol A, Emmert MY, Dijkman PE, Frese L, Sanders B, Weber B, et al. Transcatheter Implantation of Homologous “Off-the-Shelf” Tissue-Engineered Heart Valves With Self-Repair Capacity: Long-Term Functionality and Rapid In Vivo Remodeling in Sheep. Journal of the American College of Cardiology. 2014;63(13):1320-9.

114. Mol A, Smits AIPM, Bouten CVC, Baaijens FPT. Tissue engineering of heart valves: advances and current challenges. Expert Review of Medical Devices. 2009;6(3):259-75.

115. Frid MG, Kale VA, Stenmark KR. Mature Vascular Endothelium Can Give Rise to Smooth Muscle Cells via Endothelial-Mesenchymal Transdifferentiation. In Vitro Analysis. 2002;90(11):1189-96.

116. Nimjee SM, Rusconi CP, Sullenger BA. Aptamers: An Emerging Class of Therapeutics. Annual Review of Medicine. 2005;56(1):555-83.

117. CryoLife. SynerGraft Technology 2015 [Available from: https://www.cryolife.com/products/cardiac-allografts/synergraft-technology/.

118. Simon P, Kasimir MT, Seebacher G, Weigel G, Ullrich R, Salzer-Muhar U, et al. Early failure of the tissue engineered porcine heart valve SYNERGRAFT in pediatric patients. European Journal of Cardio-Thoracic Surgery: Official Journal of the European Association for Cardio-Thoracic Surgery. 2003;23(6):1002-6; discussion 6.

119. Konuma T, Devaney EJ, Bove EL, Gelehrter S, Hirsch JC, Tavakkol Z, et al. Performance of CryoValve SG Decellularized Pulmonary Allografts Compared With Standard Cryopreserved Allografts. The Annals of Thoracic Surgery.88(3):849-55.

120. Berlin AT. Matrix P 2015 [Available from: http://www.autotissue.de/seknavi/dezellularisierung/.

121. Ruffer A, Purbojo A, Cicha I, Glockler M, Potapov S, Dittrich S, et al. Early failure of xenogenous de-cellularised pulmonary valve conduits--a word of caution! European Journal of Cardio-Thoracic Surgery. 2010;38(1):78-85.

122. Konertz W, Angeli E, Tarusinov G, Christ T, Kroll J, Dohmen PM, et al. Right ventricular outflow tract reconstruction with decellularized porcine xenografts in patients with congenital heart disease. Journal of Heart Valve Disease. 2011;20(3):341-7.

123. School HM. ARISE 2016 [Available from: http://arise-clinicaltrial.eu/home.html.

124. School HM. ESPOIR 2014 [Available from: http://www.espoir-clinicaltrial.eu/home.html.

125. Sarikouch S, Horke A, Tudorache I, Beerbaum P, Westhoff-Bleck M, Boethig D, et al. Decellularized fresh homografts for pulmonary valve replacement: a decade of clinical experience. European Journal of Cardio-Thoracic Surgery. 2016:ezw050.

126. Iop L, Gerosa G. Guided Tissue Regeneration in Heart Valve Replacement: From Preclinical Research to First-in-Human Trials. BioMed Research International. 2015;2015:13.

127. Crapo PM, Gilbert TW, Badylak SF. An overview of tissue and whole organ decellularization processes. Biomaterials. 2011;32(12):3233-43.

128. Seddon AM, Curnow P, Booth PJ. Membrane proteins, lipids and detergents: not just a soap opera. Biochimica et Biophysica Acta (BBA) - Biomembranes. 2004;1666(1–2):105-17.

129. Dohmen PM, Konertz W. Tissue-engineered heart valve scaffolds. Annals of Thoracic and Cardiovascular Surgery. 2009;15(6):362-7.

130. Tudorache I, Cebotari S, Sturz G, Kirsch L, Hurschler C, Hilfiker A, et al. Tissue engineering of heart valves: biomechanical and morphological properties of decellularized heart valves. Journal of Heart Valve Disease. 2007;16(5):567-73; discussion 74.

131. Grauss RW, Hazekamp MG, Oppenhuizen F, van Munsteren CJ, Gittenberger-de Groot AC, DeRuiter MC. Histological evaluation of decellularised porcine aortic

valves: matrix changes due to different decellularisation methods☆. European Journal of Cardio-Thoracic Surgery. 2005;27(4):566-71.

132. Dahl SL, Koh J, Prabhakar V, Niklason LE. Decellularized native and engineered arterial scaffolds for transplantation. Cell Transplantation. 2003;12(6):659-66.

133. Patel N, Solanki E, Picciani R, Cavett V, Caldwell-Busby JA, Bhattacharya SK. Strategies to recover proteins from ocular tissues for proteomics. Proteomics. 2008;8(5):1055-70.

134. Prasertsung I, Kanokpanont S, Bunaprasert T, Thanakit V, Damrongsakkul S. Development of acellular dermis from porcine skin using periodic pressurized technique. Journal of Biomedical Materials Research, Part B: Applied Biomaterials. 2008;85(1):210-9.

135. Guyette JP, Gilpin SE, Charest JM, Tapias LF, Ren X, Ott HC. Perfusion decellularization of whole organs. Nature Protocols. 2014;9(6):1451-68.

136. Courtman DW, Pereira CA, Kashef V, McComb D, Lee JM, Wilson GJ. Development of a pericardial acellular matrix biomaterial: biochemical and mechanical effects of cell extraction. Journal of Biomedical Materials Research. 1994;28(6):655-66.

137. Mendoza-Novelo B, Avila EE, Cauich-Rodriguez JV, Jorge-Herrero E, Rojo FJ, Guinea GV, et al. Decellularization of pericardial tissue and its impact on tensile viscoelasticity and glycosaminoglycan content. Acta Biomaterialia. 2011;7(3):1241-8.

138. Garcia Paez JM, Herrero EJ, Carrera San Martin A, Garcia Sestafe JV, Tellez G, Millan I, et al. The influence of chemical treatment and suture on the elastic behavior of calf pericardium utilized in the construction of cardiac bioprostheses. Journal of Materials Science: Materials in Medicine. 2000;11(7):459-64.

139. Mirsadraee S, Wilcox HE, Korossis SA, Kearney JN, Watterson KG, Fisher J, et al. Development and characterization of an acellular human pericardial matrix for tissue engineering. Tissue Engineering. 2006;12(4):763-73.

140. Dong X, Wei X, Yi W, Gu C, Kang X, Liu Y, et al. RGD-modified acellular bovine pericardium as a bioprosthetic scaffold for tissue engineering. Journal of Materials Science: Materials in Medicine. 2009;20(11):2327-36.

141. Hennessy KM, Clem WC, Phipps MC, Sawyer AA, Shaikh FM, Bellis SL. The effect of RGD peptides on osseointegration of hydroxyapatite biomaterials. Biomaterials. 2008;29(21):3075-83.

142. Rémi E, Khelil N, Centa ID, Roques C, Ba M, Medjahed-Hamidi F, et al. Pericardial Processing: Challenges, Outcomes and Future Prospects2011 2011-09-15.

143. Tedder ME, Liao J, Weed B, Stabler C, Zhang H, Simionescu A, et al. Stabilized collagen scaffolds for heart valve tissue engineering. Tissue Eng Part A. 2009;15(6):1257-68.

144. Alavi SH, Groves EM, Kheradvar A. The Effects of Transcatheter Valve Crimping on Pericardial Leaflets. The Annals of Thoracic Surgery. 2014;97(4):1260-6.

145. Della Barbera M, Valente M, Basso C, Thiene G. Pericardial traumatic injury in trans-catheter aortic valve implantation. European Journal of Cardio-Thoracic Surgery. 2013;43(3):493-4.

146. Zegdi R, Bruneval P, Blanchard D, Fabiani J-N. Evidence of leaflet injury during percutaneous aortic valve deployment. European Journal of Cardio-Thoracic Surgery. 2011;40(1):257-60.

147. Amahzoune B, Bruneval P, Allam B, Lafont A, Fabiani JN, Zegdi R. Traumatic leaflet injury during the use of percutaneous valves: a comparative study of balloon- and self-expandable valved stents. European Journal of Cardio-Thoracic Surgery. 2013;43(3):488-93.

148. Kiefer P, Gruenwald F, Kempfert J, Aupperle H, Seeburger J, Mohr FW, et al. Crimping may affect the durability of transcatheter valves: an experimental analysis. Annals of Thoracic Surgery. 2011;92(1):155-60.

149. Thiene G, Basso C, Barbera MD, Valente M. Pericardial leaflet injury in transcatheter aortic valve implantation: trick or treat. European Journal of Cardio-Thoracic Surgery. 2011;40(1):259-60.

150. Woessner JF. The determination of hydroxyproline in tissue and protein samples containing small proportions of this imino acid. Archives of Biochemistry and Biophysics. 1961;93:440-7.

151. SYMETIS. ACURATE neo TF | Symetis 2017 [Available from: https://www.symetis.com/products/acurate-neo-tf.

152. Moreira R, Velz T, Alves N, Gesche VN, Malischewski A, Schmitz-Rode T, et al. Tissue-engineered heart valve with a tubular leaflet design for minimally invasive transcatheter implantation. Tissue Eng Part C Methods. 2015;21(6):530-40.

153. Weber M, Heta E, Moreira R, Gesche VN, Schermer T, Frese J, et al. Tissue-engineered fibrin-based heart valve with a tubular leaflet design. Tissue Eng Part C Methods. 2014;20(4):265-75.

154. Goetz WA, Lim HS, Lansac E, Weber PA, Duran CM. A temporarily stented, autologous pericardial aortic valve prosthesis. Journal of Heart Valve Disease. 2002;11(5):696-702.

155. Kempfert J, Mollmann H, Walther T. Symetis ACURATE TA valve. EuroIntervention. 2012;8 Suppl Q:Q102-9.

156. International Organization for Standardization. ISO 5840-3 Cardiovascular implants: Cardiac valve prostheses Part 3: Heart valve substitutes implanted by transcatheter techniques. 2013.

157. Bottio T, Caprili L, Casarotto D, Gerosa G. Small aortic annulus: the hydrodynamic performances of 5 commercially available bileaflet mechanical valves. Journal of Thoracic and Cardiovascular Surgery. 2004;128(3):457-62.

158. Bottio T, Tarzia V, Rizzoli G, Gerosa G. In-vitro testing of three totally supra-annular bileaflet mechanical valves: hydrodynamics in the Sheffield pulse duplicator. Journal of Heart Valve Disease. 2008;17(2):222-6.

159. Gerosa G, Tarzia V, Rizzoli G, Bottio T. Small aortic annulus: the hydrodynamic performances of 5 commercially available tissue valves. Journal of Thoracic and Cardiovascular Surgery. 2006;131(5):1058-64.

160. Akins CW, Travis B, Yoganathan AP. Energy loss for evaluating heart valve performance. Journal of Thoracic and Cardiovascular Surgery. 2008;136(4):820-33.

161. Berkovitz BK. Crimping of collagen in the intra-articular disc of the temporomandibular joint: a comparative study. Journal of Oral Rehabilitation. 2000;27(7):608-13.

162. Hilbert SL, Sword LC, Batchelder KF, Barrick MK, Ferrans VJ. Simultaneous assessment of bioprosthetic heart valve biomechanical properties and collagen crimp length. Journal of Biomedical Materials Research. 1996;31(4):503-9.

163. ISO. ISO 5840-3:2013 (E) (Cardiovascular implants - Cardiac valve prostheses - Part 3: Heart valve substitutes implanted by transcatheter techniques). 2013.

164. Cribier A. Commemorating the 15-year anniversary of TAVI: insights into the early stages of development, from concept to human application, and perspectives. EuroIntervention. 2017;13(1):29-37.

165. Wong ML, Wong JL, Athanasiou KA, Griffiths LG. Stepwise solubilization-based antigen removal for xenogeneic scaffold generation in tissue engineering. Acta Biomaterialia. 2013;9(5):6492-501.

166. Roosens A, Somers P, De Somer F, Carriel V, Van Nooten G, Cornelissen R. Impact of Detergent-Based Decellularization Methods on Porcine Tissues for Heart Valve Engineering. Annals of Biomedical Engineering. 2016;44(9):2827-39.

167. Theodoridis K, Müller J, Ramm R, Findeisen K, Andrée B, Korossis S, et al. Effects of combined cryopreservation and decellularization on the biomechanical, structural and biochemical properties of porcine pulmonary heart valves. Acta Biomaterialia. 2016;43(Supplement C):71-7.

168. Aguiari P, Iop L, Favaretto F, Fidalgo CM, Naso F, Milan G, et al. In vitro comparative assessment of decellularized bovine pericardial patches and commercial bioprosthetic heart valves. Biomed Mater. 2017;12(1):015021.

169. Rahmani B, Tzamtzis S, Sheridan R, Mullen MJ, Yap J, Seifalian AM, et al. In Vitro Hydrodynamic Assessment of a New Transcatheter Heart Valve Concept (the TRISKELE). Journal of Cardiovascular Translational Research. 2016.

170. Sedaghat A, Sinning J-M, Utzenrath M, Ghalati PF, Schmitz C, Werner N, et al. Hydrodynamic Performance of the Medtronic CoreValve and the Edwards SAPIEN XT Transcatheter Heart Valve in Surgical Bioprostheses: An In Vitro Valve-in-Valve Model. The Annals of Thoracic Surgery. 2016;101(1):118-24.

171. Kappetein AP, Head SJ, Généreux P, Piazza N, van Mieghem NM, Blackstone EH, et al. Updated standardized endpoint definitions for transcatheter aortic valve implantation: the Valve Academic Research Consortium-2 consensus document (VARC-2)†. European Journal of Cardio-Thoracic Surgery. 2012;42(5):S45-S60.

172. Bermejo J. The effects of hypertension on aortic valve stenosis. Heart. 2005;91(3):280-2.

173. Gallo M, Poser H, Bottio T, Bonetti A, Franci P, Naso F, et al. The Vietnamese pig as a translational animal model to evaluate tissue engineered heart valves: promising early experience. International Journal of Artificial Organs.40(4):142-9.

LIST OF TABLES

LIST OF FIGURES